Cell Adhesion and Cell Fate: An Effective Feedback Loop During Zebrafish Gastrulation

by

Vanessa Barone

March, 2017

A thesis presented to the
Graduate School
of the
Institute of Science and Technology Austria, Klosterneuburg, Austria
in partial fulfillment of the requirements
for the degree of
Doctor of Philosophy

The dissertation of Vanessa Barone, titled "*Cell Adhesion and Cell Fate: An Effective Feedback Loop During Zebrafish Gastrulation*", is approved by:

Supervisor: Carl-Philipp Heisenberg, IST Austria, Klosterneuburg, Austria

Signature:

Committee Member: Harald Janovjak, IST Austria, Klosterneuburg, Austria

Signature:

Committee Member: Patrick Lemaire, CRBM, Montpellier, France

Signature:

Exam Chair: Calin C. Guet, IST Austria, Klosterneuburg, Austria

Signature:

I hereby declare that this dissertation is my own work and that it does not contain other people's work without this being so stated; this thesis does not contain my previous work without this being stated, and the bibliography contains all the literature that I used in writing the dissertation.

I declare that this is a true copy of my thesis, including any final revisions, as approved by my thesis committee, and that this thesis has not been submitted for a higher degree to any other university or institution.

I certify that any republication of materials presented in this thesis has been approved by the relevant publishers and co-authors.

Signature:

Vanessa Barone

March 27, 2017

Abstract

Cell-cell contact formation constitutes the first step in the emergence of multicellularity in evolution, thereby allowing the differentiation of specialized cell types. In metazoan development, cell-cell contact formation is thought to influence cell fate specification, and cell fate specification has been implicated in cell-cell contact formation. However, remarkably little is yet known about whether and how the interaction and feedback between cell-cell contact formation and cell fate specification affect development. Here we identify a positive feedback loop between cell-cell contact duration, morphogen signaling and mesendoderm cell fate specification during zebrafish gastrulation. We show that long lasting cell-cell contacts enhance the competence of prechordal plate (ppl) progenitor cells to respond to Nodal signaling, required for proper ppl cell fate specification. We further show that Nodal signalling promotes ppl cell-cell contact duration, thereby generating an effective positive feedback loop between ppl cell-cell contact duration and cell fate specification. Finally, by using a combination of theoretical modeling and experimentation, we show that this feedback loop determines whether anterior axial mesendoderm cells become ppl progenitors or, instead, turn into endoderm progenitors. Our findings reveal that the gene regulatory networks leading to cell fate diversification within the developing embryo are controlled by the interdependent activities of cell-cell signaling and contact formation.

Acknowledgments

Many people accompanied me during this trip: I would not have reached my destination nor enjoyed the travelling without them. First of all, thanks to CP. Thanks for making me part of your team, always full of diverse, interesting and incredibly competent people and thanks for all the good science I witnessed and participated in. It has been a blast, an incredibly exciting one! Thanks to JLo, for teaching me how to master my pipettes and showing me that science is a lot of fun. Many, many thanks to Gabby for teaching me basically everything about zebrafish and being always there to advice, suggest, support...and play fussball! Thank you to Julien, for the critical eye on things, Pedro, for all the invaluable feedback and the amazing kicker matches, and Keisuke, for showing me the light, and to the three of them together for all the good laughs we had. My start in Vienna would have been a lot more difficult without you guys. Also it would not have been possible without Elena and Inês: thanks for helping setting up this lab and for the dinners in Gugging. Thanks to Martin, for helping me understand the physics behind biology. Thanks to Philipp, for the interest and advice, and to Michael, for the Viennise take on things. Thanks to Julia, for putting up with being our technician and becoming a friend in the process. And now to the newest members of the lab. Thanks to Daniel for the enthusiasm and the neverending energy and for all your help over the years: thank you! To Jana, for showing me that one doesn't give up, no matter what. To Shayan, for being such a motivated student. To Matt, for helping out with coding and for finding punk solutions to data analysis problems. Thanks to all the members of the lab, Verena, Hitoshi, Silvia, Conny, Karla, Nicoletta, Zoltan, Peng, Benoit, Roland, Yuuta and Feyza, for the wonderful atmosphere in the lab. Many thanks to Koni and Deborah: doing experiments would have been much more difficult without your help. Special thanks to Katjia for setting up an amazing imaging facility and for building the best team, Robert, Nasser, Anna and Doreen: thank you for putting up with all the late sortings and for helping with all the technical problems. Thanks to Eva, Verena and Matthias for keeping the fish happy. Big thanks to Harald Janovjak for being a present and helpful committee member over the years and to Patrick Lemaire for the helpful insight and extremely interesting discussion we had about the project. Also, this journey would not have been the same without all the friends that I met in Dresden and then in Vienna: Daniele, Claire, Kuba, Steffi, Harold, Dejan, Irene, Fabienne, Hande, Tiago, Marianne, Jon, Srdjan, Branca, Uli, Murat, Alex, Conny, Christoph, Caro, Simone, Barbara, Felipe, Dama, Jose, Hubert and many others that filled my days with fun and support. A special thank to my family, always close even if they are kilometers away. Grazie ai miei fratelli, Nunzio e William, e alla mia mamma, per essermi sempre vicini pur vivendo a chilometri di distanza. And, last but not least, thanks to Moritz, for putting up with the crazy life of a scientist, the living apart for so long, never knowing when things are going to happen. Thanks for being a great partner and my number one fan!

About the Author

Vanessa Barone completed a BSc in Biological Sciences and a MAs in Biomolecular Sciences at the Universita` degli Studi di Torino in 2007 and 2009, respectively. She participated in the characterization of a protein marker for liver metastasis secondary to colorectal cancer under the supervision of Dr. Serena Marchio`, Prof. Paola Taverna and Prof. Federico Bussolino at Vascular Oncology Unit, Institute of Cancer Research and Treatment (IRCC), Candiolo (Italy). The result of this work was published in the research article:

Marchiò S, Soster M, Cardaci S, Muratore A, Bartolini A, **Barone V**, Ribero D, Monti M, Bovino P, Sun J, Giavazzi R, Asioli S, Cassoni P, Capussotti L, Pucci P, Bugatti A, Rusnati M, Pasqualini R, Arap W, Bussolino F. A complex of α6 integrin and E-cadherin drives liver metastasis of colorectal cancer cells through hepatic angiopoietin-like 6. EMBO Mol Med. 2012

Afterwards, she joined Massimo Santoro group at the Molecular Biology Center (MBC, Torino) as a research assistant where she worked on vascular development in the zebrafish embryo.

List of Publications Appearing in Thesis

Barone V, Lang M, Krens G, Pradhan SJ, Shamipour S, Sako K, Sikora M, Guet CC, Heisenberg CP. An effective feedback loop between cell-cell contact duration and morphogen signaling determines cell fate specification during zebrafish gastrulation. In revision.

Krens SF, Veldhuis JH, **Barone V**, Čapek D, Maître JL, Brodland GW, Heisenberg CP. Interstitial fluid osmolarity modulates the action of differential tissue surface tension in progenitor cell segregation during gastrulation. Development. 2017

Sako K, Pradhan SJ, **Barone V**, Ingles-Prieto A, Muller P, Ruprecht V, Capek D, Galande S, Janovjak H, Heisenberg CP. Optogenetic control of Nodal signaling reveals a temporal pattern of nodal signaling regulating cell fate specification during gastrulation. Cell Reports. 2016

Ruprecht V, Wieser S, Callan-Jones A, Smutny M, Morita H, Sako K, **Barone V**, Ritsch-Marte M, Sixt M, Voituriez R, Heisenberg CP. Cortical contractility triggers a stochastic switch to fast amoeboid cell motility. Cell. 2015

Compagnon J, **Barone V**, Rajshekar S, Kottmeier R, Pranjic-Ferscha K, Behrndt M, Heisenberg CP. The notochord breaks bilateral symmetry by controlling cell shapes in the zebrafish laterality organ. Dev Cell. 2014

Tragust S, Mitteregger B, **Barone V**, Konrad M, Ugelvig LV, Cremer S. Ants disinfect fungus-exposed brood by oral uptake and spread of their poison. Curr Biol. 2013

Barone V, Heisenberg CP. Cell adhesion in embryo morphogenesis. Curr Opin Cell Biol. 2012

Table of Contents

List of Figures

List of Symbols/Abbreviations

Acvr	activin receptor-like
aldh1a2	aldheyde dehydrogenase 1a2
BMP	Bone morphogenetic protein
cas	casanova
cdc42	cell division cycle 42
Cdh	cadherin
cyp26a1	cytochrome P450 26a1
DCL	deep cell layer
dkk1	dikkopf
DMEM	Dulbecco's Modified Eagle's medium
Dpp	decapentaplegic
EGFP	enhanced green fluorescent protein
EGTA	ethylene glycol-bis(β-aminoethyl ether)-N,N,N',N'-tetraacetic acid
EVL	enveloping layer
FGF	fibroblast growth factor
flh	floating head
FoxH	forkhead box H
gapdh	glyceraldehyde-3-phosphate dehydrogenase
GEF	guanosine exchange factor
gsc	goosecoid
hpf	hours post fertilization
ikk1	inhibitor of NFkB kinase 1
irf6	interferon regulatory factor 6
lft	lefty
mir-	microRNA
mRFP	membrane bound red fluorescent protein

ndr	nodal related
ntl	notail
Oep	one eyed pinhead
p-mlc2	phosphorilated myosin light chain 2
Pan-Cad	pancadherin
PBS	phosphate buffered saline
PFA	paraformaldehyde
ppl	prechordal plate
prex1	phosphatidylinositol-3,4,5-trisphosphate-dependent Rac exchange factor 1
qDots	quantum dots
RA	retinoic acid
rac	ras-related C3 botulinum toxin substrate
rho	ras homolog gene family
SARA	smad anchor for receptor activation
TBS	triphosphate buffered saline
TGF-β	transforming growth factor beta
TL	tupfel long fin
tRFP	turbo red fluorescent protein
TST	tissue suface tension
vent	ventral expressed homeobox
vox	ventral homeobox
Wnt	wingless related integration site
YSL	yolk syncitial layer

1 Introduction

1.1 Embryogenesis: cell differentiation and morphogenesis

The sexual reproduction of multicellular organisms relies on the formation of a new individual starting from a single cell, the zygote. This entails the production of multiple cells that acquire specialized functions and, at the same time, organize into distinct tissues, structures and eventually organs. Embryogenesis, i.e. the formation of an embryo, is the first step towards the formation of a new individual. The set of events that brings about the specialization of cells into several types is referred to as cell differentiation, while the process by which cells organize in space to give the embryo its shape is named morphogenesis. Cell differentiation and morphogenesis are two inseparable sides of the same coin, as the success of embryogenesis requires the coordinated and timely unfolding of both processes.

1.1.1 Cell differentiation in the early embryo

The differentiation of a cell into a particular type is viewed as a path along which one can make several irreversible choices. Even though every cell can initially choose any possible path, each turn restricts the range of reachable destinations down to the final one[1]. However, the events that lead to an irreversible choice unfold over time. Typically, a cascade of molecular events is initiated so that the cell starts differentiating into a certain type. For a period of time, this differentiation program is reversible and can be reset towards a different cell type: the cell's fate is specified. After a certain point, the cell is committed to this particular fate: the irreversible choice is made and the cell's fate is determined.

One of the first choices an embryonic cell makes is during gastrulation, when embryonic progenitor cells, or blastomeres, differentiate and eventually separate into the three germ layers, ectoderm, mesoderm and endoderm. Ectoderm progenitor cells generate the epidermis and the nervous system. Mesoderm progenitor cells form blood, muscles, bones, kidney, gonads and connective tissues, while endoderm progenitor cells give rise to the epithelial cell types of the inner organs. In most cases, mesendoderm progenitors are first specified that then further differentiate in mesoderm or endoderm. The mechanisms that lead to the differentiation into ectoderm, mesoderm and endoderm vary among organisms. Molecules that are sufficient to initiate differentiation, i.e. determinants, may be asymmetrically distributed in the zygote, so that, after cleavage, they are inherited only by a

subset of blastomeres[2] (Fig. 1.1.1a). In the ascidian embryo, for instance, specification of primary muscle mesoderm is due to inheritance of mRNA coding for the transcription factor *macho-1*[3,4]. Similarly, asymmetric localization of Wnt signals and subsequent nuclear translocation of β-catenin is responsible for the specification of skeletogenic mesoderm in sea urchin[5–7] and of dorsal mesendoderm in zebrafish and xenopus embryos[8–11]. In these cases cell specification is autonomous and differentiation can be achieved in isolation from the rest of the embryo[6,12,13]. Nonetheless, cell specification may require direct or indirect cell communication, as one or more cells produce signals that change the fate of other embryonic cells (Fig. 1.1.1b). In the very same sea urchin embryo, contact with a skeletogenic micromere is necessary and sufficient for endoderm specification of any other embryonic cell [6]. In c.elegans the specification of the first endoderm precursor happens at the 4-cell stage and requires the interaction between the posterior most cell (P2) and the neighbouring cell (EMS)[14,15]. In the ascidian embryo, cell-cell contact between specific cell pairs is necessary for the specification of notochord and neural precursors[16,17]. In such cases, one cell induces the other by direct interaction. In other cases the molecules triggering cell specification are soluble and can act at a distance from the producing cells (Fig. 1.1.1c). Ligands of the Transforming Growth Factor beta (TGF-β) family like Nodals and Bone Morphogenetic Proteins (BMPs), as well as Fibroblast Growth Factors (FGFs) have been shown to have such functions in the early embryo and are also called morphogens [18,19]. Since morphogens can diffuse from their source, they have been shown to form gradients or to have graded activity. In these cases the inductive effect of a morphogen may vary according to the relative position of producing and receiving cell [20–22], as well as with the time the receiving cell spends within the gradient[23]. We will discuss one example of graded morphogen activity in the following section regarding nodal ligands in the zebrafish embryo.

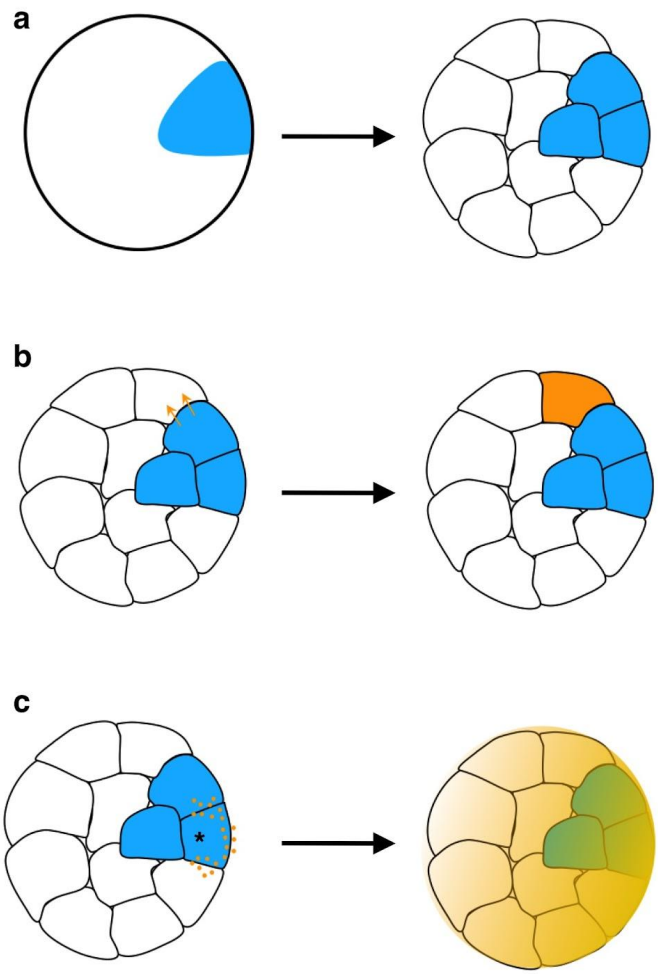

Fig. 1.1.1 - Modes of cell fate specification
(**a**) Maternal determinants are deposited locally in the egg. The blastomeres forming in that region following cell division inherit the determinants and acquire a specific cell fate. (**b**) Direct contact with an inducing blastomere specifies cell fate. (**c**) One blastomere (*) expresses a soluble morphogen that diffuses creating a gradient of inducing signal. The receiving blastomeres acquire specific cell fates according to the level and duration of morphogen signal they are exposed to.

1.1.2 Morphogenesis

The process by which embryos acquire their shape is named morphogenesis, literally the generation of form. It comprises the events that transform an initial mass of cells into a structured body and it has been most thoroughly described in the context of gastrulation.

During gastrulation the progenitor cells of the three germ layers reorganize so that the embryo becomes a multilayered structure with mesoderm and endoderm progenitor cells inside and ectoderm progenitor cells outside. This is due to subsets of embryonic cells displaying specific cell behaviors in a coordinated fashion that result in movements of whole tissues, i.e. morphogenic movements. Interestingly, only a few morphogenic movements have been repeatedly observed among metazoan: i) epiboly, the spreading of a layer of cells over another; ii) internalization, the penetration of superficial cells into the interior of the embryo; iii) emboly, the migration of internalized cells; iv) convergent-extension, narrowing of a tissue along one axis and concomitant extension along another axis [24].

Each of these morphogenic movements is the result of a set of coordinated cell behaviors. Cell behaviors that lead to morphogenic movements are cell division, cell growth, cell death,

cell shape change, extracellular matrix secretion and cell movement[25]. Even though both morphogenic movements and the cellular behaviors that cause them are conserved among metazoan there is great variation as of which set of cellular behaviors drives a specific morphogenic movement[26]. The internalization of mesendoderm cells, for instance, happens by invagination in invertebrate embryos such as ascidians[27] and drosophila[28,29]. This kind of internalization is caused mainly by cell shape changes within a continuous epithelium, namely the apical constriction of mesendoderm progenitor cells[30]. In amphibian embryos, instead, mesendoderm cells internalize by involution, the folding of a coherent tissue[31], while in the zebrafish embryo they ingress singularly but synchronously[32]. In other cases, different mesendoderm types use different behaviors to ingress. In the sea urchin the skeletogenic mesoderm cells internalize by ingression, followed by invagination of the other mesendoderm progenitor cells[33,34].

Gastrulation is the result of several morphogenic movements that are coordinated in space and time. Internalization of mesendoderm is coupled to epiboly of the overlying ectoderm in organisms as diverse as ctenophores, amphibians and teleost fish, and further coordinated with convergent-extension in vertebrate embryos[24].

1.2 Zebrafish embryogenesis

Embryonic development of the zebrafish, *Danio rerio*, begins with the deposition of mature oocytes surrounded by an a-cellular membrane, the chorion. Fertilization is external and sperm entry is restricted spatially, as it can only happen through a small opening in the chorion, the micropyle[35]. The zygote is a mix of yolk and cytoplasm that are separated by means of cytoplasmic streaming, which results in the accumulation of cytoplasm at one pole of the embryo (Fig.1.2.1). The embryo is then intrinsically asymmetric, with a cytoplasmic animal pole and a yolk rich vegetal pole. This first embryonic asymmetry determines the first body axis, as the animal pole will be the anterior and the vegetal pole the posterior end of the embryo.

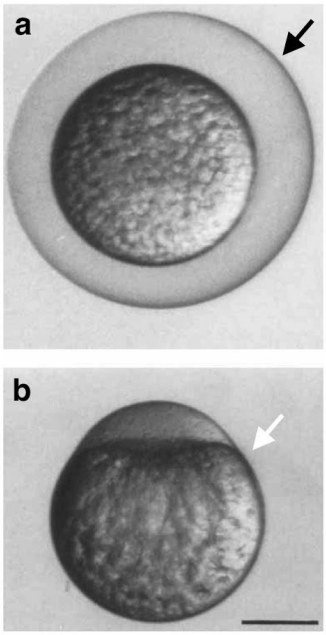

Fig. 1.2.1 Cytoplasmic streaming in the zebrafish embryo
(**a**) Zebrafish oocyte immediately after deposition, with the protective chorion (black arrow). (**b**) One-cell stage zebrafish embryo. Cytoplasmic streams result in the accumulation of cytosol at the animal pole (white arrow), i.e. the first cell and the future anterior end of the embryo. Scale bar, 250 um. Adapted from Kimmel et al., 1995.

The animal-vegetal (or antero-posterior) axis is actually established during the early phases of oocyte maturation, when the Balbiani body is positioned at the future vegetal pole of the oocyte (Fig. 1.2.2). The Balbiani body is a transient aggregate of organelles that forms near the early oocyte nucleus, moves towards the future vegetal pole and is then dissolved[36]. The identification of the *bucky ball* mutant, that does not form a Balbiani body, has clearly shown how this structure is necessary for the establishment of the antero-posterior axis[37]. Not only: the determinants that establish the dorso-ventral body axis are also transported vegetally by the Balbiani body. It has been recently shown that *wnt8a* mRNA is localized in the Balbiani body during oocyte maturation, then vegetally in the zygote and later moved along transient microtubules bundles to the future dorsal side of the embryo[38,39]. Wnt8a is sufficient to induce differentiation of embryonic cells into dorsal types, making it the *bona fide* maternal determinant of dorsal identity in the zebrafish embryo[38]. The fact that both the antero-posterior and dorso-ventral body axes are already set up in the oocyte is emblematic of the importance of maternally inherited factors in the patterning of the early embryo, which we will discuss in the following session.

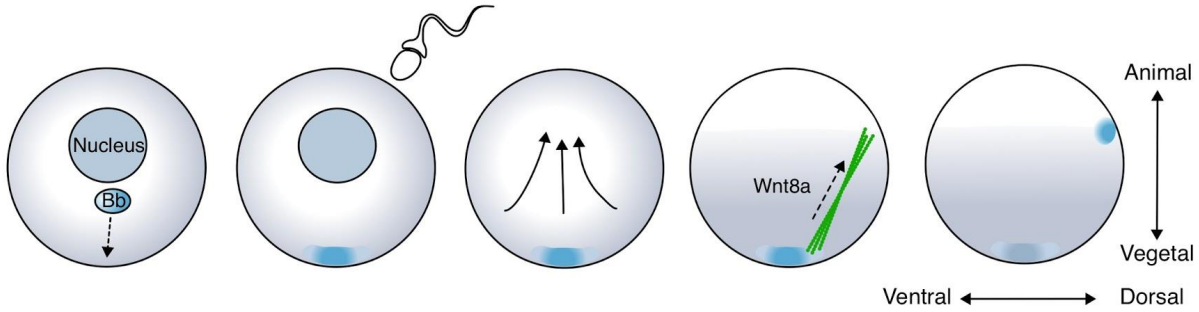

Fig. 1.2.2 Early determinants of axes specification in zebrafish.
During oogenesis, the Balbiani body (Bb) migrates and deposits its content vegetally. After egg deposition and fertilization wnt8a mRNA is transported animally on a transient microtubule bundle, where it acts to determine the future dorsal side of the embryo.

1.2.1 Early embryo morphogenesis

Cytoplasmic streaming and the transport of maternal determinants to the dorsal side continue during the first cell divisions, starting 45 min after fertilization and proceeding synchronously at 15 min intervals. Cytokinesis starts at the animal pole and is incomplete, leaving the blastomeres connected to the yolk by numerous cytoplasmic bridges (meroblastic cleavage). At the 16-cell stage, the central most blastomeres are completely cellularized and, during the following divisions, only the marginal most blastomeres remain connected with the yolk[40] (Fig. 1.2.1.1a).

At the 512-cell stage the zygotic genome starts to be transcribed (mid-blastula transition)[41] and, shortly after, one can recognize three different tissues. The outer cells differentiate into a squamous monolayered epithelium, the enveloping layer (EVL). The cells that are in contact with the yolk collapse into it and form a syncitium, the yolk syncitial layer (YSL)[40]. In between are the deep cells, that will form the embryo proper (Fig. 1.2.1.1b). As cell divisions continue the blastomeres compact and the embryo acquires different shapes that have been used to describe specific stages of development, such as high (3.3 hpf) and sphere (4 hpf). At 4.3 hpf the yolk appears to bulge towards the animal pole, defining the dome stage and being the clearest sign that epiboly is beginning. During epiboly, YSL, deep cells and EVL move vegetally and engulf the yolk. When the embryonic cells have reached the equator (50% epiboly, 5.3 hpf), gastrulation begins. While the ectoderm progenitor cells keep moving towards the vegetal pole of the embryo, mesendoderm progenitor cells separate by synchronized cell ingression at the margin between deep cells and YSL[32,42] (Fig. 1.2.1.1a,c). The ingressed cells then move animally while further differentiating in mesoderm and endoderm[32,42–44]. At this point the dorsal side of the embryo becomes evident, as the ingression of mesendoderm progenitor cells starts earlier and results in a compact structure,

the embryonic shield. The axial mesendoderm progenitor cells that form the shield will collectively migrate in a compact cluster, the prechordal plate[32,42,43]. Starting from 7 hpf, concomitantly with the separation of the three germ layers, the deep cells move towards the dorsal side of the embryo (convergence) and intercalate radially, resulting in an elongation of the antero-posterior axis (extension). At 10 hpf, tailbud stage, the embryonic tissues have engulfed completely the yolk cell and gastrulation is completed. It is followed by the segmentation period, during which the tail is extended away from the yolk while the somites and neuromeres are formed. At 24 hpf embryos have reached the pharyngula stage, characterized by the beginning of organogenesis. Organ morphogenesis and the formation of organ systems continue in the next two days of development, when the larva hatches, the swimming bladder is inflated and the larva starts seeking food and avoid perils[45].

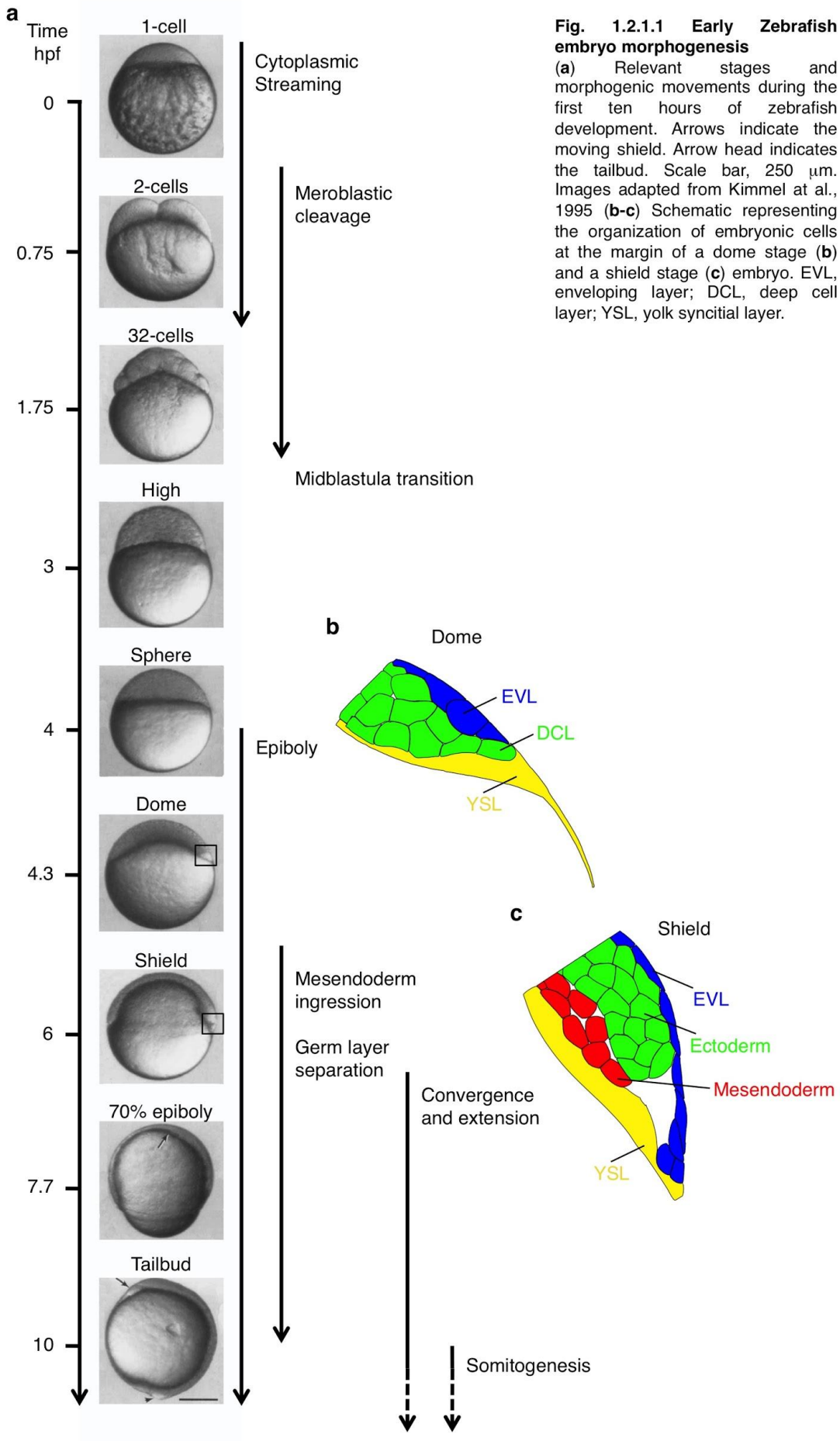

Fig. 1.2.1.1 Early Zebrafish embryo morphogenesis
(**a**) Relevant stages and morphogenic movements during the first ten hours of zebrafish development. Arrows indicate the moving shield. Arrow head indicates the tailbud. Scale bar, 250 μm. Images adapted from Kimmel at al., 1995 (**b-c**) Schematic representing the organization of embryonic cells at the margin of a dome stage (**b**) and a shield stage (**c**) embryo. EVL, enveloping layer; DCL, deep cell layer; YSL, yolk syncitial layer.

1.2.2 Early embryo patterning: fate maps

Similarly to the situation in the xenopus embryo, the prospective dorsal side of the zebrafish embryo is specified by the position of maternal determinants within the zygote. However, differently from xenopus, the plane of early cell divisions are not predictive of the future embryonic axes in the zebrafish embryo: the plane of bilateral symmetry does not correspond to the first cleavage plane and the dorsoventral axis does not align with the second cleavage plane[40,46]. Moreover, extensive cell mixing occurs during the early phases of epiboly so that the progenies of different blastomeres occupy partially overlapping regions at later stages of development[46]. Therefore, the origin of differentiated cells within the zebrafish embryo cannot be traced back to singular early blastomeres. Not cell lineage, but the position of zebrafish progenitor cells within the embryo is predictive of cell fate (Fig. 1.2.2.1). The cells at the outer edge of the embryo, in contact with culture medium, will differentiate into EVL, while the marginal blastomeres that keep cytoplasmic connection with the yolk cell will form the YSL[40]. The position along the animal-vegetal axis at 50% epiboly determines the likelihood of deep cells becoming endoderm, mesoderm or ectoderm. Endoderm progenitor cells are closest to the margin with the YSL, mesoderm progenitor cells occupy the first 6 tiers from the margin and ectoderm progenitor cells are located in animal regions[47]. Moreover, the position of deep cells along the dorsoventral axis predicts the tissue or organ they will form[47], as well as their position along the antero-posterior axis. Due to the movements of convergence and extension taking place during gastrulation, cells located dorsally will give rise to anterior structures while cells located ventrally will form posterior structures.

Interestingly, cell fate specification is a relatively long process in zebrafish development, as deep cells are not irreversibly committed to their fate until 50% epiboly[48]. Before this stage, a mesendoderm progenitor cell transplanted to an ectopic animal region of the embryo acquires the fate typical of that region and integrates in the specified tissue. This potential is gradually lost after gastrulation starts and cells are terminally committed by mid-gastrulation stages[49].

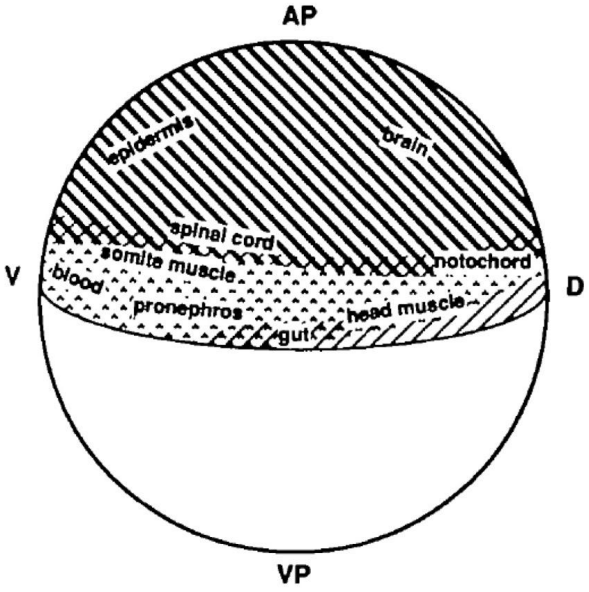

Fig. 1.2.2.1 Zebrafish embryo fate map
Fate map of the zebrafish embryo at 5 hpf. The domain of presumptive ectoderm, mesoderm and endoderm progenitor cells were drawn by labelling single blastomeres at 3 hpf and following their progeny until 24 hpf, when the primary organs are formed. Thick lines depict ectoderm domain, dots the mesoderm domain and thin lines the endoderm domain. AP, animal pole; VP, vegetal pole; D, dorsal; V, ventral.
Kimmel et al.,1990.

1.2.3 Early embryo patterning: molecular mechanisms

The first lineages to be specified in the zebrafish embryos are the YSL and EVL. The YSL plays important roles in the patterning and morphogenesis of the deep cells, however the mechanisms that lead to YSL differentiation have not been elucidated yet[40,50]. EVL differentiation depends on the expression of *inhibitor of NFkB kinase 1* (*ikk1*) and of the transcription factor *interferon regulatory factor 6* (*ifr6*)[51,52]. Messenger RNAs for both factors are maternally provided and ubiquitously expressed, necessary but not sufficient for EVL specification. Interestingly, EVL differentiation depends on cell-cell contact[53] and can be induced in aggregates formed either by ectoderm, mesoderm or endoderm progenitor cells[54], suggesting that the asymmetry between cell to cell and cell to medium interfaces may represent the signal for EVL specification.

The molecular processes leading to deep cells patterning start already during oogenesis, when maternal determinants are deposited asymmetrically within the egg. *Wnt8a* mRNA is localized in the Balbiani body during oocyte maturation and translocated to the future dorsal side of the embryo during early cleavage stages [38,39]. Wnt8 activates canonical Wnt pathway and causes nuclear localization of β-catenin in a subset of dorsal blastomeres, which form the zebrafish Nieuwkoop center[55]. At the 512-cell stage the zygotic genome starts to be transcribed and expression of β-catenin target genes is initiated in the dorsal blastomeres. At the same time other Wnt genes as well as *ventral homeobox/ventral expressed homeobox* (*vox/vent*) and *bmp2b* and *bmp7* are expressed in the rest of the embryo. β-catenin targets include *dharma*, *dikkopf 1* (*dkk1*)[56] and *nodal related 1 (ndr1*, also

known as *squint*)[57]. Dharma is a transcription factor that represses *vox/vent* which, in turn, repress expression of *chordin*[58]. Chordin is an inhibitor of BMP signaling, while Dkk1 is an inhibitor of Wnt signaling[56,59]. As a consequence, BMP and Wnt activity gradients are formed, with high activity at the ventral side and low activity at the dorsal side. Concomitantly, Ndr1 activates nodal signaling, inducing expression of itself and *ndr2* (or *Cyclops*) and creating a nodal activity gradient with higher activity at the dorsal side and lower at the ventral side of the embryo[57,60,61]. After YSL formation, expression of *ndr1* and *ndr2* is detected in the YSL and in the blastomeres immediately adjacent to it[62,63]. Consequently, the shape of nodal graded activity changes considerably, so that nodal activity is detected along the whole margin of the embryo. Nodal signalling also initiates expression of the FGF ligands fgf8 and fgf3, so that a gradient of FGF signalling forms, expanding slightly further than the nodal activity area[64]. Moreover, marginal cells express *aldheyde dehydrogenase 1a2* (*aldh1a2*), which catalyses the synthesis of retinoic acid (RA), while expression of *cytochrome P450 26a1* (*cyp26a1*), which degrades RA, is detected at the dorsal and vegetal margin areas and in the animal pole of the embryo[65–67]. This creates a source-sink system by which a gradient of RA is formed as well[68].

By sphere stage (4hpf), the graded activities of Wnt, BMP, Nodal, FGF and RA create a map: the position of blastomeres within the embryo determines the amount and type of signals they will receive and this combinatorial information is thought to specify the different cell types of the early embryo[69]. High levels of nodal signaling are sufficient to induce endoderm and dorsal mesoderm, while decreasing levels of nodal specify progressively posterior/ventral mesodermal cell fates[70–73]. However, the concerted action of nodal and FGF signals is required for maintenance of mesoderm during late gastrulation[64], while the interaction between nodal, BMP and FGF signaling is thought to regulate the number of differentiating endoderm cells[74]. Moreover, FGF inhibition causes the loss of trunk and posterior mesodermal structure, while the expression of posterior markers in both mesoderm and ectoderm is increased upon over-expression of FGF ligands[75]. BMP and RA are implicated in the antero-posterior patterning of the brain, as inhibition of BMP or RA signalling causes the loss of posterior structures while their upregulation results in the loss of anterior domains[66,67,76,77]. Therefore, cell fate specification and cell differentiation in the zebrafish early embryo depend on the formation of multiple morphogen gradients, whose combined signalling activities determine the fate of cells in different domains of the embryo (Fig. 1.2.3). However, the graded activity of morphogens has been inferred mainly by assessing the expression levels of target genes. That morphogen ligands can form diffusion gradients has been shown for FGF and Nodal, using overexpression of fluorescently tagged ligands[21,78]. Nonetheless, the shape and temporal establishment of the endogenous morphogen gradients have been described only for RA during gastrulation. The use of a

genetically encoded probe allowed to visualize endogenous RA and to show that a RA gradient progressively forms from 50% epiboly to 3-4 somite stages, as predicted by the expression domains of *aldh1a2* and *cyp26a1*[68]. Therefore, how the graded activity of BMP, FGF, Wnt and Nodal relates to expression levels and spatio-temporal distribution of ligands remains unclear.

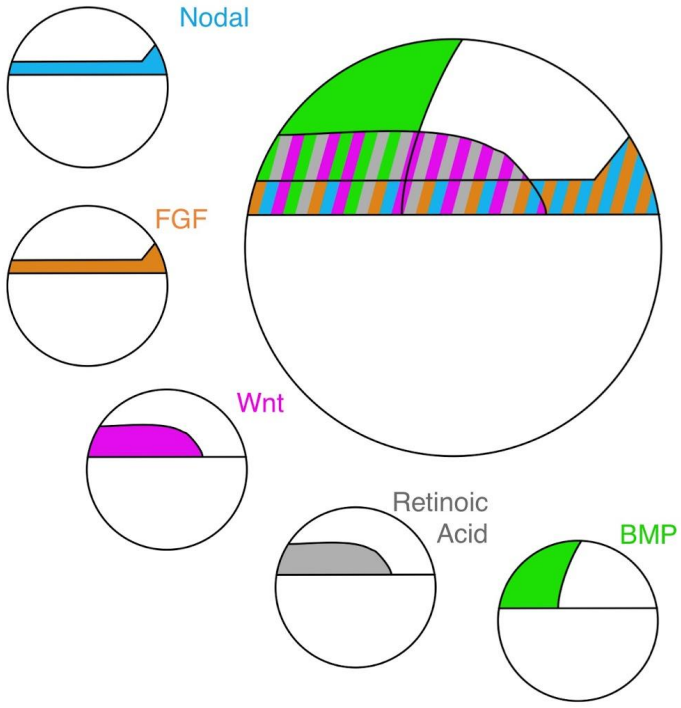

Fig 1.2.3 Morphogen gradients in the zebrafish blastula
Map of the expression domains of the main morphogens involved in cell fate specification in the zebrafish embryo at 4 hpf. Morphogen activity domains are depicted according to Schier and Talbot, 2005.

1.2.4 Nodal signaling and mesendoderm specification in the zebrafish embryo

Nodals belong to the TGFβ family of extracellular ligands. Nodal homologs have been identified in a wide range of both vertebrate and invertebrate species, where they have been implicated in early embryonic patterning and establishment of left-right asymmetry. However, their role in early development seems to have transitioned: nodal ligands are expressed solely in ectoderm in invertebrate species while they are necessary and sufficient to induce mesendoderm cell fates in vertebrates. Three nodal ligands have been identified in zebrafish, *ndr1* (*squint*), *ndr2* (*cyclops*)[60] and *ndr3* (*southpaw*)[79]. While ndr1 and ndr2 are necessary for early specification of mesendodermal cell types, ndr3 is required for the establishment of left-right asymmetries during late gastrulation stages[62,79]. Nodal ligands are produced as pro-proteins that need to be secreted and cleaved by Furin proteases to become active[80,81]. Once active they can signal through serine/threonine kinase receptor

complexes comprising two type I receptors (activin receptor-like 1ba, Acvr1ba), two type II receptors (Acvr2a/b), and the co-receptor one eyed pinhead (Oep)[82,83]. Ligand binding causes receptor heterodimerisation, which is followed by mutual phosphorylation.

Following receptor phosphorylation, the complex of ligand, receptors and co-receptor is internalized by endocytosis[84]. Once endocytosed, the complex is bound by the scaffold protein Smad Anchor for Receptor Activation (SARA), that facilitates the interaction between the receptors and their effector molecule, Smad2[85,86]. Smad2 is a transcription factor that shuffles between nucleus and cytoplasm via kinesin mediated transport over microtubules[87]. Once phosphorylated by active nodal receptors, Smad2 binds Smad4 and complexes formed by Smad2/Smad4 and Forkhead Box H1/3 (FoxH1/3) bind to activin responsive elements (ARE) in the genome, activating transcription of target genes[88] (see Fig. 1.2.4 for a schematic representation of Nodal signaling). While unphosphorylated Smad2 and Smad4 shuttle between cytoplasm and nucleus, complexes of phosphorylated Smad2 with Smad4 are thought to be retained in the nucleus, so that activation of nodal signaling results in nuclear accumulation of Smad2/Smad4[89]. The degree of Smad2 nuclear accumulation correlates with the concentration of nodal ligands a cell is exposed to, so that Smad2 nuclear to cytoplasmic ratios can be used to infer the level of nodal signaling within a cell[90]. The level of nodal signaling, in turn, determines the set of genes that are activated in a particular cell. High levels of nodal signalling are required for the expression of the target genes *goosecoid* (*gsc*) and *casanova* (*cas*)[61,71,72], marker genes for dorsal axial mesendoderm[91] and endoderm[92,93], respectively. Progressively lower levels are sufficient to trigger expression of *floating-head* (*flh*), a notochord marker gene[94], and *notail* (*ntl*), a pan-mesodermal marker gene[91,94].

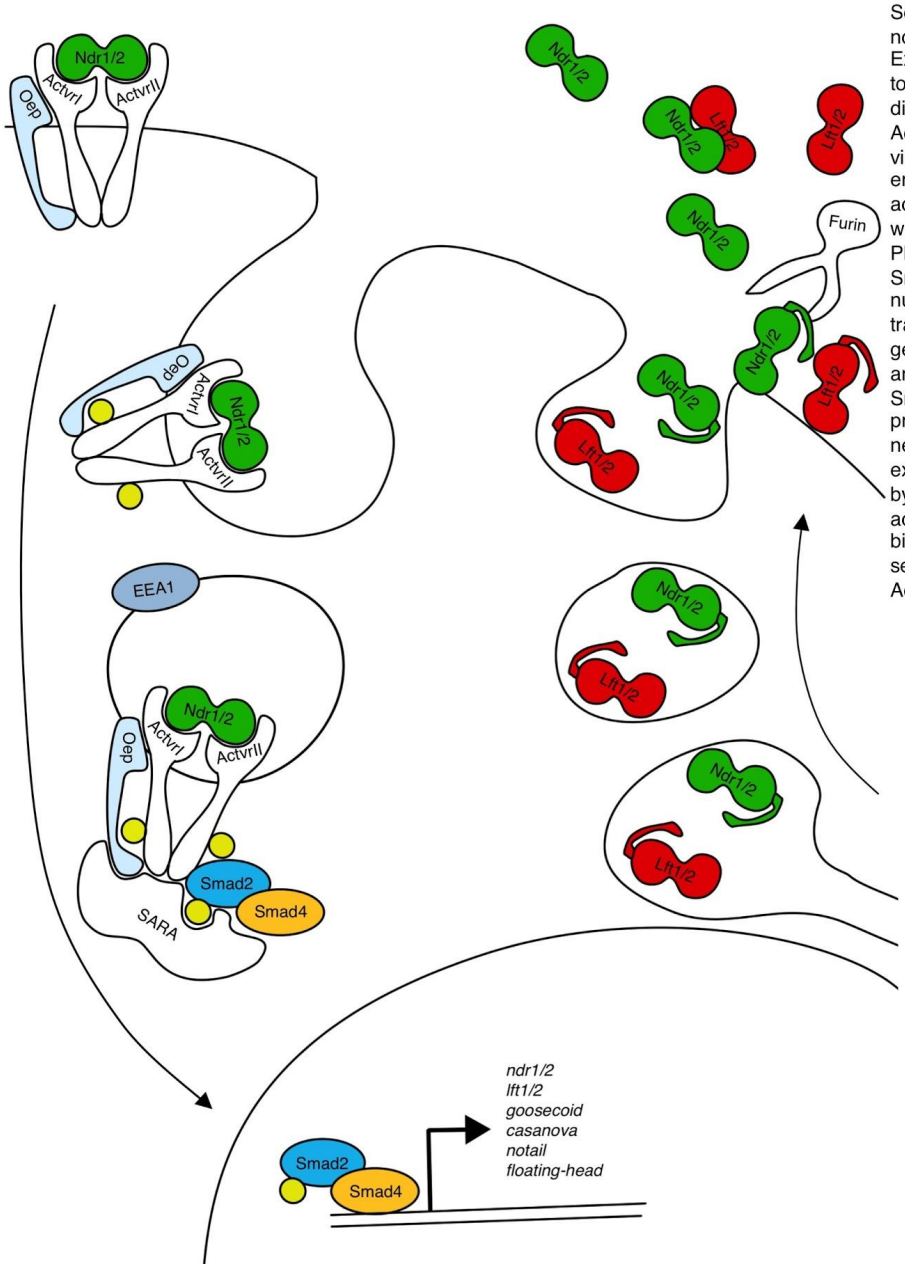

Fig. 1.2.4 Nodal signaling
Schematic representation of nodal signaling pathway. Extracellular nodal ligands bind to Actvrl and Actvrll causing their dimerization and activation. Active receptors are internalized via endocytosis. While in early endosomes, Smad2 binds to active Actvrl/ll/Oep complexes, which promotes phosphorilation. Phosphorilated Smad2 binds to Smad4 and translocates in the nucleus where it activates transcription of multiple target genes. Nodal ligands (Ndr1/2 and Lft1/2) are among Smad2/ Smad4 targets. They are produced a pro-proteins, which need to be secreted in the extracellular space and cleaved by Furin proteases to become active. Once active, Ndr1/2 can bind to Actvrl/ll, while Lft1/2 can sequester Ndr1/2 and/or bind to Actvrl/ll.

Among the direct target genes of nodal signaling in the zebrafish are *ndr1*, *ndr2* and other two members of the family of nodal related ligands, *lefty 1* and *lefty 2* (*lft1/2*)[60,61,95]. Lft1/2 are secreted inhibitors of nodal signaling that act by both sequestering Ndr1/2 in the intra-cellular space and preventing Oep from participating in receptor complexes[96]. It has been proposed that the expression of both Ndr1/2 and Lft1/2 by the marginal most blastomeres of the zebrafish embryo ensures graded nodal activity along the animal-vegetal axis. Over-expression studies of tagged versions of Ndr1/2 and lft1/2 show that Ndr1/2 present lower diffusivity than Lefty1/2 so that nodal activity is ensured at short distances from the source and inhibited further away[78]. In this view, nodal behaves according to the model of reaction-diffusion first postulated by Turing, where the interaction between a short range activator and

a long range inhibitor creates patterns of target genes expression. This view is supported by the evidence that Ndr1 can activate target genes at a distance[72] and the signalling activity of Ndr1/2 can be inhibited by Lft1/2 in a dose dependent manner[73]. However, Ndr2 can diffuse and induce target genes expression only at a very short distance from the source[72,78], even though Ndr2 is necessary for the maintenance of axial mesendoderm marker genes, such as *gcs*[97,98], and it is thought to contribute to the graded nodal activity along the antero-posterior axis. Recently an alternative model has been proposed in which not diffusivity but temporal control of *ndr1/2* and *lft1/2* expression allows the determination of domains with different nodal activity. Van Boxtel et al., show that Ndr1/2 expressed by the YSL induces Ndr1/2 expression in the adjacent blastomeres, that, in turn, signal to the blastomeres closest to them. *Lft1/2* are also direct target of nodal signaling and so transcribed in the signal receiving cells at similar rates as Ndr1/2; however their translation is delayed due to the action of the microRNA mir-403. This results in Lft1/2 proteins reaching levels necessary to block Ndr1/2 mediated signaling only at 50% epiboly stages, three hours after the onset of nodal signaling. Within this time window, the cells that were closer to the YSL had been exposed to nodal signal for longer time than the ones situated further away: the duration of signalling determines nodal graded activity along the animal-vegetal axis and not diffusion of nodal ligands[63]. Similarly, it has been shown that the duration of nodal signalling may account for the specification of different mesendodermal cell types along the antero-posterior axis[23]. The notion that the duration and not only the maximum level of signalling plays a role in mesendodermal fate specification relies on cells being able to integrate signalling events over long periods of time. The fact that Smad2 nuclear accumulation persists long after nodal signalling has ceased suggests that such a mechanism might be in place[63]. The persistence of active signaling complexes within early endosomes has been proposed to enable the integration of nodal signalling over time and regulation of ligand and receptor recycling has been shown to affect target gene expression[84,99,100]. These findings have led to the formulation of the cumulative dose hypothesis: mesendodermal cell fate specification depends on both the level and the duration of nodal signalling. Recently, we have used a light activatable form of the nodal receptor to study the effect of controlled level and duration of nodal signalling on zebrafish gene expression[98]. We found that gene expression varied according to the developmental stage at which nodal signalling was activated, suggesting that not only the level and duration of signalling but also the intracellular state of receiving cells determines mesendodermal cell fate specification.

1.3 Cell-cell adhesion as a driver of morphogenesis

Morphogenic movements of tissues depend on the mechanical coupling of the cells they are composed of so that cell-cell adhesion is one of the major drivers of morphogenesis. Absence or mis-regulation of cell-cell adhesion molecules result in gross morphological defects in virtually all organisms described so far. The mechanisms by which cell-cell adhesion is ensured and controlled in early embryos have been the focus of intense study in the past decades. We will here limit our attention to cadherin mediated cell-cell adhesion and how its regulation is thought to influence morphogenic movements.

1.3.1 Cadherin mediated cell-cell adhesion: the cadherin superfamily

The family of cadherin proteins is an extended one and comprises classical, desmosomal, proto- and receptor cadherins[101,102]. Their functionality depends on calcium and they are composed of an N- terminal extracellular domain, a one pass transmembrane domain and a C-terminal intracellular domain[102,103]. The extracellular domain is composed of a variable number of EC repeats, a conserved motif typical of cadherins. Each cadherin subfamily presents a characteristic number of EC repeats, with classical and desmosomal cadherins having 5, protocadherins 6 to 34 and receptor cadherins 7[101]. The other subfamily defining feature of cadherin resides in their intracellular domain, or cytoplasmic tail. While receptor cadherins have a very short cytoplasmic tail, classical, desmosomal and proto-cadherins present an extended intracellular domain[101,104]. A certain level of conservation has been observed in the intracellular domains of protochaderins, even though their intracellular binding partners remain largely uncharacterized[104,105]. However, increasing evidence points to protocadherins being involved in signalling controlling cell-cell adhesion, more than mechanically mediating cell-cell contact[105,106]. The cytoplasmic tail of desmosomal and classical cadherins, instead, mediates the binding to elements of the cell cytoskeleton. Desmosomal cadherins have a variable cytoplasmic tail and bind to intermediate filaments, mediating the formation of stable junctional complexes found at the basal side of epithelia, the desmosomes[101]. Desmosomal cadherins are therefore essential to functional epithelia: in the zebrafish they are necessary for epiboly as they ensure EVL integrity[107]. However, desmosomes have not been observed within cell-cell contacts formed by deep cells[32]. The morphogenetic defects due to knock-out of desmosomal cadherin are likely to be secondary to loss of the osmoregulative functions of EVL.

Classical cadherins present a highly conserved cytoplasmic tail that binds to the actomyosin cortex through various linker proteins including β-catenin, p120-catenin and α-catenin[102,108]. Therefore, classical cadherins act as molecular bridges connecting the cortices of contacting

cells. Interestingly, classical cadherins mediate adhesion between cells that express the same cadherin type and tissue specific cadherins have been identified that are expressed predominantly in epithelia (E-cadherin), nervous system (N-cadherin), vasculature (VE-cadherin), retina (R-cadherin) and placenta (P-cadherin).

E-cadherin (Cdh1) is expressed in all cells of the zebrafish early embryo and is indispensable for zebrafish development[109–111]. Moreover, N-cadherin (Cdh2) is expressed in the YSL and mesendoderm progenitor cells show expression of N-cadherin from 60% epiboly stages[112]. Mutants for *n-cadherin* show convergence and extension defects[112,113], pointing at a prominent role for E- and N-cadherin in mediating cell-cell adhesion of embryonic deep cells during zebrafish gastrulation.

1.3.2 Cadherin mediated cell-cell adhesion: E-cadherin

The molecular mechanisms at the basis of classical cadherin function have been shown to be remarkably conserved, although having been studied most extensively for E-cadherin.

E-cadherin molecules exposed on the same cell surface form homodimers, via *cis* interactions between parallel molecules, and subsequently bind cognate homodimers on the surface of adjacent cells, via *trans* interactions between antiparallel molecules[114–117]. Both *cis* and *trans* interactions are mediated by the N-terminal EC repeat (EC1) and require calcium[115,117]. However calcium ions are not directly involved in the interactions between cadherin molecules, as they do not bind anywhere near the intermolecular binding regions of EC1[114,115,118]. Calcium ions are, instead, found in pockets between two consecutive EC domains and are necessary for the structural integrity of cadherins[114,115,118]. In the absence of calcium the cadherin extracellular domain folds on itself, making the EC1 unavailable for binding. In the presence of calcium, the 5 EC repeats are aligned to each other and the extracellular domain takes up a rod-like structure that allows *cis* and *trans* interactions[119]. The EC1 repeat is also responsible for the homophilic binding of classical cadherins, i.e. the preference for binding to cadherins of the same type[118,120,121]. Even though the extracellular domain of classical cadherins mediates homophilic molecular binding, effective cell-cell adhesion requires the cytoplasmic tail[122,123]. The mechanical coupling between classical cadherins and the actomyosin cortex is, in fact, mediated by catenins binding to cadherin intracellular domain. E-cadherin dependent cell-cell adhesion is primarily mediated by β-catenin, that can be replaced by γ-catenin (or plakoglobin) in certain cases. β-catenin binds directly to E-cadherin and E-cadherin/β-catenin complexes are formed already in the endoplasmic reticulum[124–126]. Once reached the membrane, β-catenin binds α-catenin, an actin binding protein necessary for cadherin mediated cell-cell adhesion[124–128] (Fig. 1.3.2.1).

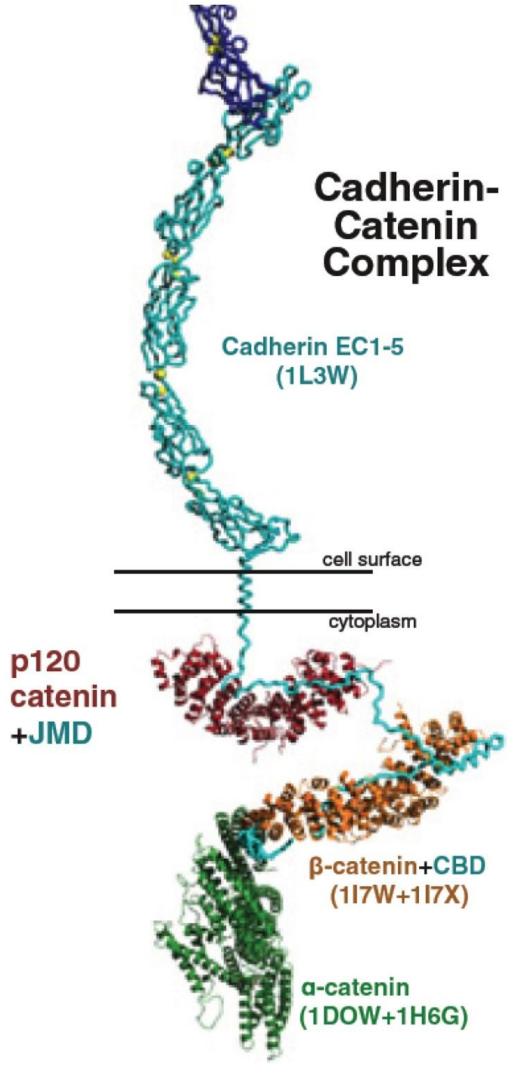

Fig. 1.3.2.1 The E-cadherin adhesion complex
Model of cadherin-catenin complex based on the protein structure of its components. E-cadherin (light blue) presents an extracellular domain composed of 5 EC repeats (EC1-5) that interact with Ca++ (yellow). EC-1 mediates trans-interactions with E-cadherin molecules exposed on the surface of adjacent cells (dark blue). The cytoplasmic tail of E-cadherin binds to p120 catenin (red) via the juxtamembrane domain (JMD) and to β-catenin (orange) via the catenin binding domain (CBD). β-catenin binds to α-catenin (green), which, under tension, can bind to actin. Ishiyama et al., 2010.

When under minimal tension, E-cadherin/β-catenin/α-catenin complexes can bind to actin, providing a mechanical link between cell surface and cell cortex[129]. Therefore, E-cadherin based junctions couple the cortices of contacting cells, allowing the transmission of forces across cell boundaries and creating a continuous contractile network within tissues. Interestingly, actomyosin contractility is regulated by cadherin adhesion complexes, primarily via p120 catenin. The latter binds to the cytoplasmic tail of E-cadherin[130,131], so that it is localized predominantly at cell-cell contact sites[132], while it can regulate the activity of the small GTPases RhoA, Rac1 and Cdc42[133–136]. Moreover, cell-cell contact formation causes extensive reorganization of the actomyosin cortex in contacting cells. This effect is most obvious when observing two cells in contact, forming a cell doublet: in this case the actomyosin cortex is delocalized at the cell to cell interface and enriched at the cell to medium interfaces, so that it forms a sort of cage encompassing and connecting the two cells[137–139]. On the other hand, actomyosin contractility is necessary for cell-cell contact formation, so that cells with lowered contractility due to inhibition of myosin activity fail to

expand cell-cell contacts[137–139]. At the molecular level, interaction with the actomyosin cytoskeleton influences clustering of E-cadherin/catenins complexes on the membrane as well as the immobilization of E-cadherin molecules at cell-cell contact sites, possibly influencing the likelihood of cell-cell contact formation, expansion and persistence[139,140141,142]. Given this mutual influence of cell-cell contact and actomyosin contractility, cell-cell contact sites are not only passive bonds allowing the transmission of forces but behave as reactive links, allowing cells to adjust and possibly respond to mechanical stimuli[143,144]. It follows that regulation of cell-cell adhesion and actomyosin contractility are intimately linked and play important roles in morphogenesis.

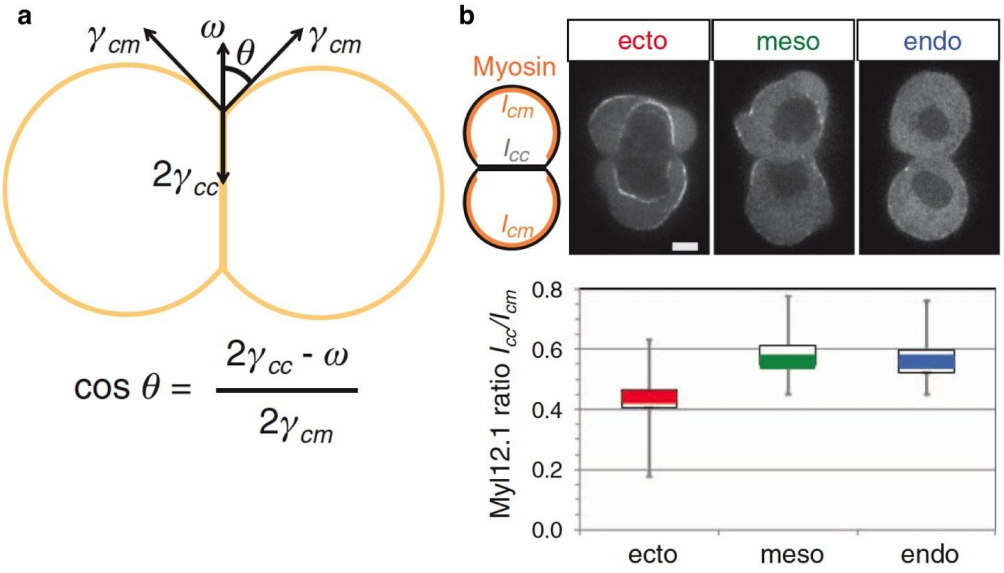

Fig. 1.3.2.2 Actomyosin contractility, surface tensions and contact shape in zebrafish progenitor cell doublets.
(**a**) Surface tensions controlling cell doublet shape at steady state. The contact angle θ results from the balance between the adhesion tension ω and the cortex tensions at the cell-medium γcm and cell-cell interfaces γcc (**b**) Delocalization of actomyosin cortex at cell-cell interface controls cell-cell contact size. Sketch of myosin (Myl12.1-eGFP) localization in homotypic doublets of pTol2-b-actin::myl12.1-eGFP transgenic zebrafish. Measured mean fluorescence intensity at the cell-cell interface (Icc) is normalized to the mean intensities at the cell-medium interfaces (Icm) of both cells for ectoderm, mesoderm and endoderm doublets. Scale bar, 5 µm. Maître et al., 2012.

1.3.2 Regulation of cell-cell adhesion and morphogenesis

Cadherins, being the glue that keeps together embryonic cells, are required for morphogenesis in both vertebrate and invertebrate embryos[109–111,113,145–148]. However, morphogenic processes most often require positional rearrangement or shape changes of cells within a tissue, so that embryonic cells not only need to adhere to each other but also to regulate the extent in which they do so for morphogenesis to take place. Regulation of cell-cell adhesion can result from changes in the types and levels of cadherins exposed on the cell surface [120,149,150] and/or to variation in cortical contractility of cells [138,143,151]. Lowered levels of E-cadherin at the cell surface, due to transcriptional inactivation or endocytosis, and concomitant increase of N-cadherin have been implicated in the ingression of mesoderm progenitor cells in mouse, chick, drosophila and sea urchin embryos[152–156]. Lowered E-

cadherin would reduce cell-cell adhesion and allow mesoderm progenitors to delaminate from the epithelium they originate from. However, neither E-cadherin overexpression nor N-cadherin knock-out affect ingression of mesoderm cells in the drosophila[157], and mesoderm cells can detach from the neighbouring ectoderm cells only after a decrease in myosin activity[157,158]. This suggests that a balance between cadherin surface levels and cell contractility determines lowered cell-cell adhesion.

On the other hand, impaired E-cadherin expression or increased E-cadherin endocytosis affect collective migration of mesoderm progenitor cells in the zebrafish embryo[43,159,160]. Even though mesoderm cells are less adhesive than ectoderm cells, they need to adhere homotypically to migrate effectively and directionally. Similarly, interfering with cell-cell adhesion affects convergence and extension movements in both zebrafish and xenopus embryos[109–111,161]. Given that cells need to intercalate radially for convergence and extension to take place, both inhibiting and increasing cell-cell adhesion disturb this process; in the first case intercalating cells cannot apply the necessary traction forces on their neighbours, while, in the second, they fail to disrupt cell-cell contacts, necessary to slide through neighbours and contact new ones.

Finally, cortex contractility controls cell-cell contact size, ultimately determining compaction of tissues, in zebrafish and mouse embryos[138,162,163]. Cortical contractility of zebrafish progenitor cells in culture regulates cell-cell contact size and tissue surface tension (TST) of cell aggregates. Ectoderm progenitor cells are more contractile than mesoderm progenitor cells: therefore, ectoderm progenitor cells form larger cell-cell contacts and present higher TST than mesoderm progenitor cells[138,150,162,164]. Ultimately, this causes zebrafish progenitor cells to sort *in vitro*: clusters initially formed of intermixed ectoderm and mesoderm cells unmix and reach a final configuration in which mesoderm cells surround ectoderm[150,162,164]. However, it is unclear if and how regulation of cell-cell contact size and cortex contractility are involved in unmixing of mesoderm from ectoderm progenitor cells and ingression of mesoderm during zebrafish gastrulation[150]. On the other hand, a direct role for actomyosin contractility in tissue compaction *in vivo* has been shown in the early mouse embryo[163]. During the 8-cell stage, mouse embryonic cells enlarge their cell-cell contacts, thereby reducing the embryo surface area. While E-cadherin is necessary to allow cell-cell adhesion, the enlargement of cell-cell contacts is driven by a cell autonomous increase in actomyosin contractility[145,163].

Therefore, multiple and diverse processes, such as cadherin expression, localization, turnover, as well as variations in actomyosin contractility, contribute to the control of cell-cell contact size, strength and persistence, which is necessary for successful morphogenesis.

Review: Cell adhesion in embryo morphogenesis

1.4 Cell differentiation controls cell-cell adhesion

The differentiation of embryonic cells entails the regulation of cell-cell adhesion and cell contractility, that ultimately allows cells of different types to sort and organize into tissues and organs. The signaling pathways that induce differentiation by upregulating the expression of cell-type specific transcription factors have been also implicated in the control of cell-cell adhesion. The FGF signaling pathway, responsible for mesoderm differentiation, activates Snail expression that, in turn, suppresses E-cadherin expression[152,156]. Snail is also thought to affect E-cadherin turnover at junctions, so that FGF signaling indirectly causes decreased cell-cell adhesion in mesoderm progenitor cells compared to ectoderm progenitor cells[154,157]. Similarly, BMP signaling has been implicated in reducing cell-cell adhesion of mesendoderm progenitor cells in the zebrafish embryo, so that the graded activity of BMP not only patterns the embryo cell fates but also cell-cell adhesion properties[165]. Finally, Nodal signaling regulates cadherin activity and actomyosin contractility in zebrafish, xenopus and mouse embryos. Xenopus embryonic cells exposed to Nodal signaling show higher rates of endocytosis and lower C-cadherin activity, resulting in reduced cell-cell adhesion[106,166,167]. Interestingly, zebrafish mesendoderm progenitor cells, exposed to Nodal, show higher E-cadherin expression levels but lower actomyosin contractility and, ultimately, lower cell-cell adhesion compared to ectoderm progenitor cells[32,109,138,162]. The molecular mechanism underlying the Nodal dependent reduction in actomyosin contractility in mesendoderm cells are not known, however Nodal signaling also controls migration of endoderm progenitor cells during late gastrulation[168]. Nodal activates the expression of *prex1*, a Rac Guanosine Exchange Factor (Rac-GEF) that induces Rac activity and directional migration in zebrafish endoderm progenitor cells[168]. It is currently unknown if and how Nodal signaling controls the activity of small GTPases during mesendoderm cell fate specification, which would help clarify how Nodal regulates cell-cell adhesion during early stages of zebrafish gastrulation.

The notion that the same signaling pathways involved in cell fate specification act in parallel to regulate adhesion and contractility has led to the view that morphogenesis is a result of cell differentiation. However, the response of differentiating cells to inducing signals depends on mechanical cues such as substrate stiffness and the extent of cell-cell adhesion[169–173]. This leads to the hypothesis that differentiation and morphogenesis may not be independent processes unfolding in parallel but, instead, parts of a reciprocal feedback mechanism resulting in embryogenesis[174].

1.5 Cell adhesion controls cell differentiation

Evidence for cell-cell adhesion influencing cell fate dates back to the 90's when Larue and colleagues showed that mouse embryonic stem cells in culture would differentiate only in epithelial cell types when over-expressing E-cadherin and only in mesenchymal and neuroepithelial cell types when over-expressing N-cadherin[175]. Since then, it has been shown that the pattern of cell-cell adhesion and the shape of cell aggregates affect stem cell differentiation in culture[169,170,176,177], pointing at cell-cell adhesion as a regulator of cell fate specification. In fact, cadherins can interact with components of several signaling pathways, influencing signal transduction within a cell. On the other hand, cell-cell adhesion determines the position of cells within a tissue, influencing the types and amount of signals received. Therefore, cell-cell adhesion regulates cell signaling at a molecular and cellular scale.

1.5.2 Classical cadherins and signaling

Cadherins may regulate cell signaling by binding to components of a signaling pathway and sequester them to the cell membrane. This is the case for β-catenin, which is both a core component of the cadherin adhesion complex and the main effector of canonical Wnt signaling[178]. Wnt signaling functions by increasing cytoplasmic levels of β-catenin that subsequently translocates in the nucleus and activates transcription of target genes[179]. E-cadherin adhesion complexes sequester β-catenin to the membrane, thought to counteract Wnt signaling[152,157,178]. Similarly, E-cadherin heterodimerizes with Epidermal Growth Factor Receptor (EGFR) and prevents its endocytosis, necessary for effective EGF signaling[180–183]. Alternatively, cadherins can participate in the formation of complexes with several components of a signaling pathway, which can either facilitate or repress signaling. For instance, the formation of multimeric complexes including N-cadherin, N-CAM and FGF receptors enhances FGF signaling in metastatic cancer cell lines[184,185]. Similarly, VE-cadherin, expressed by endothelial cells, binds to TGFβ receptor I and II, promoting their clustering and internalization, which increases signaling[186]. Repression of signaling, instead, has been described in the case of VE-cadherin binding to both VEGF Receptor (VEGFR) and a phosphatase specific for VEGFR, DEP-1, which represses VEGF signaling[187]. Likewise, Wnt signaling can be dampened by interaction of N-cadherin with LRP5/6 and axin, core components of the Wnt signaling pathway[188].

Molecular interactions between cadherins and components of signaling pathways as diverse as EGF, FGF, TGF-β and Wnt, point to a general, although context specific, role of cadherins in regulating intracellular signaling.

1.5.2 Cell-cell contact and cell fate specification

Besides regulating cell signaling at a molecular level, cell-cell adhesion induces cell polarity and compartmentalization that can affect signaling events[189,190]. How this reflects on differentiation is most evident in the case of asymmetric cell divisions, after which each of two daughter cells acquire a distinct fate. The asymmetry may be established before cell division by the mother cell being polarized due to cell-cell contact to a specific neighbour. If the plane of cell division is parallel to the cell-cell contact, the two daughter cells will inherit membrane and cytoplasmic domains that differ in their molecular composition, possibly affecting cell fates.

In the ascidian embryo, for instance, a single blastomere (cell A6.2/6.4) divides asymmetrically to give rise to one neural and one notochord precursor. The asymmetry is established by the mother cell contacting an animal blastomere that expresses the ephrin ligand A3, eliciting asymmetric Ephrin signaling[17]. This is necessary and sufficient for the mother cell to give rise to one notochord and one neural precursor cell, even if isolated from the rest of embryo[17]. Ephrin ligands and their receptors are membrane bound, so that Ephrin signaling requires cell-cell adhesion. However, also signaling triggered by soluble ligands of the TGF-β family may become asymmetric following cell-cell adhesion. In the drosophila testis, adhesion between germline stem cells and somatic stromal cells causes accumulation of the BMP ligand Decapentaplegic (Dpp) at cell-cell contacts[191]. This is necessary to mediate effective Dpp signaling and prevents germline stem cells from differentiating[191]. In both these cases the presence or absence of contact between specific pairs of cells determines cell fate, suggesting that the effect of cell-cell adhesion is all or nothing, binary so to speak. However, there is at least one example in which the extent of cell-cell adhesion may be important for correct differentiation: in the ascidian embryo, induction of anterior neural precursors at the 32-cell stage takes place only when the contact area between the inducing cell, expressing FGF ligands, and the receiving cells exceeds a certain threshold, suggesting that regulation of cell-cell adhesion may play a role in cell differentiation[16].

More generally, cell-cell adhesion between embryonic cells determines their relative positions within the embryo. Therefore, changes in the size, strength or persistence of cell-cell contacts may affect cell differentiation due to inductive events by (i) changing the relative positions of inducing and receiving cells or (ii) altering the time of exposure to inducing signals[192]. While it is plausible that cell-cell adhesion may influence cell fate just by imparting positional information on embryonic cells, experimental evidence for such an effect is arduous to produce. In fact, when tinkering with the adhesive properties of embryonic cells, it is difficult to distinguish between the cell autonomous effects of, for instance, a loss of cell-cell contacts and the non autonomous effects due to positional variations within the embryo.

Finally, cell-cell adhesion may influence differentiation by determining the shape of tissues and, therefore the shape of morphogen gradients[192]. That the shape of a tissue can determine cell differentiation by modifying morphogen concentration has been shown by Shyer et al[193]. During intestine organogenesis, the intestinal epithelium expresses Sonic hedgehog (Shh) that is received by the underlying mesenchyme. When the endothelium buckles to form the characteristic villi, the mesenchyme cells at the tip of the villi receive higher concentrations of Shh, due to the geometry of the tissue. This, in turn, induces the tip mesenchymal cells to express signals that induce differentiation of the epithelial cells, restricting the pool of undifferentiated intestinal stem cells to the bottom part of the villi[193]. While this study provides the proof of principle that tissue shape can determine morphogen gradient shape and so differentiation, if and how such mechanisms are at play during early stages of embryonic development and their dependence on cell-cell adhesion remain unclear.

2 Materials and Methods

2.1 Reagents, Media and Buffers

Agarose solutions	0.7% (w/v) low melting point agarose (Invitrogen) in distilled water for mounting live embryos 2% (w/v) agarose in distilled water for molds and 96 well plate coating
Danieau's buffer	58 mM, 0.7 mM KCl, 0.4 mM MgSO4, 0.6 mM Ca(NO3)2, 5 mM HEPES, pH 7.6
E3 medium	5 mM NaCl, 0.17 mM KCl, 0.33 mM CaCl2 x 2 H2O, 0.33 mM MgSO4 x 7 H2O, pH 6.5
PenStrep	10000 units penicillin/ml and 10000 µg/ml streptomycin (Invitrogen)
PBS	1.7 mM KH2PO4; 5.2 mM Na2HPO4; 150 mM NaCl
PBT	0.05 (v/v) Triton X-100 in PBS
PFA	4% (w/v) paraformaldehyde, 81 mM Na2HPO4 19 mM, NaH2PO4, pH 7.4
Brinkley Buffer 1980 (BRB80)	80mM PIPES, 1mM MgCl2, 1mM EGTA, pH 6.8
Microtubule Fixative: glutaraldehyde	1% (v/v) in BRB80
Microtubule Quenching Solution	0.1% (w/v) NaBH4 in PBS.
TBS	50 mM Tris-Cl, 150 mM NaCl, pH 7.5
TBST	0.1% (w/v) Triton-X in TBS

RIPA	Cell signaling
Protease Inhibitor	Complete Mini, Roche
Phosphatase Inhibitor	Phospho-STOP, Roche
DMEM-F12	Gibco
EGTA	5 mM in DMEM-F12
Activin	10-100 ng/ml in DMEM-F12 (120-14 - Preprotech)
Nodal Inhibitor	30 µM in DMEM-F12 (SB-431542, 1614 - Tocris)
qDots 625 ITK	40 nM in Nuclease free water (A10200, Thermo Fisher Scientific)
Dextran-AlexaFluor647	D-22914, Thermo Fisher Scientific
Dextran-Tetramethylrhodamine	D-1817, Thermo Fisher Scientific
Dextran-Cascade Blue	D-1976, Thermo Fisher Scientific

2.2 Antibodies

Ab	IF	WB	Clone and producer
myc	1:5000		9E10, produced by MPI-CBG, Dresden - Germany
EEA1	1:200		ab2900, Abcam
Pan-Cad		1:1000	C3678, Sigma
GAPDH		1:1000	NB300-221, Novus Biologicals
P-MLC2		1:500	3674, Cell Signalling

2.3 Primers

Cloning

Mezzo-attB1r	5’-GGGGACTTTTTTGTACAAACTTGACACATCTAAGGAAAAAAGTCA-3’
Mezzo-attB4	5’-GGGGACAACTTTGTATAGAAAAGTTGCATCACAACGGGTTATGAAT-3’
TurboRFP_attB1	5’-GGGGACAAGTTTGTACAAAAAAGCAGGCTCCACCATGAGCGAGCTGATCAAG-3’
TurboRFP_attB2	5’GGGGACCACTTTGTACAAGAAAGCTGGGTtTCATCTGTGCCCCAGTTTGCT-3’
caRock2a_attB1	5’-GGGGACAAGTTTGTACAAAAAAGCAGGCTACAACATGTCGCTAGGAGCGGAGAGAAG-3’
caRock2a_attB2	5’-GGGGACCACTTTGTACAAGAAAGCTGGGTCCTCTTCATCGAGCTCTTTGGT-3’
Rab5c-attB2r	5’-GGGGACAGCTTTCTTGTACAAAGTGGctATGGCGGGGCGAGGTGGACCA-3’
Rab5c-attB3	5’-GGGGACAACTTTGTATAATAAAGTTGgTTAGTTTCCGCCTCCACAGCA-3’

RT-PCR

β-actin fw	5’-gatcttcactccccttgttca-3’
β-actin rw	5’-ggcagcgatttcctcatc-3’
Goosecoid fw	5’-tgcacctacgtgaagagaagg-3’
Goosecoid rw	5’-ttgttccatttctgtgagttttct-3’
EGFP fw	5’-gaagcgcgatcacatggt-3’
EGFP rw	5’-ccatgccgagagtgatcc-3’

2.4 Technical Equipment

Ball-joint-holder	World Precision Instruments (WPI)

Glass capillaries	Harvard GC100F-15 (injection)
Magnet holder	MB-B (Kanetec)
Microinjectors	PV820 and Pico-Pump with foot pedal (WPI)
Micromanipulators	Narishige MN-15 (injection set up) MO-155 (transplantation set up)
Needle puller	Flaming/Brown P87 (Sutter instruments)
Pipette holders	MN-151 (injection) MPH3 (transplantation)
NanoPhotometer spectrometer	Nanodrop 2000 spectrophotometer (Thermo scientific)
Glass-bottom Petri dishes	P35G-0-10-C case (Matek)
Heating block	Dri-block DB-2D (Techne)
Temperature chamber	IST Austria Bioimaging Facility
Objective heater	IST Austria Workshop
Stage incubation chamber	Workshop IST Austria and Peacon heating stage
Stereomicroscopes	Leica MZ 125 Leica M165 FC
Confocal microscopes	Leica SP5 upright Leica SP5 inverted LaVision Biotec TrimScope Zeiss Lsm800

2.5 Fish maintenance and embryo collection

Fish maintenance and embryo collection were carried out as previously described [194]. Briefly, adult TL or AB zebrafish were couples were set up in separate tanks in the evening so that they would mate in the morning. A sieve separates the adult fish from the embryos

and, optionally, male and female can be separated as well, to allow timing of mating. The deposited eggs were collected and embryos were raised in either E3 medium or Danieau's buffer, kept at 28 or 31°C and staged according to Kimmel et al[45].

2.6 qDots, mRNA, morpholino and dextran injections

Embryos at the 1-cell stage were injected as previously described [194]. Embryos were collected and aligned on an 2% agarose mold to allow orienting. A previously prepared needle (Harvard GC100F-15 capillaries pulled with a Flaming/Brown P87 needle puller - Sutter instruments) was filled with the injection mix and loaded on an pressure controlled injection setup (a WPI needle holder mounted on a Narishige MN-15 micromanipulator and connected to a PV820 and Pico-Pump with foot pedal (WPI) microinjector). The tip of needle was broken with forceps and the pressure of microinjector was calibrated to obtain a 0.5 nl drop. The needle was then inserted in the embryo through the chorion and the injection mix was delivered in the cell. The cell cytoplasm was labelled by injection of either 0.5 nl of a 40 nM solution of qDots 625 ITK (A10200, Thermo Fisher Scientific) or 2.5 ng of fluorescently labelled 10000 MW dextran, i.e. Dextran-AlexaFluor647, Dextran-Tetramethylrhodamine or Dextran-Cascade Blue (D-22914, D-1817 and D-1976, respectively; Thermo Fisher Scientific). The cell nuclei were labelled by injection of 30 pg *H2B-BFP* or *H2A-mCherry* mRNA. Cell membranes were labelled by injection of 30-50 pg of *mRFP* or *lyn-EGFP* mRNA. Induction of prechordal plate (ppl) progenitors was achieved by injecting 100 pg of either *ndr2* or *ndr2-EGFP* mRNA in combination with 2 ng *casanova morpholino* (MO; 5'---GCATCCGGTCGAGATACATGCTGTT---3',GeneTools;)[138]. To reduce cell-cell adhesion, 2 ng *e-cadherin* MO (5'---TAAATCGCAGCTCTTCCTTCCAACG---3', GeneTools) was injected at the 1-cell stage, while control embryos were injected with 2 ng scramble *morpholino* (5'--ATGCCAGAGTTCTTACAGAAGCGAT--3'). For modulating the level of Nodal signaling in ppl progenitor cells by light, *Opto-Actvr1b* and *Opto-Actvr2b* mRNA (20 pg each[98]) were injected at the one-cell stage, while control embryos were injected with mRNA encoding for Chem-Actvr1b and Chem-Actvr2b, chemically inducible versions of the respective Nodal receptors (20 pg each).

2.7 Transgenic and mutant lines

The following transgenic and mutant lines were used in this study: *Tg(gsc::mEGFP)*[195], *Tg(β-actin::mEGFP)*[196], *Tg(sox17::EGFP)*[197], MZ*oep*[198], *Tg(gsc::tRFP)* and *Tg(mezzo::EGFP).*

The Tol2/Gateway technology[199,200] was used to generate the *Tg(gsc::tRFP)* and *Tg(mezzo::EGFP)* lines. For the *Tg(gsc::tRFP)* line, expressing TurboRFP under the control of the goosecoid promoter, the p5E-goosecoid plasmid, containing -1.8Kb promoter region of the zebrafish *gsc* gene was a gift from the Solnica-Krezel lab[201]. The cDNA sequence of TurboRFP was amplified from the pCLX-UBI-Tred plasmid (a gift from Patrick Salmon – Addgene plasmid #27246) using sequence specific primers with additional Gateway recombination arms. The resulting PCR product was recombined with the pDONRP221 (Chien#218) and subsequently with the pDestTol2pA2 (Chien#394), p5E-goosecoid and p3E-polyA (Chien#302) to obtain pTol2-*gsc*::tRFP.

For the *Tg(mezzo::EGFP)* line, expressing EGFP under the control of the mezzo promoter, a region encompassing 2 kb upstream of the TSS, first exon and first intron of the mezzo gene was amplified from zebrafish genomic DNA using sequence specific primers with additional Gateway recombination arms. The resulting PCR product was recombined with the pDONRP4-P1R (Chien#219) and subsequently with the pDestTol2pA2 (Chien#394), pME-EGFP (Chien#383) and p3E-polyA (Chien#302) to obtain pTol2-mezzo::EGFP. The final vectors were injected in wild type TL embryos together with mRNA encoding for a transposase (Invitrogen).

Fluorescent embryos were raised (P0) and screened for germ line transmission once they reached adulthood. The fluorescnetly positive progeny was raised (F1) and outcrossed to WT until a stable line with a single insertion of the transgene was established.

2.8 Prechordal plate cell transplantations

To assess *goosecoid* (*gsc*) expression rates, donor *Tg(gsc::mEGFP)* embryos were injected with qDots at the one-cell stage and both donor and uninjected *Tg(gsc::mEGFP)* host embryos were kept at 31 °C until early shield stage (5 hpf). Embryos were dechorionated with forceps and transferred into an agarose dish with Danieau's buffer, and 5-15 cells were taken from the ppl of a donor embryo, using a beveled borosilicate needle with a 20 µm inner diameter attached to a syringe system, and immediately transplanted in front of the forming shield of a host embryo. To test the effect of (1) reduced cell-cell adhesion and (2) increased Nodal signalling on ppl cell behavior, a mixture of control and experimental ppl cells was transplanted into a host embryo. For reducing ppl cell-cell adhesion (1), *Tg(gsc::mEGFP)* donor embryos were injected either with qDots together with scramble/control MO and dextran-Cascade Blue (control cells) or with qDots together with *e-cadherin* MO (experimental cells). For increasing Nodal signaling (2), *Tg(gsc::mEGFP)* donor embryos were injected with either qDots together with *Chem-Actvr1b,2b* mRNA and

dextran-Cascade Blue (control cells) or with qDots together with *Opto-Acvr1b,2b* mRNA (experimental cells). The transplanted host embryos were then mounted in 0.7 % agarose in E3 medium or Danieau's buffer and imaged with a LaVision upright multi-photon microscope equipped with a Zeiss Plan-Apochromat 20x/1.0 water immersion objective and Ti:Sa laser (Chameleon, Coherent) set at 820 nm, allowing simultaneous excitation of EGFP, qDots and dextran-Cascade Blue. Image analysis was performed with Imaris version 7.4 (Bitplane) as follows: transplanted cells were tracked and assigned a 3D spot object. Mean EGFP and qDots intensities were then calculated over the volume of the spot and a linear regression of mean EGFP/qDots ratio as a function of time was used to compute a linear coefficient normalized to the median initial EGFP/qDots value (Lc). Cell-cell contacts formed by each transplanted cell were tracked manually over a period of 60 min, and mean contact duration was computed as described in the Supplementary Note - Appendix 1. Transplanted cells dividing during the time of acquisition were not considered for analysis. To assess the likelihood of ppl cells differentiating into endoderm, transplantations were performed using *Tg(sox17::EGFP)* donor and host embryos. Transplanted host embryos were incubated for 3 h at 31 °C, mounted in 0.7 % agarose in Danieu's buffer and imaged with a Leica upright SP5 confocal microscope equipped with a Leica 25x/0.95 NA water immersion objective. Total and sox17::EGFP positive transplanted cells were counted manually.

2.9 Light activation of Opto-Actvr

Embryos were light stimulated using an incubator (Herp Nursery II, 69802, Lucky Reptile) equipped with 300 light-emitting diodes (SMD5050) [202] with a measured light intensity of 5.12 mW/mm^2. Control embryos were incubated under the same conditions in a light-tight box and imaged with a stereomicroscope (M165 FC, Leica). For multi-photon imaging, embryos were mounted in an incubation chamber equipped with LED that was remotely controlled using custom Matlab scripts via an USB analog switch. LED light activation was achieved by cycles of 180 sec illumination followed by 120 sec multi-photon imaging.

2.10 3D cell-cell contact *in vivo*

To estimate the average number of cell-cell contacts established by ppl progenitor cells in vivo, *Tg(gsc::mEGFP)* embryos were injected with H2A-mCherry mRNA and kept at 31 °C until shield stage (6 hpf), mounted in 0.7 % agarose in E3 medium and imaged with a

LaVision upright multi-photon microscope equipped with a Zeiss Plan-Apochromat 20x/1.0 water immersion objective, Ti:Sa laser (Chameleon, Coherent) set at 820 nm and OPO laser set at 1150 nm, allowing simultaneous excitation of EGFP and mCherry. Image analysis was performed with Imaris version 7.4 (Bitplane) and with custom Matlab scripts, as follows: first, nuclear mCherry signal was used to create a spot object for each ppl cell and their x,y,z coordinates were used as nodes of a Delaunay triangulation. The edges whose midpoint is closer to another vertex than it is to one of its end vertices were eliminated from the triangulation. For each node, the number of connecting edges was extracted and used as a measure of the number of simultaneous cell-cell contacts formed by each cell.

2.11 Fluorescence activated cell sorting (FACS)

For FACS, 100-150 shield stage (6hpf) embryos were dechorionated and transferred to 1 mL of 5 mM EGTA containing CO_2-independent DMEM/F12 (Invitrogen, complemented with L Glut, 15 mM Hepes and 100 U/mL penicillin plus streptomycin, adjusted at pH 7.5, sterilized using 0.45 µm pore filters, and preheated to 28 °C). Embryos were then mechanically dissociated into single cells by mild shaking, and yolk proteins were removed by 2 successive wash steps with 1 mL fresh medium, followed by centrifugation at 100 G for 2 min. Dissociated cells were processed with a flow cytometer (FACSAria III, BD Bioscience) and sorted into glass bottom 96-well plates (655892, Greiner) containing DMEM-F12 medium and coated with 2 % agarose in distilled water or heat inactivated fetal calf serum (FCS).

2.12 In vitro cell assays

For analyzing gsc::mEGFP expression over time in cultured ppl cell, FACS was used to isolate ppl cells from *Tg(gsc::mEGFP)* or *MZoep;Tg(gsc:mEGFP)* embryos injected with dextran-Alexa647. The isolated cells were imaged with a Leica inverted SP5 confocal microscope equipped with a Leica 20x/0.7 NA air objective (temperature controlled at 28.5 °C), and image analysis was performed with Imaris (Bitplane) as follows: first, the dextran-Alexa647 signal was used to build a surface object for each single cell or doublet. Mean EGFP intensities over the volume of the surface object were then measured and normalized to the initial value. For analyzing Smad2 nuclear-to-cytoplasmic ratios, ppl cells were isolated by FACS from *Tg(gsc::tRFP)* embryos injected with *smad2-EGFP* and *H2B-BFP* mRNAs. The isolated cells were then imaged with a Zeiss inverted LSM800 confocal

microscope equipped with a Zeiss 40x/1.2 NA water objective (temperature controlled at 28.5 °C) every 10 min for a period of 90 min. For image analysis Imaris (Bitplane) was used as follows: first, a surface object was built using the H2B-BFP signal and used to mask the Smad2-EGFP signal. A second surface object was then built on the cytoplasmic Smad2-EGFP signal, and the mean EGFP intensities were measured over the volume of the nuclear and cytoplasmic surface objects. Only a portion of the single cells and doublets were detected and analyzed for multiple timepoints, due to cell division or cell death. For measuring the effect of Nodal signaling on cell-cell contact formation, wild type embryos were injected with both *ndr2-EGFP* mRNA and dextran-Alexa647 and incubated at 31 °C until they had reached shield stage (6 hpf). Cells expressing different levels of Ndr2-EGFP were isolated via FACS and imaged with a Leica inverted Sp5 confocal microscope equipped with a Leica 20x/0.7 NA air objective (temperature controlled at 28.5°C) for 120 min. Image analysis was performed with Imaris (Bitplane) and custom python scripts as follows: first, the dextran-Alexa647 signal was used to determine the shape of cell doublets after 120 min in culture. The axes of the maximum and minimum rotational inertia of the doublet shape were then identified and their ratio used as a proxy for compaction. For measuring the dynamics of Nodal accumulation at cell-cell contacts, wild type embryos were injected with both *ndr2-EGFP* and membrane bound RFP (mRFP) mRNAs and incubated at 31 °C until they had reached shield stage (6 hpf). Cells expressing Ndr2-EGFP were isolated and imaged with a Leica inverted Sp5 confocal microscope equipped with a Leica 63x/1.4 NA oil objective (temperature controlled at 28.5°C). Cell-cell contact formation was initiated by gently bringing two cells together using micropipettes[138], and the newly formed cell doublet was imaged over a period of 10 min at 30 sec intervals. Image analysis was performed with Imaris (Bitplane) measuring average Ndr2-EGFP intensities at the cell-cell and cell-medium interfaces over time.

2.13 Myc and EEA1 immunofluorescence staining.

Wild type embryos were injected with either *Actvr1b-myc* plus *ndr2-EGFP* mRNA and *casanova* MO (experimental) or *H2A-mCherry* plus *ndr2* mRNA and *casanova* MO (control). Embryos were then incubated at 31 °C until they had reached shield stage (6 hpf), and progenitor cells were isolated by FACS. A mix of differently labelled cells was sorted into glass bottom 96-well plates containing DMEM-F12 medium and incubated for 60 min. The cells were then fixed with 2 % PFA, and Actvr1b-myc was detected with an anti-myc antibody (1:5000, 9E10, produced by MPI-CBG, Dresden - Germany), while early

endosomes were detected using an anti-EEA1 antibody (1:200, ab2900, Abcam). As secondary antibodies goat alexa-568 conjugated anti-mouse (1:500, A-11004, Molecular Probes) and goat Cy5-conjugated anti-rabbit (1:500, 111-175-003, Jackson ImmunoReasearch) antibodies were used. Doublets formed by a Actvr1b-myc and Ndr2-EGFP coexpressing cell in contact with another H2A-mCherry expressing cell were imaged using a Leica inverted SP5 confocal microscope equipped with a Leica 63x/1.4 NA oil objective. Triple colocalization of Actvr1b-myc, Ndr2-EGFP and EEA1 was analysed with Imaris (Bitplane), and the subcellular localization of Actvr1b-myc and Ndr2-EGFP double-positive early endosomes was analyzed using Fiji-ImageJ. The intensity of the colocalization signal was measured in an area of 3 µm below the membrane at the cell outline. The average intensity was calculated for the cell-medium and cell-cell interface separately.

2.14 Western blotting

Wild type embryos were injected with *ndr2-EGFP* mRNA and incubated at 31 °C until they had reached shield stage (6 hpf). Cells expressing different levels of Ndr2-EGFP were isolated using FACS, and 100.000 cells per sample were lysed in RIPA buffer (9806, Cell signaling) supplemented with protease (Complete Mini, Roche) and phosphatase (Phospho-STOP, Roche) inhibitors. Total protein was transferred to a 12 % polyacrylamide gel for Western blotting. Cadherins were detected with an anti-pan-cadherin antibody (1:1000, C3678, Sigma), while phosphorylated myosin II was detected with an anti-phospho-myosin light chain II antibody (1:500, 3674, Cell Signalling). Both antibodies were used in combination with a goat HRP conjugated secondary anti-rabbit antibody (111-035-003, Jackson ImmunoResearch). As a loading control, GAPDH was detected using an anti-GAPDH antibody (1:1000, NB300-221, Novus Biologicals) in combination with a goat HRP-conjugated anti-mouse secondary antibody (111-035-006, Jackson ImmunoResearch). Chemiluminescence was detected with a VersaDoc MP4000 (Biorad) imaging system, and western blot band densitometry was performed using the QuantityOne (Biorad) software.

2.15 qPCR

Tg(gsc::mEGFP) embryos were dechorionated manually and exposed to either DMSO, 50-100 µM nodal inhibitor (SB-505124, Sigma) or 20 nM human Activin (120-14E, Preprotech) in E3 for 3h, starting at early shield stage (5.5 hpf). Total RNA was extracted using Trizol, starting from 20 embryos per group. One µg of total RNA was retro-transcribed using

Superscript III reverse transcriptase (Invitrogen) and qPCR was performed using the SYBR-green method (Absolute qPCR SYBR green mix plus ROX, AB-1166A, ABgene), optically clear plates 96 well plates (AB-0600, ABgene) and a C1000 BioRad QPCR thermal cycler. Levels of gsc and mEGFP mRNA were normalized to b-actin and relative expression to the DMSO control was calculated using the CFX Manager 3.1 software (BioRad).

2.16 Statistical analysis

Statistical analysis of data was performed using the GraphPad Prism 5 software, as indicated in the figure captions. Pairwise comparisons of normally distributed samples with similar variances were performed with Student t test, while Mann-Whitney test was used in case of not normally distributed data. Comparisons between multiple treatments (Fig. 1a) was performed via one-way ANOVA followed by Bonferroni post-test correction for multiple comparisons. Comparisons between multiple treatments of two different samples (Fig. 2d) was performed via two-way ANOVA followed by Bonferroni post-test correction for multiple comparisons. No statistical method was used to predetermine sample size, the experiments were not randomized and the investigators were not blinded to allocation during experiments and outcome assessment.

3 Results

The data presented in this section is result of collaborative work, in which I was the leading scientist. In case I did not perform an experiment presented, this is stated in the legend of the relative figure, along with the reference to whom did the work. Moritz Lang developed the theory and stochastic modeling included in this project: for completeness, his work is added to this Thesis as Appendix 1.

3.1 Cell-cell adhesion and *goosecoid* expression positively correlate within the prechordal plate in vivo.

Cell-cell contact formation is thought to be important for cell fate specification in both vertebrate and invertebrate development [15–17,109,145,175,191,203]. In mouse embryogenesis, for instance, cell-cell contact formation is required for the induction of the pluripotent inner cell mass giving rise to the embryo proper[145]. Conversely, cell fate specification determines the ability of cells to form contacts of different size and strength [138,162,163,166,167,204], a process important for cell segregation and tissue formation [106,150,204–207]. Finally, there is increasing evidence that morphogen signaling not only controls cell fate specification, but also influences cell-cell contact formation by modulating cell mechanics and dynamics [138,162,165,208–212]. While these observations suggest that cell fate specification and cell-cell contact formation are tightly interconnected processes, little is yet known about how their interplay affects embryo patterning and morphogenesis in development.

In the zebrafish embryo, anterior axial mesendoderm cells are the first population of mesendoderm progenitor cells to be specified at the dorsal germ ring margin and to segregate from the ectoderm progenitor cells via synchronized cell ingression[32]. Once ingressed, they form a compact cell cluster, the prospective prechordal plate (ppl), and collectively migrate towards the animal pole of the gastrula [32,42,43]. Ppl cell fate specification becomes apparent in progenitor cells by the expression of the marker gene *goosecoid (gsc)*, a direct target of the Nodal/TGFβ signalling pathway[91]. Previous studies have suggested that persistent *gsc* expression in ppl progenitors requires continuous expression of the cell-cell adhesion receptor e-cadherin (cdh1) [109], pointing to the intriguing possibility that e-cadherin-mediated cell-cell adhesion is required for proper ppl cell fate specification.

To address this possibility, we used a zebrafish transgenic line expressing membrane-bound EGFP (mEGFP) under the control of the *gsc* promoter[195] and analyzed *gsc::mEGFP* expression as a readout of ppl cell fate specification within individual cells of the ppl as a function of time and cell-cell contact formation. Firstly, we sought to verify the validity of the *gsc::mEGFP* reporter. Given that *gsc* is a direct target of Nodal signaling[91], we treated *Tg(gsc::mEGFP)* embryos with either a Nodal inhibitor[213] or with Activin, known to activate Nodal signaling[73], for three hours starting at shield stage (6pf) and then used qPCR to measure mRNA levels of both *gsc::mEGFP* and endogenous *gsc*. We found that both endogenous *gsc* and *gsc::mEGFP* levels decreased upon Nodal signaling inhibition and increased upon Nodal signaling stimulation, even though the *gsc::mEGFP* is more responsive to Activin that the endogenous *gsc* (Fig. 3.1.1a). These results confirm that *gsc*::mEGFP is a valid reporter for *gsc* promoter activity and that zebrafish embryonic cells are responsive to Nodal signaling during late gastrulation.

To analyze cell-cell contact formation, we first determined cell-cell contact size, assuming that highly adhesive cells form bigger contacts than less adhesive cells. Cell-cell contact size within a cluster of cells reflects on cell density, with cells forming bigger contacts being closer to their neighbours. Therefore, we used *Tg(gsc::mEGFP)* embryos expressing the nuclear marker H2A-mCherry and measured average nuclear distance to the first six neighbors of each ppl cell as an estimate of its adhesive properties (Fig. 3.1.1b). We found an inverse correlation between *gsc*::mEGFP intensity and nuclear distance, becoming more evident over time (Fig. 3.1.1c). We repeated the same analysis using Tg(β-*actin*::mEGFP);Tg(*gsc*::tRFP) embryos expressing mEGFP under a control promoter (β-*actin)*[196] and the nuclear marker H2B-BFP. We found no correlation between β-*actin::*mEGFP expression level and nuclear distance (Fig. 3.1.1d), suggesting that *gsc*::mEGFP but not β-*actin::*mEGFP expression correlates with cell density within the ppl. Nuclear distances between cells, however, can be influenced by both cell-cell contact size and cell volume, with smaller cells presenting lower distance to their neighbours than bigger cells. To have a measure of cell adhesion independent of cell size, we determined cell-cell contact number and duration for single ppl cells over time, assuming that highly adhesive cells form more and/or longer-lasting contacts than less adhesive cells.

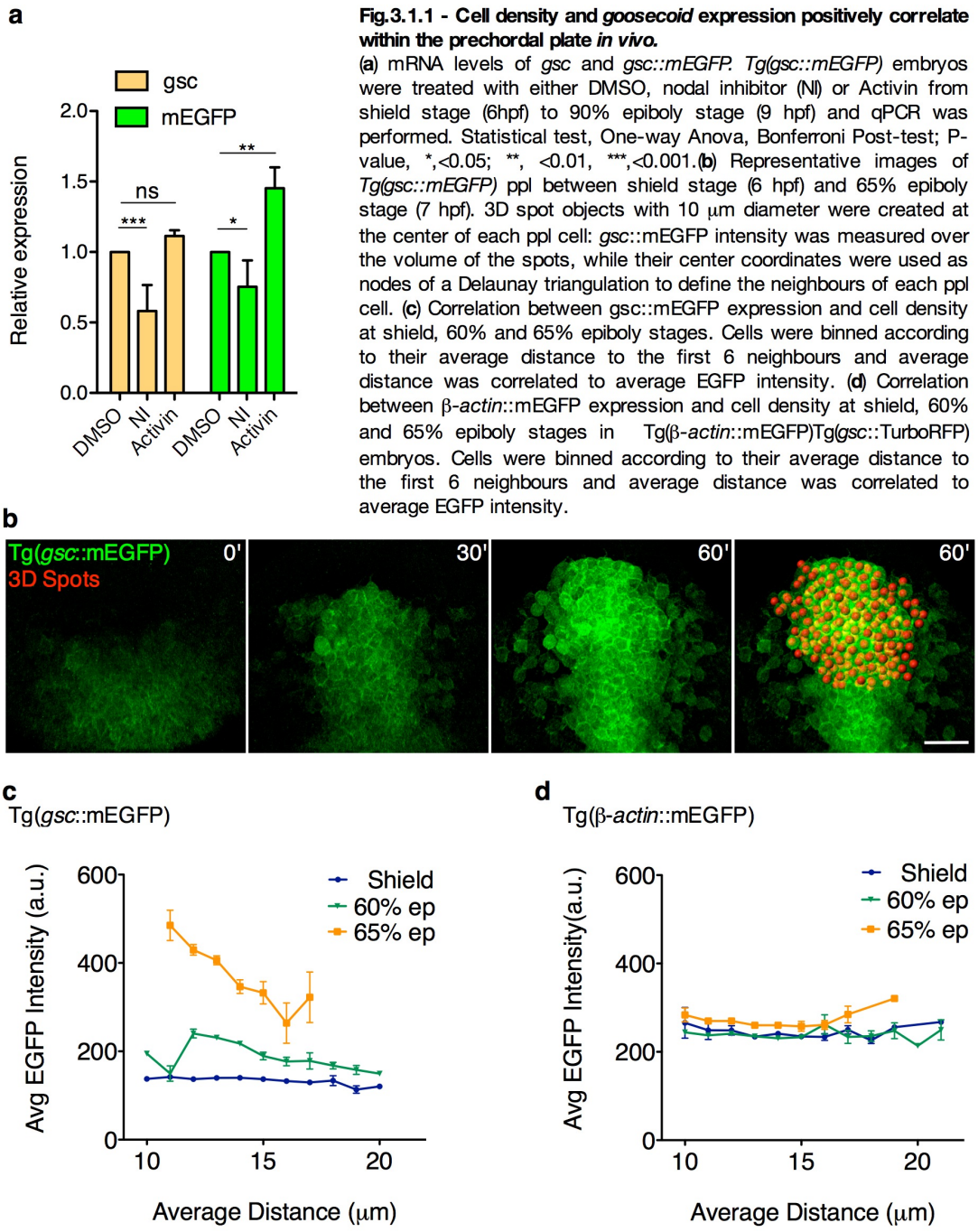

Fig.3.1.1 - Cell density and *goosecoid* expression positively correlate within the prechordal plate *in vivo*.
(**a**) mRNA levels of *gsc* and *gsc::mEGFP*. *Tg(gsc::mEGFP)* embryos were treated with either DMSO, nodal inhibitor (NI) or Activin from shield stage (6hpf) to 90% epiboly stage (9 hpf) and qPCR was performed. Statistical test, One-way Anova, Bonferroni Post-test; P-value, *,<0.05; **, <0.01, ***,<0.001.(**b**) Representative images of *Tg(gsc::mEGFP)* ppl between shield stage (6 hpf) and 65% epiboly stage (7 hpf). 3D spot objects with 10 μm diameter were created at the center of each ppl cell: *gsc*::mEGFP intensity was measured over the volume of the spots, while their center coordinates were used as nodes of a Delaunay triangulation to define the neighbours of each ppl cell. (**c**) Correlation between gsc::mEGFP expression and cell density at shield, 60% and 65% epiboly stages. Cells were binned according to their average distance to the first 6 neighbours and average distance was correlated to average EGFP intensity. (**d**) Correlation between β-*actin*::mEGFP expression and cell density at shield, 60% and 65% epiboly stages in Tg(β-*actin*::mEGFP)Tg(*gsc*::TurboRFP) embryos. Cells were binned according to their average distance to the first 6 neighbours and average distance was correlated to average EGFP intensity.

To analyse cell-cell contact number and duration over time, we performed homotypic and homochronic transplantation of ppl progenitors from donor *Tg(gsc::mEGFP)* embryos containing qDots into the ppl of host *Tg(gsc::mEGFP)* embryos devoid of qDots (Fig. 3.1.2a,b, Video 1). This allowed us to measure *gsc*::mEGFP levels in each of the transplanted cells over time (Fig 3.1.2c-e) and to unambiguously identify cell-cell contacts between individual host and donor cells (Fig. 3.1.2f,g). To account for variations in *gsc*::EGFP intensity due to imaging we corrected *gsc*::mEGFP by qDots average fluorescence intensities in each transplanted cell over time (Fig 3.1.2c-e). We found that

gsc::mEGFP expression in ppl cells steadily increased as a function of time between 60% (6.5 hours post fertilization, hpf) and 70% (7.5 hpf) epiboly stages: therefore we performed a linear fit on the gsc::mEGFP/qDots ratios for each transplanted cell and used the linear coefficient normalized on the median initial gsc::mEGFP/qDots value of each experiment (Lc) as a proxy of gsc::mEGFP expression rate (Fig. 3.1.2e). To measure cell-cell contact duration and number for each transplanted cell, we tracked all cell-cell contacts between individual host and donor cells that were clearly visible in the x,y axis between 60% (6.5 hpf) and 70% (7.5 hpf) epiboly stages (Fig. 3.1.2f,g) and then measured the average duration and number of contacts for each transplanted cell. We found that the average duration and average number of contacts for any given ppl cell varied between 10 and 40 mins (Fig. 3.1.2h) and 3 and 10 contacts (Fig. 3.1.2i), respectively. Importantly, we also observed that the level of *gsc*::mEGFP expression in individual ppl cells positively correlated with cell-cell contact duration (Fig. 3.1.2h), pointing to the possibility that these two features could be functionally linked. Given the low amount of data points, we confirmed the observed correlation using the Kendall correlation coefficient, known to be robust to outliers [214] (Fig. 3.1.2h). In contrast, there was no significant correlation between number of simultaneous cell-cell contacts and *gsc*::mEGFP expression levels (Fig. 3.1.2i), suggesting that the duration rather than the number of contacts is critical for *gsc* expression within ppl cells.

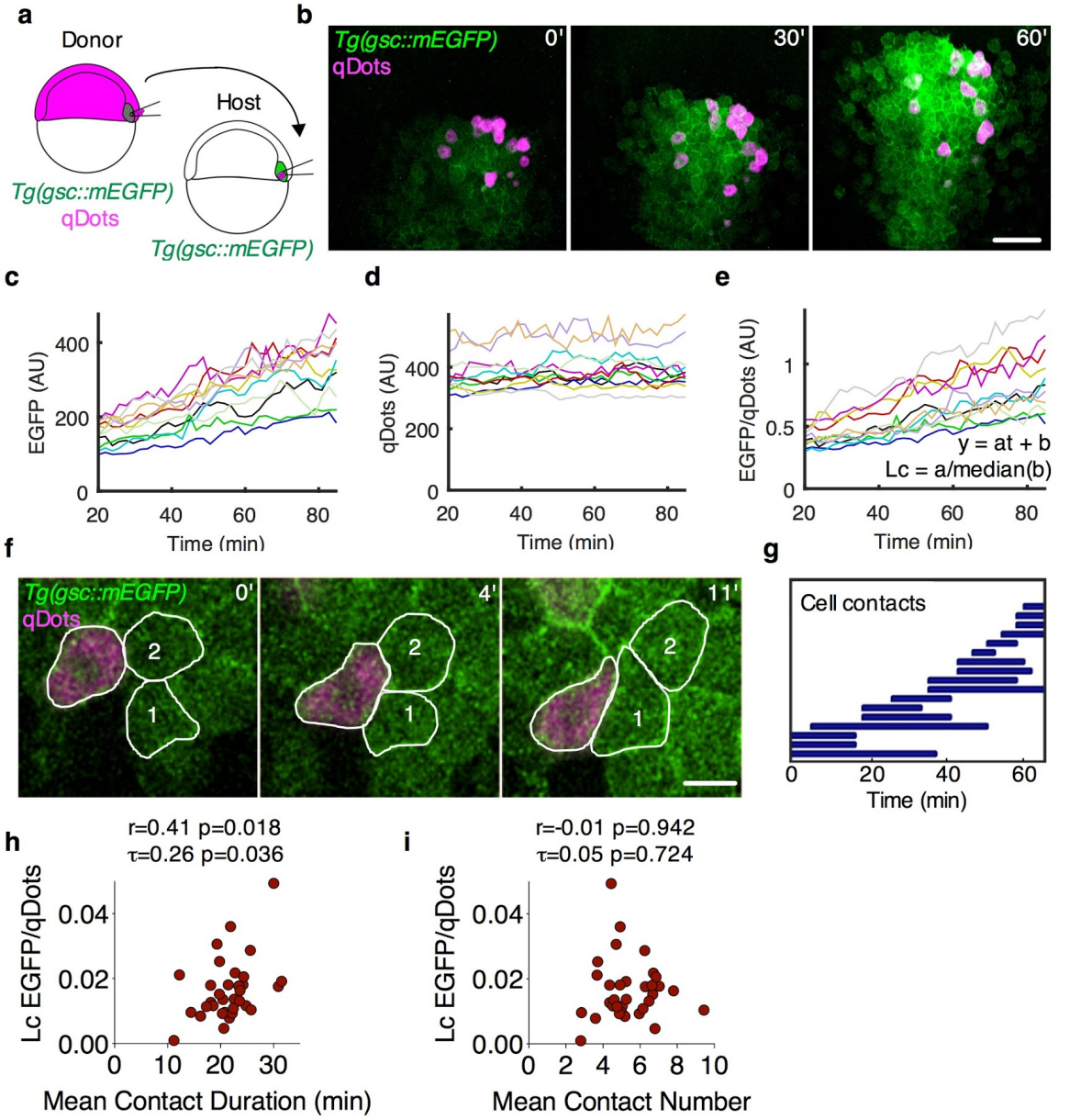

Fig. 3.1.2 - Cell-cell adhesion and *goosecoid* expression positively correlate within the prechordal plate *in vivo*.
(**a**) Schematic representation of a homotypic/homochronic transplantation assay. (**b**) Representative images of ppl cells transplanted from a *Tg(gsc::mEGFP)* embryo injected with qDots into a *Tg(gsc::mEGFP)* non-injected embryo. Transplantation was performed at shield stage (6 hpf) and images were taken between 60% epiboly stage (6.5 hpf) and 70% epiboly stage (7.5 hpf). Scale bar, 50 μm. (**c-e**) Average fluorescence intensities measured for the 11 transplanted ppl cells as a function of time. Each line represents one cell. Transplanted cells were tracked for 60 min and average EGFP (**c**) and qDots (**d**) intensities were measured for each cell at 2 min intervals. The ratio between EGFP and qDots average intensities was then calculated for each time point (**e**) and used to compute the linear coefficient (Lc) (**f**) Representative images of cell-cell contact dynamics between transplanted and host ppl cells at 60% epiboly stage (6.5 hpf). Scale bar, 20 μm.(**g**) Cell-cell contacts of one exemplary transplanted ppl cell, manually tracked for 60 min. Each line within a graph represents one tracked cell-cell contact. (**h**) Correlation between *gsc::*mEGFP expression rate and average contact duration in ppl progenitors between 6.5 and 7.5 hpf. (**i**) Correlation between *gsc*::mEGFP expression rate and average number of contact in ppl progenitors between 6.5 and 7.5 hpf. n (cells), 34; 4 embryos. Pearson (r) and Kendall (τ) correlations and relative p values (p) are shown.

3.2 Prechordal plate cell-cell contact formation promotes Nodal signalling *in vitro*.

3.2.1 Cell-cell contact formation promotes nodal dependent goosecoid expression

To experimentally address the possibility that cell-cell adhesion is critical for *gsc* expression within ppl cells, we first took a reductionist approach and isolated *gsc*::mEGFP positive cells from *Tg(gsc::mEGFP)* embryos at the onset of gastrulation (6 hpf) using fluorescence activated cell sorting (FACS). We then seeded these cells at low density on non-adhesive substrates (Fig. 3.2.1a), allowing us to follow *gsc*::mEGFP expression in single cells versus cells that were in contact with another cell (cell doublets) (Fig. 3.2.1b, Video 2). We found that ppl cell doublets showed a significantly higher rate of *gsc*::mEGFP expression than single ppl cells (Fig. 3.2.1c,d). This increased expression rate was specific for the *gsc* promoter, as mEGFP driven by a control promoter (β-*actin)* showed equal expression in single cells compared to doublets isolated from *Tg(*β-*actin::mEGFP)*;*Tg(gsc::tRFP)* embryos (Fig. 3.2.1c,d). Collectively, these results suggest that *gsc* expression in ppl progenitors is enhanced by cell-cell contact formation.

Gsc expression is directly controlled by Nodal signaling [60,91]. It is thus conceivable that cell-cell contact formation promotes *gsc* expression by enhancing Nodal signaling in the contacting ppl cells. To address this possibility, we turned to maternal zygotic *one-eyed-pinhead* mutant embryos (MZ*oep*), which are defective in Nodal signal reception and thus endogenous mesendoderm specification [198]. We reasoned that if cell-cell contact formation indeed promotes *gsc* expression by enhancing Nodal signaling, *gsc* expression should not be affected by cell-cell contact formation in Nodal signaling-defective MZ*oep* mutant cells. To trigger ppl specification in MZ*oep* cells, we took advantage of previous observations that mutant cells are still able to respond to the exogenously applied Nodal ligand Activin [215], although being unresponsive to endogenously produced Nodal ligands. We then isolated cells from *Tg(gsc::mEGFP);*MZ*oep* mutant embryos, exposed them to the Nodal ligand Activin to induce ppl specification, and compared *gsc* expression in cultured single cells versus cell doublets (Fig. 3.2.1a). Interestingly, we found that *gsc*::mEGFP expression was only enhanced in doublets compared to single cells when the exogenous Nodal ligand Activin was continuously present in the culture medium during the measurements. In contrast, no such enhancement was observed when Activin was removed from the culture

medium shortly before the measurements (Fig. 3.2.1d). This suggests that cell-cell contact formation promotes the competence of progenitor cells to respond to Nodal signals inducing *gsc* expression and thus ppl specification.

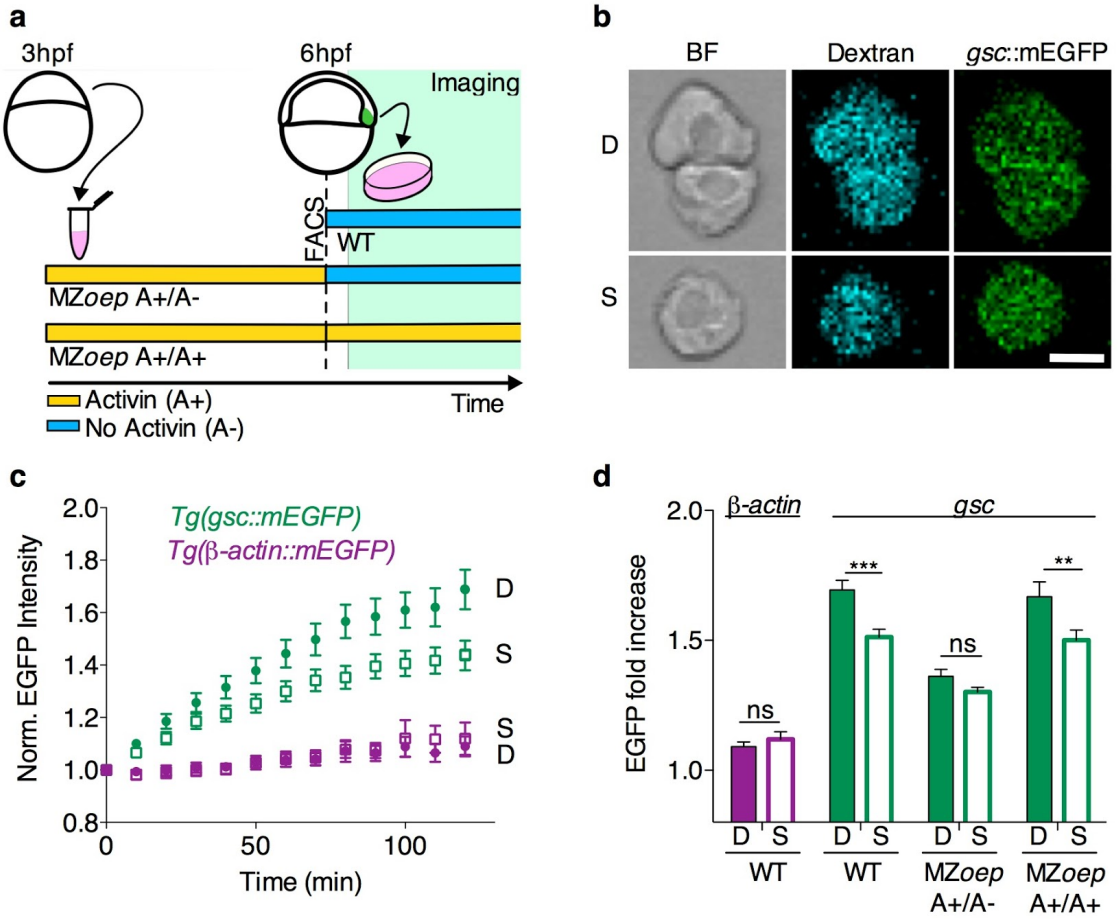

Fig. 3.2.1 - Prechordal plate cell-cell contact formation promotes Nodal signalling *in vitro*.
(**a**) Schematic representation of the experimental design. *Gsc*::mEGFP positive cells were isolated via FACS from WT *Tg(gsc::mEGFP)* embryos injected with fluorescent dextran-Alexa648 at shield stage (6 hpf) and seeded on non-adhesive substrates for subsequent imaging. MZ*oep;Tg(gsc::mEGFP)* embryos injected with dextran-Alexa648 were dissociated at 3 hpf, and cells were exposed to Activin for 3h in culture. Activin-induced *Gsc*::mEGFP positive cells were then selected by FACS and seeded on non-adhesive substrates for subsequent imaging. During imaging, selected cells were kept in culture medium either containing Activin (MZ*oep* A+/A+) or not (MZ*oep* A+/A-). (**b**) Representative images of doublets (D) and single cells (S) obtained from WT *Tg(gsc::mEGFP)* at shield stage (6 hpf) after 160 min in culture. Brightfield (BF) images show cell morphology (left column) and confocal images (middle and right columns) show dextran and *gsc*::mEGFP expression in the same cells. Scale bar, 10 μm. (**c**) Fold increase of average *gsc*::mEGFP intensities in single cells (S) versus cell doublets (D) as a function of time in culture for ppl cells isolated from *Tg(gsc::mEGFP)* or *Tg(gsc::tRFP);Tg(β-actin::mEGFP)* at shield stage (6 hpf). Plotted values, mean ± 95% CI. n (*gsc::*mEGFP, single cells), 41; n (*gsc::*mEGFP, doublets), 40; 5 independent experiments. n (β-*actin::*mEGFP, single cells), 18; n (β-*actin::*mEGFP, doublets), 19; 5 independent experiments. (**d**) Average *gsc*::mEGFP fold increase for doublets (D) and single (S) ppl cells taken from WT or MZ*oep*;*Tg(gsc::mEGFP)* embryos at shield stage (6 hpf) and cultured for 120 min in the presence (A+/A+) or absence (A+/A-) of Activin within the culture medium. Plotted values, mean ± s.e.m. n (β-*actin::*mEGFP, single cells), 18; n (β-*actin::*mEGFP, doublets), 19; 5 independent experiments. n (*gsc::*mEGFP, single cells), 52; n (*gsc::*mEGFP, doublets), 42; 5 independent experiments. n (MZ*oep*, *gsc::*mEGFP, (A+/A-), single cells), 52; n ((MZ*oep*, *gsc::*mEGFP, (A+/A-), doublets), 47; n (MZ*oep*, *gsc::*mEGFP, (A+/A+), single cells), 36; n ((MZ*oep*, *gsc::*mEGFP, (A+/A+), doublets), 36; 7 independent experiments. Statistical test, two-way anova and Bonferroni post test; P values, *< 0.05; **< 0.005; ***< 0.001, ns = not significant.

3.2.2 Cell-cell contact formation induces polarization of nodal signaling pathway components.

Next we asked how cell-cell contact formation affects the competence of progenitors to respond to Nodal signals. Cell-cell contact formation has previously been shown to trigger cell polarization [189]. We thus speculated that the Nodal signal transduction pathway might be polarized upon cell-cell contact formation, and that such polarization might affect the competence of contacting cells to receive Nodal signals. To test this hypothesis, we analyzed the subcellular distribution of various components previously associated with Nodal signal transduction in ppl cell doublets. Microtubules have been shown to be necessary for Nodal signaling, as they allow shuttling of Smad2 between cytoplasm and nucleus as well as endosome trafficking[87]. Moreover, activation of Smad2 by Nodal receptor takes place predominantly at the level of early endosomes[100]. We found that in cell doublets expressing the microtubule binding protein DCLK-EGFP, microtubules accumulated at cell-cell contacts (Fig. 3.2.2a,d). We also observed that early endosome, marked by mCherry-Rab5, preferentially localized at cell-cell contacts (Fig. 3.2.2b,d), while late endosomes, positive for mCherry-Rab7, were uniformly distributed (Fig. 3.2.2c,d). Moreover, in cell doublets expressing an EGFP-tagged version of the Nodal ligand Ndr2[78], the ligand preferentially localized to cell-cell contacts (Fig. 3.2.2e). We further found that a myc-tagged version of the Nodal receptor ActvR1b and the early endosomal marker EEA1 colocalized with Ndr2 at cell-cell contacts (Fig. 3.2.2e,f), suggesting that ligand-induced Nodal receptor internalization into early endosomes becomes polarized in ppl progenitors upon contact formation. To determine whether such polarized receptor internalization leads to increased Nodal signaling in cell doublets, we measured nuclear accumulation of the Nodal/TGFβ signaling mediator Smad2 [216] in ppl cell doublets versus single cells (Fig. 3.2.2g,h). We found that the nuclear-to-cytoplasmic ratio of EGFP-Smad2 was significantly increased in cell doublets compared to single ppl cells after 1 hour in culture (Fig. 3.2.2h). This supports the assumption that cell-cell contact formation promotes Nodal signaling and thus ppl specification by polarizing the Nodal signal transducing machinery to cell-cell contacts.

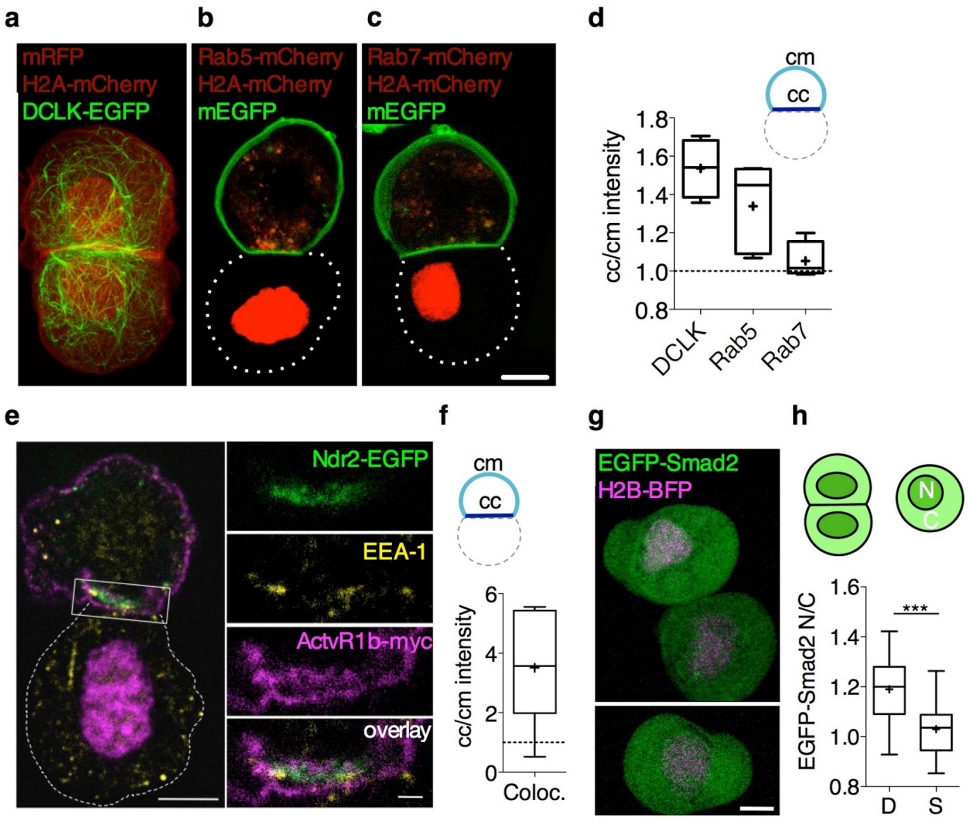

Fig. 3.2.2 - Cell-cell contact formation polarizes components of the Nodal signaling patwhay
Confocal images of ppl cell doublets isolated from embryos over-expressing (**a**) Ndr2, H2A-mCherry, mRFP and DCLK-EGFP, showing microtubules (**b**) Ndr2, mEGFP and Rab5-mCherry, showing early endosomes or (**c**) Ndr2, mEGFP and Rab7-mCherry, showing late endosomes.The bottom cell in (b) and (c) is outlined by white dashed line and only expresses H2A-Cherry to mark its nucleus. Scale bar, 5 μm. (**d**) Intensity ratios of DCLK-EGFP, Rab5-mCherry and Rab7-mCherry at cell-cell (cc) versus cell-medium (cm) interfaces of ppl cell doublets obtained from embryos at 6hpf and kept in culture for 60 min. Values are shown as Tukey box-and-whiskers plots with median (bar) and average values (cross). n (doublets), 4, 5, 4; 2 independent experiments. (**e**) Confocal image of a ppl cell doublet isolated from embryos over-expressing Ndr2-EGFP and ActvR1b-myc at 6 hpf and kept in culture for 60 min, showing the subcellular localization of Ndr2-EGFP relative to ActvR1b-myc and EEA1 visualized by immunohistochemistry in the top cell. The bottom cell (outlined by white dashed line) only expresses H2A-Cherry to mark its nucleus. Scale bar, 5 μm. Inset shows high magnification of the colocalization between EEA1, Ndr2-EGFP and ActvR1b-myc at the cell-cell contact. Scale bar, 1 μm. (**f**) Intensity ratios of colocalizing EEA1, Ndr2-EGFP and Actvr1b-myc at cell-cell (cc) versus cell-medium (cm) interfaces of ppl cell doublets obtained from embryos at 6hpf and kept in culture for 60 min. Values are shown as Tukey box-and-whiskers plots with median (bar) and average values (cross). n (doublets), 6; 2 independent experiments. (**g**) Representative images of ppl cells isolated from *Tg(gsc::tRFP)* embryos at shield stage (6 hpf) expressing EGFP-Smad2 and H2B-BFP after 60 min in culture. Scale bar, 5 μm. (**h**) EGFP-Smad2 nuclear-to-cytoplasmic (N/C) ratios for ppl cell doublets (D) and single cells (S) taken from WT *Tg(gsc::tRFP)* embryos expressing EGFP-Smad2 and H2B-BFP after 60 min in culture. Values are shown as Tukey box-and-whiskers plots with median (bar) and average values (cross). n (single cells), 27; n (doublets), 22; 3 independent experiments. Statistical test, Student t test, two tailed; P values,***< 0.001.

3.3 Nodal signaling promotes prechordal plate cell-cell contact formation *in vitro*.

Nodal signaling has previously been implicated in modulating cell-cell adhesion and contact formation [138,162,166,168,217]. We thus asked whether there might be feedback from enhanced Nodal signaling in ppl cell-cell doublets on cell-cell contact formation. To address this possibility, we ubiquitously expressed Ndr2-EGFP in wild type (WT) embryos and utilized FACS to isolate induced mesendoderm progenitor cells expressing different levels of Ndr2 (Fig. 3.3.1a). We then analyzed the ability of those isolated mesendoderm progenitors to form cell-cell contacts *in vitro* as a function of their Ndr2 expression level. To evaluate contact formation, we analyzed the shape of cell doublets, indicative of the relative size of cell-cell contacts formed in those doublets. We found that the contact size scaled with the amount of Ndr2 expressed in mesendoderm progenitors (Fig. 3.3.1b). To test if physiological levels of Nodal signaling could regulate cell-cell contact formation we compared the shape of doublets formed by mesendoderm progenitor cells that receive high or lower levels of Nodal signaling, i.e. ppl cells (expressing *gsc::mEGFP*) or all mesendoderm cells (expressing *mezzo::EGFP*). We found that contact size was higher in ppl cells (Fig. 3.3.1b), suggesting that Nodal signaling promotes cell-cell contact formation.
To determine how Nodal signaling functions in this process, we analyzed actomyosin contractility and e-cadherin expression, which have previously been shown to constitute key cell properties controlling germ layer progenitor cell-cell contact formation [138,151,162]. We found that with increasing levels of Ndr2 expression, the amount of both phosphorylated and thus activated myosin II as well as e-cadherin increased (Fig. 3.3.1c), suggesting that Nodal signaling promotes progenitor cell-cell contact formation by both up-regulating actomyosin contractility and cell-cell adhesion molecule expression. Together, these findings suggest that Nodal signaling mediates a positive feedback loop between ppl cell fate specification and cell-cell contact formation.

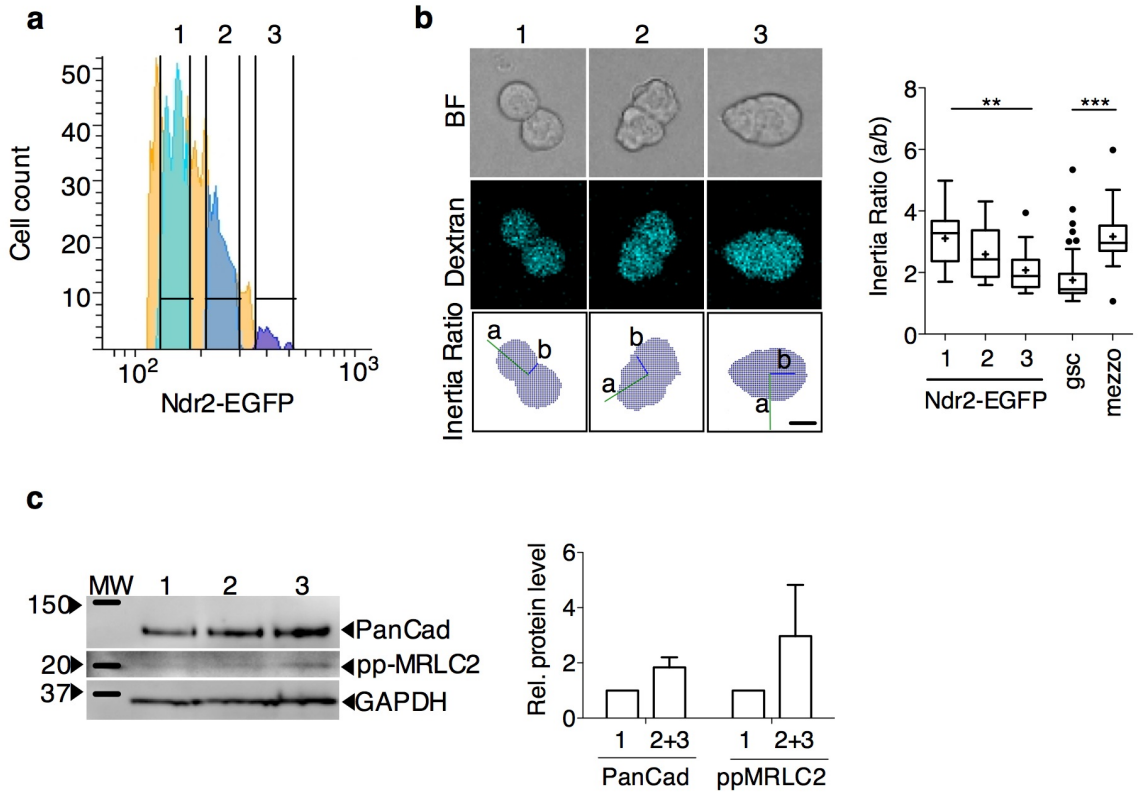

Fig. 3.3.1 - Nodal signalling promotes prechordal plate cell-cell contact formation *in vitro*.
(**a**) FACS sorting strategy: mesendoderm (ppl) cells were obtained from 6 hpf embryos injected with *ndr2-GFP* mRNA (100 pg/embryo) at the one-cell stage and sorted into 3 groups according to their Ndr2-EGFP expression levels. (**b**) Representative brightfield images of cell doublet shapes from the 3 groups. Cell doublet compaction was quantified as the ratio of rotational inertia along the longest and shortest axis n (1), 18, n(2), 19, n(3), 16; 3 independent experiments. Compaction was also quantified for endogenous ppl cells (gsc) and mesendoderm progenitor cells (mezzo). n(gsc), 69, n(mezzo), 20; 5 indipendent experiments. Scale bar: 5 μm. Statistical test, Student t test, two tailed. P value, **< 0.01. (**c**) Representative western blot showing the level of Pan-Cadherin (anti-PanCad antibody), phosphorylated myosin regulatory light chain 2 (anti-pp-MRLC2 antibody) and glyceraldehyde 3-phosphate dehydrogenase (anti-GAPDH antibody; control) expression in the 3 groups. Average PanCad/GAPDH and pp-MRLC2/GAPDH ratios were calculated after densitometry of 3 different experiments, using the square box method coupled with background subtraction.

3.4 Mutual enhancement between prechordal plate cell-cell contact formation and Nodal signaling *in vivo*.

To determine how far such mechanism might apply to the physiological context of the developing embryo, we asked whether interfering with ppl cell-cell contact duration would affect *gsc* expression within the ppl. To this end, we reduced the level of e-cadherin expression in ppl progenitors by injecting previously characterized *morpholinos* (MO) targeted against *e-cadherin* [109]. We then transplanted a mixture of control and *e-cadherin* MO injected ppl cells from donor to host *Tg(gsc::mEGFP*) embryos (Fig. 3.4.1a, Video 3). We found that both the level of *gsc::*mEGFP expression and average contact duration were diminished in *e-cadherin* morphant compared to control ppl cells (Fig. 3.4.1b), consistent with our hypothesis of cell-cell contact duration promoting ppl cell fate specification. To further test whether Nodal signaling controls the positive feedback loop between ppl cell-cell contact duration and cell-fate specification, as suggested by our *in vitro* experiments (sections 3.2 and 3.3), we analyzed if increasing Nodal signaling in ppl cells *in vivo* would promote both cell-cell contact duration and ppl cell fate specification. To specifically increase Nodal signaling in individual ppl progenitor *in vivo*, we took advantage of a light-activatable Nodal receptor (Opto-Actvr)[98], and transplanted a mixture of Opto-Actvr-expressing ppl cells and control cells expressing a version of the Nodal receptor insensitive to light activation from donor to host *Tg(gsc::mEGFP)* embryos (Fig. 3.4.1c, Video 4). We then triggered ectopic Nodal signaling in the transplanted Opto-Actvr expressing ppl cells by exposure of the transplanted embryo to LED light and monitored cell-cell contact duration and *gsc* expression in the light activated versus control cells (Fig. 3.4.2). Strikingly, we found that both the duration of cell-cell contacts and the level of *gsc::*mEGFP expression was strongly increased in the light-activated cells (Fig. 3.4.1d, 3.4.2e-g), supporting the notion that Nodal signaling plays an important role in mediating the interplay between ppl cell-cell contact duration and cell fate specification. Interestingly, cell-cell contact duration was increased in light activated cells only after a certain time delay, indicating that it could be due to a transcriptional response (Fig. 3.4.2e-g). Moreover, gsc::mEGFP expression in these assay was lower than in the single transplantation assay (Fig. 3.1.2 h,i), probably due to our analysis of a later time window, to maximize the effects of cell adhesion and Nodal signaling manipulation.

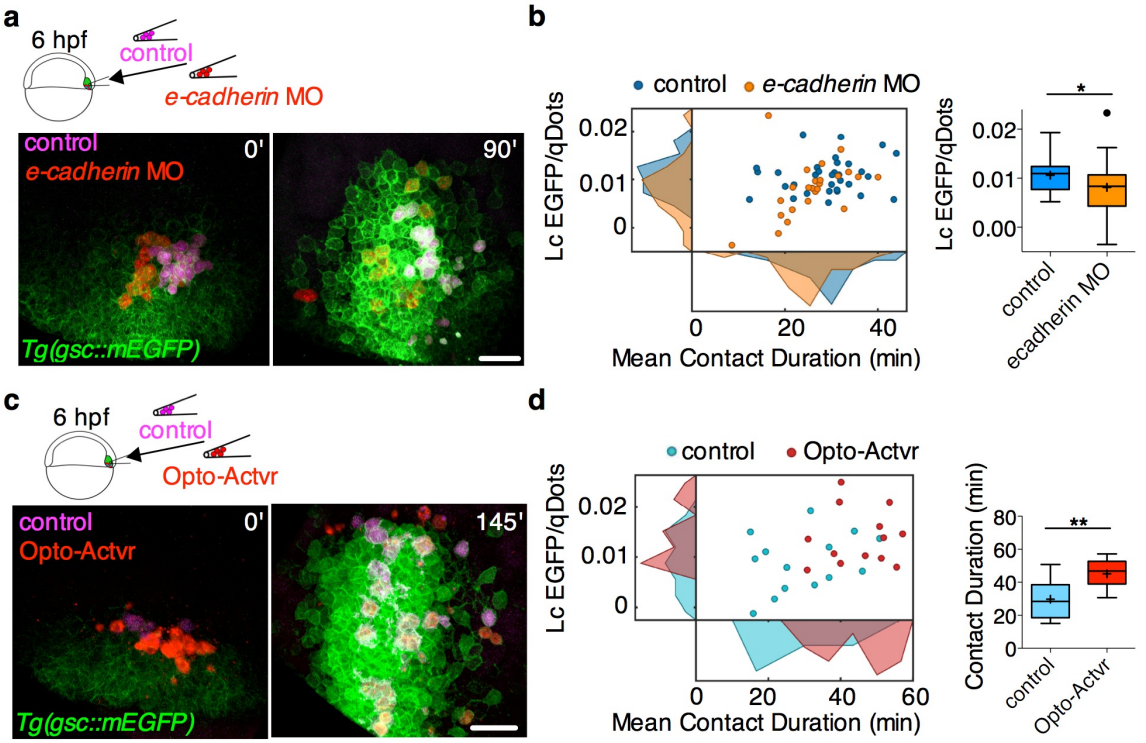

Fig. 3.4.1 - Mutual enhancement between prechordal plate cell-cell contact formation and Nodal signaling *in vivo*.
(**a**) Representative multi-photon images of ppl cells transplanted from *Tg(gsc::mEGFP)* embryos injected with either control MOs, qDots and dextran-Cascade Blue (control cells) or *e-cadherin* MOs and qDots (*e-cadherin* morphant cells) into similar staged WT *Tg(gsc::mEGFP)* embryos. Transplantation was performed at shield stage (6 hpf) and images were taken between 65% epiboly stage (7 hpf) and 75% epiboly stage (8 hpf). Scale bar, 50 μm (**b**) Linear coefficient (Lc) of gsc::mEGFP/qDots increase as a function of mean contact duration for transplanted control and *e-cadherin* morphant cells between 7 and 8 hpf. Frequency distributions of linear coefficients and mean contact durations are shown on the respective axes. Lc values are also shown as Tukey box-and-whiskers plots. n (control cells), 33; n (e-cadherin morphant cells) 24; 2 independent experiments. Statistical test, Student t test, two tailed. P value, *< 0.05. (**c**) Representative multi-photon images of ppl cells transplanted from *Tg(gsc::mEGFP)* embryos injected with either mRNA encoding for a chemically-activated form of Actvr1, qDots and dextran-cascadeblue (control cells) or mRNA encoding for a light-activated form of Actvr1 and qDtos (Opto-Actvr1 cells) into similar staged WT *Tg(gsc::mEGFP)* embryos. Transplantation was performed at shield stage (6 hpf) and images were taken between 75% epiboly stage (8 hpf) and 90% epiboly stage (9hpf). Scale bar, 50 μm. (**d**) Linear coefficient (Lc) of gsc::mEGFP/qDots increase as a function of mean contact duration for transplanted control and Opto-Actvr1 expressing cells between 8 and 9 hpf. Frequency distributions of linear coefficients and mean contact durations are shown on the respective axes. Mean contact durations are also shown as Tukey box-and-whiskers plots. n (control cells), 14; n (Opto-Actvr1 cells), 13; 2 independent experiments. Statistical test, Student t test, two tailed. P value, **< 0.01. The control and Opto-Actvr1 were cloned and optimized by Keisuke Sako.

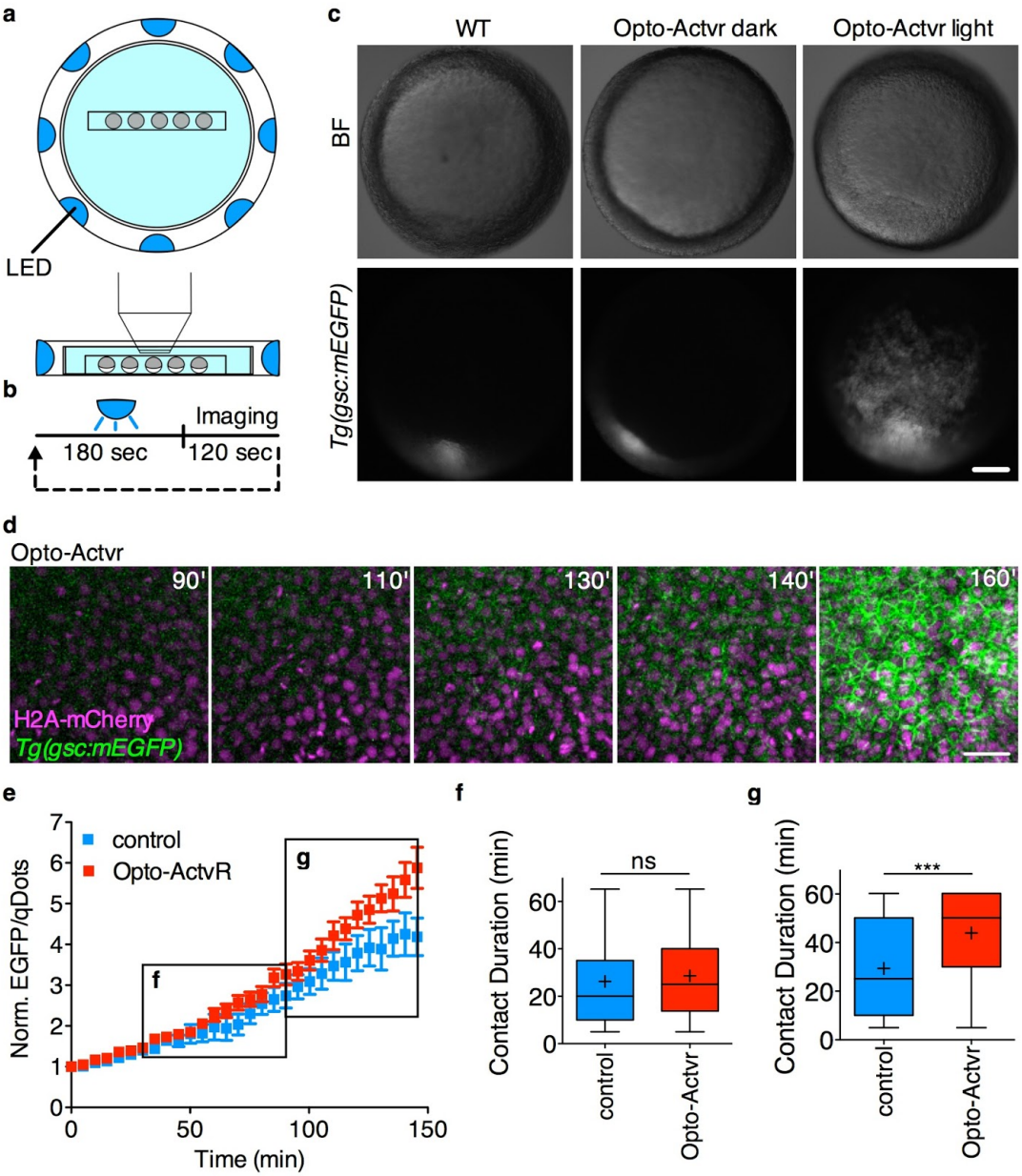

Fig.3.4.2 - Light activation of Opto-Actvr expressing prechordal plate progenitor cells

(**a**) Schematic representation of the LED illumination system coupled to a multi-photon imaging setup. (**b**) The sample was exposed to LED light for 180 sec and then imaged for 120 sec. These cycles were repeated for a period of 160 min. (**c**) Stereoscope images of *Tg(gsc::mEGFP)* embryos ubiquitously expressing Opto-Actvr. WT *Tg(gsc::mEGFP)* or *Tg(gsc::mEGFP)* embryos injected with Opto-Actvr mRNA were imaged from sphere stage (3 hpf) to shield stage (6 hpf) with a multi-photon microscope coupled to a LED illumination system. Control *Tg(gsc::mEGFP)* embryos injected with Opto-Actvr mRNA were kept in a light tight box for the duration of the experiment (Opto-Actvr dark). Images were taken at shield stage (6 hpf). Scale bar, 100 μm. (**d**) Representative images of a time-lapse recording of a *Tg(gsc::mEGFP)* embryo ubiquitously expressing Opto-Actvr and H2A-mCherry. Images were taken between sphere stage (3 hpf) and shield stage (6 hpf), alternating LED illumination and imaging. Animal pole views with cells ectopically expressing *gsc*::mEGFP. Scale bar, 40 μm (**e**) *gsc*::EGFP expression in ppl cells transplanted from *Tg(gsc::mEGFP)* embryos injected with mRNA encoding for a chemically-activated form of Actvr1 together with qDots and dextran-cascadeblue (control cells) or Opto-Actvr1 mRNA together with qDots (Opto-Actvr1 cells) into similarly staged WT *Tg(gsc::mEGFP)* host embryos. Transplantation was performed at shield stage (6 hpf) and images were taken between 60% epiboly stage (6.5 hpf) and 90% epiboly stage (9hpf). Average EGFP/qDots ratios were computed for each cell, normalized on the first imaging time point and plotted as a function of time. n (control cells), 14; n (Opto-Actvr1 cells), 13; 2 independent experiments. (**f-g**) Cell-cell contact duration in transplanted ppl cells. Cell-cell contacts formed between transplanted ppl donor cells and host cells were tracked between (**f**) 65% epiboly stage (7 hpf) and 80% epiboly (8 hpf) stages and (**g**) between 80% epiboly (8 hpf) and 90% epiboly stages (9 hpf). In (g) n (control), 173; n (Opto-Actvr), 146; In (f) n (control), 159; n (Opto-Actvr), 113; 2 independent experiments. Statistical test, Mann Whitney t-tes; P values, ***< 0.001, ns = not significant.
Optimization of Opto-Actvr light activation was performed by Keisuke Sako.

3.5 Stochastic modeling of the positive feedback loop between cell-cell contact formation and nodal signaling

3.5.1 Model rational and parametrization based on *in vitro* data

To formally test the plausibility of our assumption that a positive feedback loop between cell-cell contact duration and Nodal signaling determines ppl cell fate specification within the gastrulating embryo, we constructed a stochastic model *in silico* describing the interactions between cell-cell contact duration, Nodal signaling and ppl cell fate specification. Following our experimental observations, we assume in our model (Fig. 3.5.1a) that components of the Nodal signaling pathway accumulate at ppl cell-cell contacts. Once this accumulation reaches a sufficient level, the cell-cell contact starts to trigger Nodal signaling by increasing the rate of Smad2 phosphorylation resulting in higher Smad2 nuclear-to-cytoplasmic ratios. Nuclear Smad2, in turn, promotes transcription of *gsc* and other downstream genes.

The parameters of the model, corresponding to the effect of cell-cell contacts on Smad2 nuclear localization and subsequent gene transcription, were identified based on our experimental data of cultured primary progenitor cells. To measure the dynamics of accumulation of nodal pathway components at cell-cell contacts, we analysed the accumulation of nodal ligand in Ndr2-EGFP expressing cells upon contact formation as a function of time (Fig. 3.5.1b, Video 5). We found that the accumulation of Ndr2-EGFP at cell-cell contact is well described by an exponential curve, with the time of half-maximal accumulation representing the time after which half of newly formed cell-cell contacts actively increase Smad2 phosphorylation (Fig. 3.5.1c). Modeling of Smad2 nuclear import and export dynamics were based on a previously published model[218] and the relevant parameters were adjusted to the characteristics of ppl cells. In particular, Smad2 nuclear import and export rates in the absence of nodal signaling were derived from measurements of Smad2-EGFP nuclear-to-cytoplasmic ratios in cells isolated from MZ*oep* embryos, defective for Nodal signaling (Fig. 3.5.1d). To determine the extent of increased Smad2 phosphorylation due to one long lasting cell-cell contact, we isolated ppl cells from *Tg(gsc::tRFP)* embryos also expressing Smad2-EGFP at 6 hpf and compared Smad2 nuclear-to cytoplasmic ratios of single cells and doublets in culture (Fig. 3.5.1e).

We then tested our partial model, accounting for the effect of cell-cell contact on Nodal signaling but not for Nodal signaling promoting cell-cell contact formation, simulating Smad2 nuclear accumulation and *gsc*::mEGFP dynamics in single ppl cells and doublets in culture. Even though the values of the parameters were tightly constrained by previously

published data[89], the dynamics of Smad2 nuclear accumulation and *gsc* expression in our stochastic model showed remarkable quantitative agreement with the experimentally observed dynamics in single ppl progenitor cells as well as cell doublets *in vitro* (Fig. 3.5.1e).

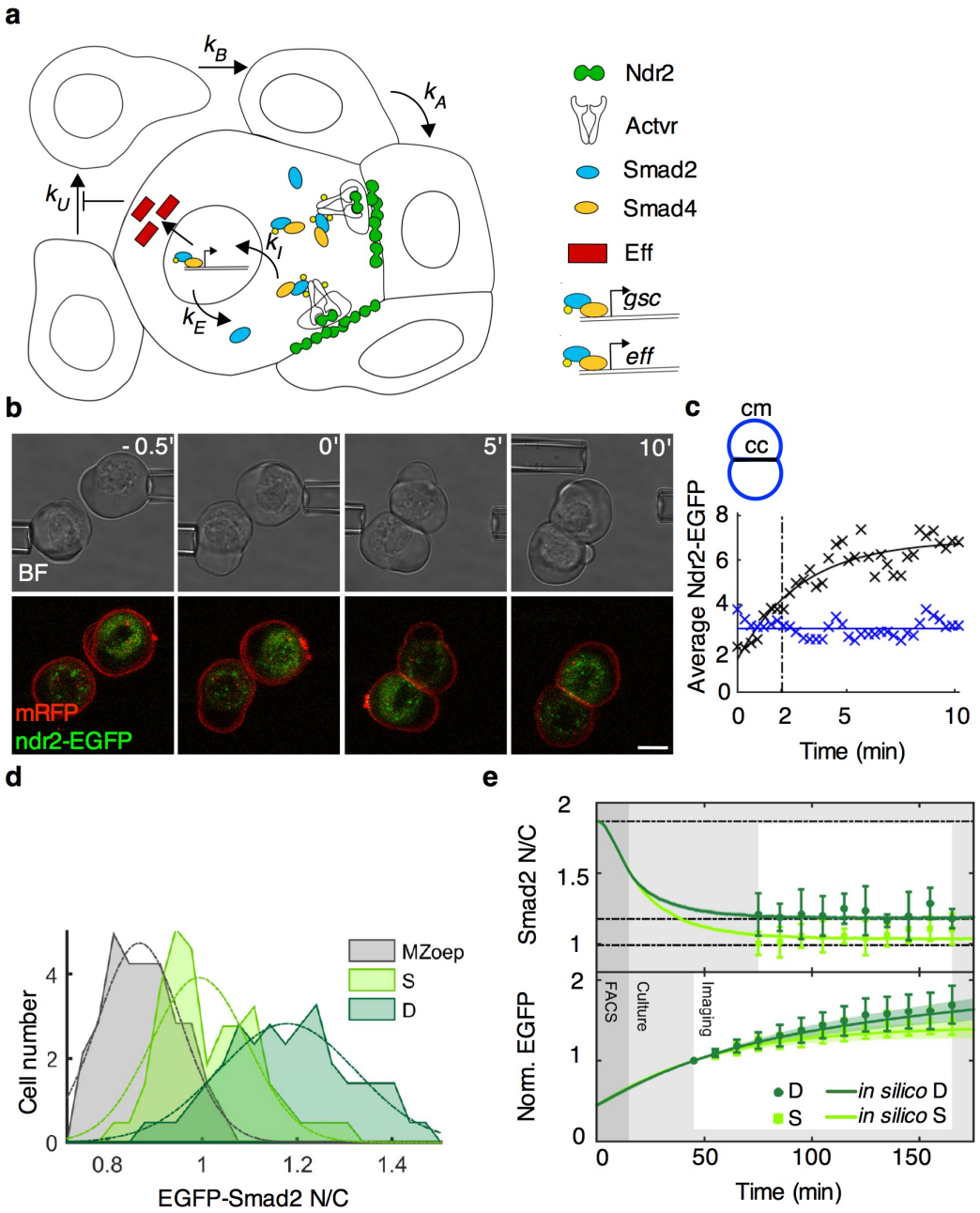

Fig. 3.5.1 - A stochastic model for ppl cell-cell contact formation and nodal signaling *in vitro*
(**a**) In silico modelling of the positive feedback loop between cell-cell contact formation and Nodal signaling. (**b-c**) Dynamics of Nodal accumulation at cell-cell contact sites. (**b**) Bright-field and confocal images of cell-cell contact formation between ppl progenitor cells in culture. Induced ppl progenitor cells were isolated from shield stage (6 hpf) embryos expressing Ndr2-EGFP and mRFP. Cell-cell contact formation was initiated by gently bringing two cells together using micropipettes, and the newly formed cell doublet was imaged over a period of 10 min at 30 sec intervals. Scale bar, 5 μm (**c**) Example of Ndr2-EGFP localization in a newly formed ppl cell doublet. Average Ndr2-EGFP intensities at the cell-cell (cc, black crosses) and cell-medium (cm, blue crosses) interfaces. Exponential fit on Ndr2-EGFP intensities at cc (black curve) and linear fit of Ndr2-EGFP intensities at cm (blue line). (**d**) Frequency distributions of EGFP-Smad2 nuclear-to-cytoplasmic (N/C) ratios of embryonic progenitor cells in culture,isolated via FACS from shield stage (6 hpf) MZ*oep* mutant embryos expressing EGFP-smad2 and H2A-mCherry or from shield stage (6 hpf) *Tg(gsc::tRFP)* embryos also expressing EGFP-Smad2 and H2B-BFP. n (MZ*oep*), 14; n (single cells), 22; n (doublets), 21; 3 independent experiments.(**e**) Experimentally observed and model predictions for Smad2 nuclear localization and gsc::mEGFP expression in single ppl cells (S) versus doublets (D) obtained from shield stage embryos (6 hpf) as a function of time since cell isolation from the embryo. Experimental data points are shown as green squares (doublets) and dots (single cells), error bars show STDV. n (Smad2 N/C, single cells), 22; n (Smad2 N/C, doublets), 21; 3 independent experiments. n (gsc::EGFP, single cells), 41; n (gsc::EGFP, doublets), 40; 5 independent experiments. Green lines and filled areas show mean values and STDV of model predictions. n (simulated single cells), 100; n (simulated doublets), 100. Curve fitting, modeling and simulation by Moritz Lang.

3.5.2 Stochastic modeling predicts cell-cell contact and goosecoid expression dynamics of ppl cells *in vivo*

We next asked whether our model, which was identified based exclusively on *in vitro* data, could also qualitatively reproduce the dynamic effects of the feedback mechanism between cell-cell contact duration and *gsc* expression within ppl cells *in vivo.* Since the molecular details by which Nodal signaling affects cell-cell contact duration are not yet fully understood, we assumed that Smad2 acts as a transcriptional activator of a yet unidentified factor (Eff) controlling cell-cell contact formation (Fig. 3.5.1a). We assumed the simplest possible relation between the concentration of Eff and contact duration, namely that the adhesion energy linearly depends on the concentration of Eff. Eff is assumed to have the same maturation time as EGFP (30 min) and a short half-life (also 30 min). We further assumed that the rate of cell-cell unbinding decreases exponentially with the adhesion energy, while all other parameters were kept at their respective values identified from the *in vitro* experiments (for more details see Supplementary Note - Appendix 1). We then assumed that multiple cell-cell contacts have additive effects on Smad2 phosphorylation and we measured the average number of contacts for ppl cells in vivo. To this aim, we imaged *Tg(gsc::mEGFP)* embryos also expressing the nuclear marker H2A-mCherry and used the nuclear signal to define a three dimensional center point for each ppl cell (Fig 3.5.2.1a). We then used those center points as the nodes of a Delaunay triangulation and the number of edges connected to each node (number of neighbours) as a measure of the number of simultaneous cell-cell contacts for each ppl cell (Fig 3.5.2.1b). We found that cell-cell contact numbers are well described by a binomial distribution with average and maximum number of cell-cell contacts equal to 8.1 and 16, respectively (Fig. 3.5.2.1c). Finally, we derived the average rates of cell-cell binding and unbinding within the ppl from our analysis of cell-cell contact durations of transplanted ppl cells *in vivo* (Fig. 3.1.2f,g, Supplementary Note - Appendix 1).

Simulations of the complete model led to a remarkably close qualitative match between experimentally observed and theoretically predicted values of *gsc* expression levels as a function of cell-cell contact duration in ppl progenitors *in vivo* (Fig. 3.5.2.1d). Together, these findings strongly support the plausibility of our assumption that a positive feedback loop between cell-cell contact duration and Nodal signaling controls ppl cell fate specification during gastrulation.

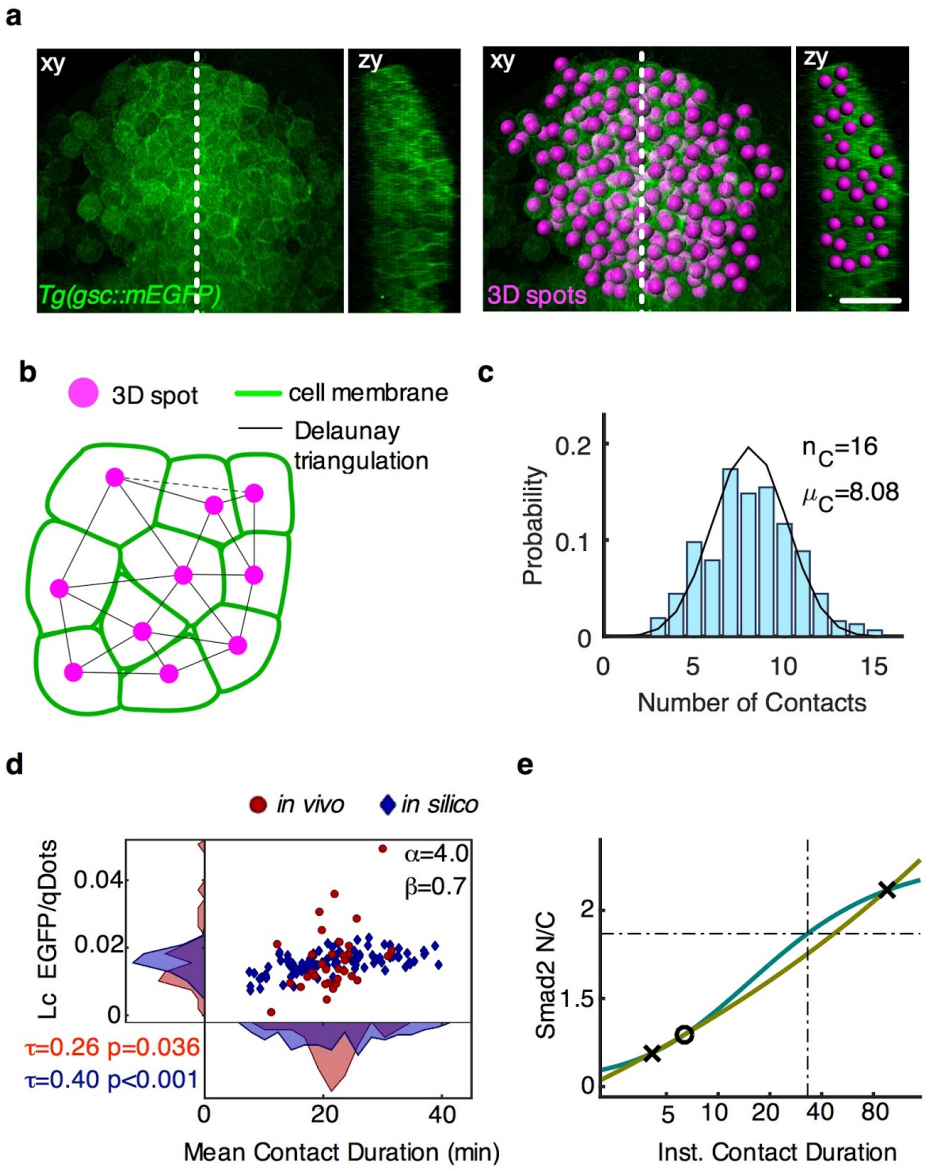

Fig. 3.5.2.1 Stochastic modeling predicts cell-cell contact and *goosecoid* expression dynamics of ppl cells *in vivo*
(**a**) Multi-photon images of the ppl of *Tg(gsc::mEGFP)* embryos at 65% epiboly stage (7 hpf). A 3D spot object was created at the center of each ppl cell, shown in magenta. Scale bar, 50 μm (**b**) Quantification of cell-cell contact number within the ppl *in vivo*. A Delaunay triangulation was computed using 3D coordinates of the spots and used to infer the number of cell-cell contacts (direct neighbours) of each cell. All edges whose midpoint was closer to another vertex than it was to one of its end vertices were eliminated from the triangulation (dotted edge). (**c**) Probability distribution of ppl cells as a function of their number of cell-cell contacts *in vivo*. Black curve shows the fit for a binomial distribution with a maximum and an average number of contacts of 16 and 8.08, respectively. (**d**) In vivo observed (red circles) and in silico simulated (blue diamonds) correlation between mean cell-cell contact durations and the linear coefficient (Lc) of gsc::mEGFP/qDots. The contact loss rate depends on the two parameters α and β, with α representing the sensitivity of cell-cell contact energy to the concentration of Eff, whereas β scales the propensity to lose a contact independently of the intrinsic state of a cell. Frequency distributions of linear coefficients and mean contact durations for both experimental data and model predictions are shown on the respective axes. n (experimental cells), 33; 4 independent experiments. n (simulated cells), 100. Kendall correlations (τ) and relative p-values (p) are shown. (**e**) Smad2 nuclear localization as a function of the instantaneous cell-cell contact duration (dark green), and instantaneous cell-cell contact duration as a function of Smad2 nuclear localization (light green) as predicted by the deterministic version of our model. The intersections of the curves (commonly referred to as "nullclines") correspond to stable (crosses) or unstable (circles) steady-states of the model when the positive feedback loop is closed. Modeling and simulations by Moritz Lang.

With a working model in hand, we further asked if the model can provide additional insight into the role of the feedback loop between cell-cell contact duration and Nodal signaling in ppl cell fate specification. Notably, we found that when assuming a dependency of the cell-cell unbinding rate on the Eff concentration leading to the best agreement of model predictions with the experimentally observed data (Fig. 3.5.2.1d, 3.5.2.2), the deterministic version of our model was bistable (Fig. 3.5.2.1e). Bistability is often associated to cellular decision making, with each of the stable steady-states corresponding, for example, to different cell fates [219]. However, stochastic models typically show rather gradual dynamic changes during the transition between mono- and bistable regions of the parameter space, in contrast to the sharp transition of deterministic models [220,221]. We found that our model lies in one such transition area, as small variations in the parameters resulted in the deterministic version of the model being monostable (Fig. 3.5.2.2). Translated to the situation within the ppl, the observation that the network is bistable, but also close to monostable, could mean that ppl cells remain sufficiently long in their respective state of cell-cell contact formation and associated *gsc* expression to decisively influence their fate. This reasoning was further supported by the observation that both *in vivo* and *in silico*, cells showing low *gsc::mEGFP* expression rates and low contact durations at the beginning of the experiment typically did not change their behavior until the end of the imaging period (Figs. 3.1.2c-e and 3.7.1a).

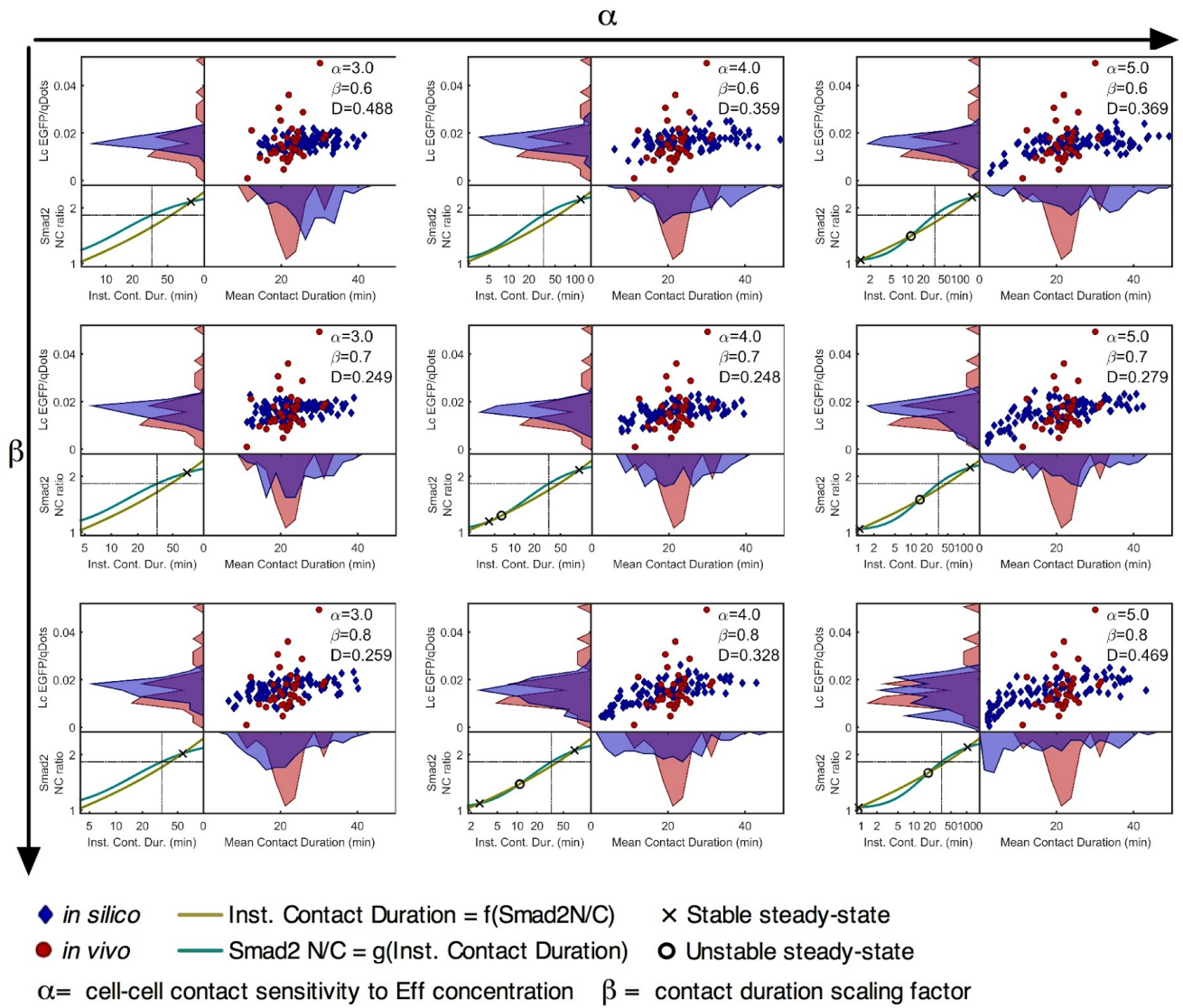

Fig. 3.5.2.2 - Parameter optimization of closed-loop model

In vivo observed (red circles) and *in silico* simulated (blue diamonds) correlation between mean cell-cell contact durations and the linear coefficient (Lc) of *gsc*::mEGFP/qDots, for increasing values of α (columns) and β (rows). The strength of the feedback loop increases as α increases, whereas β scales the propensity to lose a contact independently of the intrinsic state of a cell. Probability distributions of linear coefficients and mean contact durations for both experimental data and model predictions are shown on the respective axes. Insets, Smad2 nuclear localization as a function of the average cell-cell contact duration (dark green), and average instantaneous contact duration as a function of Smad2 nuclear localization (light green) as predicted by the deterministic version of our model. The intersections of the curves (commonly referred to as "nullclines") correspond to stable (crosses) or unstable (circles) steady-states of the model when the positive feedback loop is closed. The values α=4 and β=0.7 lead to the smallest Kolmogorov–Smirnov distance D=T |FD(T)-FS(T)| between the empirical distributions FD(T) and FS(T) of the observed and simulated mean contact durations T, which was used as the cost function for optimization. n (experimental cells), 33; 4 independent experiments. n (simulated cells), 100, for each combination of α and β. Modeling and simulation by Moritz Lang

3.6 A positive feedback loop between prechordal plate cell-cell contact formation and Nodal signaling determines cell fate specification.

Previous and our own observations suggest that the ppl gives rise to both mesoderm and endoderm structures of the zebrafish head [47,94,222], and that the duration of Nodal signaling determines whether cells within the region of the anterior axial mesendoderm remain within the ppl or turn into endoderm progenitors[98]. Based on our model predictions, we thus hypothesized that ppl cells displaying either long contact times and high *gsc* expression levels or very short contact times and low *gsc* expression levels remain sufficiently long in their respective states in order to influence, or even determine, whether they become ppl or endoderm. To test this hypothesis, we monitored simultaneously the expression of *gsc*, as a marker for ppl cell fate specification, and *sox17*, as a marker for endoderm specification, within the individual cells of the forming ppl in double transgenic *Tg(gsc::tRFP)*;*Tg(sox17::EGFP)* embryos from shield to 75% epiboly stage (6-8 hpf; Fig. 3.6.1a, Video 6). Consistent with our previous observations, we found that cells were either positioned in the bulk of the ppl expressing high levels of *gsc::*tRFP and low levels of *sox17::*EGFP*,* or were found outside of the ppl expressing only very low levels of *gsc::*tRFP and high levels of *sox17::*EGFP[98]. We further observed that *gsc::*tRFP expressing cells were occasionally leaving the ppl plate cell cluster and switching on *sox17:*EGFP expression (Fig. 3.6.1a, Video 6). Interestingly, those leaving cells displayed considerably shorter contact duration with neighboring cells when compared to cells that remained within the ppl (Fig. 3.6.1b), suggesting that reduced ppl cell-cell contact duration leads to ppl cells turning into endoderm. To further test whether the proportion of *sox17* expressing cells leaving the ppl is under the control of a positive feedback loop between cell-cell contact duration and Nodal signalling, we analyzed the proportion of *sox17::*EGFP positive cells in experiments where we transplanted a mixture of control and *e-cadherin* morphant ppl cells from donor to host *Tg(sox17::EGFP)*[197] embryos (Fig. 3.6.1c). We found an increased proportion of *sox17::*EGFP positive cells originating from transplanted *e-cadherin* morphant cells compared to control cells (Fig. 3.6.1d), suggesting that reducing ppl cell-cell contact duration increases their likelihood of becoming endoderm. Finally, we determined the proportion of *sox17:*EGFP positive cells in experiments where we transplanted a mixture of control and Opto-Actvr-expressing ppl cells from donor to host *Tg(sox17:EGFP*) embryos. Consistent with the notion that Nodal signaling mediates the positive feedback loop between cell-cell contact duration and ppl cell fate specification, we found that after light-

activation of Nodal signaling in the transplanted cells, their likelihood of leaving the ppl and turning into *sox17* expressing endoderm cells was reduced (Fig. 3.6.1d). Taken together, these results suggest that the positive feedback loop between ppl cell-cell contact duration and Nodal signaling within the ppl controls whether cells become mesoderm or endoderm.

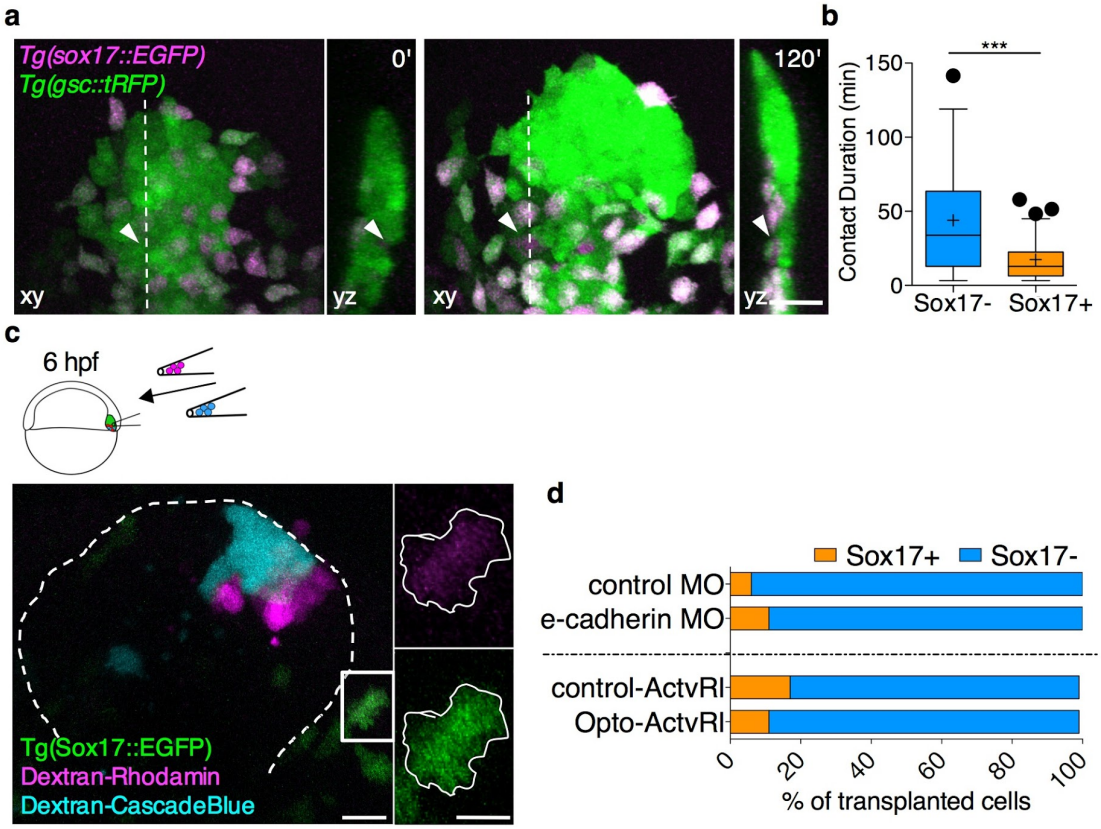

Fig. 3.6 - A positive feedback loop between prechordal plate cell-cell contact formation and Nodal signaling determines cell fate specification.
(**a**) Representative images of cells within the ppl of *Tg(gsc::tRFP);Tg(sox17::EGFP)* embryos at shield (6 hpf, 0 min) and 75% epiboly stages (8 hpf, 120 min). Each image contains a planar x,y view (left) of the ppl and y,z cross-section (right) through the ppl at the level indicated by the dashed white line in the planar view. Arrowheads indicate a tracked ppl cell eventually expressing sox17::EGFP. Scale bar, 50 μm. (**b**) Average contact durations for ppl cells either remaining within the ppl or ppl cells that are about to leave the ppl and turn into *sox17*::EGFP expressing endoderm cells. Values are shown as Tukey box-and-whiskers plots with median (bar) and average (cross) values. n (sox17-), 56; n (sox17+), 85. Statistical test, Mann Whitney t test, two tailed. P value: ***<0.001 (**c**) Representative confocal image of the ppl of a *Tg(sox17::EGFP)* host embryo at 90% epiboly stage (9 hpf) containing a mix of transplanted ppl cells from *Tg(sox17::EGFP)* donor embryos injected with either dextran-Rhodamine or dextran-Cascade Blue. Transplantation was performed at shield stage (6 hpf) and images were taken at 90% epiboly stage (9 hpf). Dashed line, ppl outline. Scale bar, 50 μm. Insets, transplanted cell expressing *sox17*::EGFP with its shape outlined in white. Scale bar, 20 μm. (**d**) Relative distribution of *sox17*::EGFP positive versus negative cells within the population of transplanted ppl cells for 2 different experimental setups: in the first experiment, a mix of control cells expressing control MOs and experimental cells expressing *e-cadherin* MOs were transplanted. n (control transplanted cells), 174;n (*e-cadherin*-MO transplanted cells), 112; 2 independent experiments. In the second experiment, a mix of control cells expressing a chemically inducible Actvr1 and experimental cells expressing a light-activatable Opto-Actvr1 were transplanted followed by exposition of the transplanted embryos to blue LED light. n (control transplanted cells), 140; n (Opto-Actvr1 transplanted cells), 113; 3 independent experiments.

3.7 Model prediction: isolation of ppl increases the likelihood of acquiring endoderm fate

One key prediction of our stochastic model is that the duration of past cell-cell contacts is memorized by the molecular state of ppl cells long after the respective contacts ceased to exist. As a consequence, the model also predicted that temporarily preventing cell-cell contact formation might represent a sufficiently strong perturbation to have a significant effect on the later specification of those cells (Fig. 3.7.1a). To test this model prediction, we isolated ppl cells from Tg(sox17:EGFP) embryos and kept them in isolation for a prolonged period of time before transplanting them into the ppl of a WT host embryo. Consistent with the model predictions, we found that the likelihood of transplanted ppl cells to transform into endoderm was increased in cells kept in isolation for 20min before transplantation when compared to control cells that were transplanted immediately after isolation from the donor embryo (Fig. 3.7.1b-d). However, transplanted ppl cells tend to express sox17::EGFP at lower (as in Fig 3.7.1c) or higher (in other cases) levels than host endoderm cells. This may be due to asynchrony between donor and host ppl cells or to transplanted ppl cells initiating sox17 expression at variable times. Moreover, it is difficult to decide on the statistical significance of the results presented here and in the previous paragraph as, at the best of my knowledge, there are no accepted statistical tests that apply to this experimental set up (multiple tests of the effect of a treatment on population percentages). However, the result that prolonged Nodal signaling promotes *gsc* expression over *sox17* has been independently shown in Sako et al[98]. Also the fact that impaired cell-cell adhesion is responsible for an increase in *sox17* positive ppl cells is shown here with two independent experimental approaches (Fig. 3.6 and 3.7). The greater effect observed following isolation of ppl could be due to a more dramatic disruption of cell-cell contacts or to the cumulative effect of impairing cell-cell contact and Nodal signaling. Taken together, these findings strongly support the view that the formation of durable cell-cell contacts constitutes a key mode of modulating the activity of Nodal signaling in inducing mesoderm and endoderm cell fates during zebrafish gastrulation. It also indicates that the right assumptions have been made and the appropriate parameters have been included in our model.

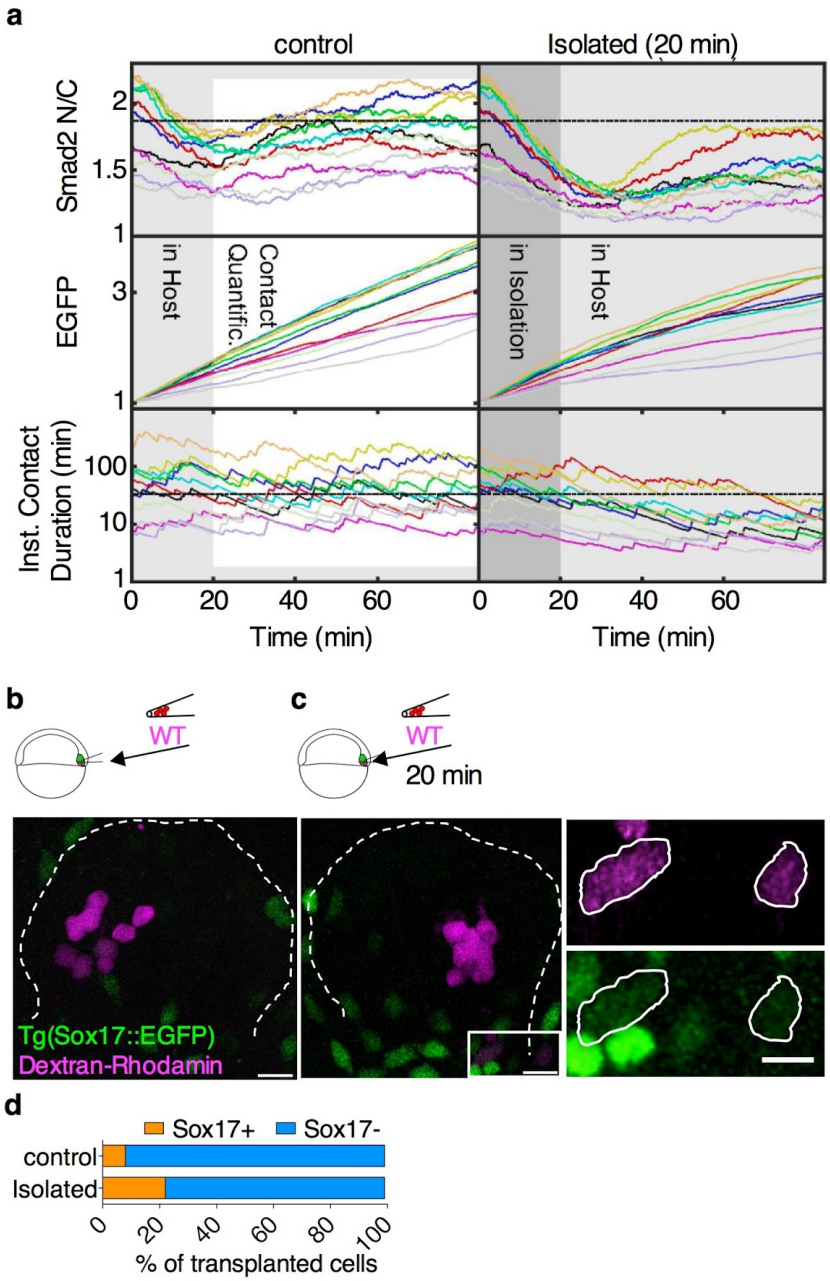

Fig. 3.7.1 - Ppl isolation induces endoderm fate

(**a**) Model predictions of the nuclear-to-cytoplasmic (N/C) ratio of Smad2, gsc::EGFP accumulation and instantaneous contact duration as a function of time for simulated cells. A transplantation experiment was simulated as an instantaneous (control) or prolonged (isolation, 20 min) loss of all cell-cell contacts, after which cells stochastically reacquired cell-cell contacts. Upper panels, simulated Smad2 N/C ratios for 11 realization of the model. Dashed line, estimated average Smad2 N/C ratio for unperturbed ppl cells *in vivo*. Middle panels, simulated gsc::EGFP levels. Lower panels, simulated instantaneous contact duration, i.e. the inverse of the contact loss rate. Dashed line, average instantaneous contact duration. (**b-d**) Experimental verification of model prediction.Representative confocal image of the ppl of a *Tg(sox17::EGFP)* host embryo at 90% epiboly stage (9 hpf) containing ppl cells from *Tg(sox17::EGFP)* donor embryos injected with dextran-Rhodamine transplanted immediately (**b**) or after 20 min isolation (**c**). Transplantation was performed at shield stage (6 hpf) and images were taken at 90% epiboly stage (9 hpf). Dashed line, ppl outline. Scale bar, 50 μm. Insets, transplanted cells expressing *sox17::*EGFP with their shape outlined in white. Scale bar, 20 μm. (**d**) Relative distribution of *sox17::*EGFP positive versus negative cells within the population of transplanted ppl cells for control cells and experimental cells that were kept for 20 min in isolation before transplanting. n (control transplanted cells), 89; n (isolated transplanted cells), 145; 3 independent experiments. Simulations and model predictions by Moritz Lang.

4 Discussion

Our results demonstrate that a positive feedback loop between cell-cell contact duration and Nodal signaling determines whether anterior axial mesendoderm cells either become ppl progenitors or endoderm progenitors. Positive feedback loops have previously been implicated in cell fate decisions, although in the large majority of those cases the positive feedback was thought to act on a transcriptional level [223–227]. Our data demonstrate that the regulation of cell fate decisions is not restricted to positive feedback loops at the transcriptional level, but represents a generic form or regulation spanning different scales of organization ranging from transcriptional control on a molecular level to cell-cell contact formation on a cellular and tissue scale.

We show that cell-cell contact formation causes a polarization of Nodal signaling pathway components, enhancing the competence of ppl cells to respond to Nodal signals. As the absence of specific antibodies or appropriate transgenic lines precludes the observation of the endogenous proteins, we assessed localization of over-expressed tagged versions of Nodal ligand and receptor, which may be artifactual. However, endogenous early endosomes, detected with EEA1, localize at cell-cell contacts suggesting that the subpopulation of Nodal signaling endosomes may also be polarized following cell-cell contact formation. This may result from directed transport of early endosomes or from longer half-life of endosomes at cell-cell contacts, or both. Experiments aimed at tracking endosomes will be required to determine the mechanisms underlying accumulation at cell-cell contact. However, we found that MZ*oep* ppl doublets exposed to Activin showed enhanced *gsc* expression compared to single cells, suggesting that cell polarization may increase Nodal signaling also independently from accumulation of ligand at cell-cell contacts. It is plausible that enrichment of early endosomes correlates with longer half-life of Nodal signaling endosomes, thereby resulting in increased Smad2 phosphorylation per active receptor. To test these hypotheses, It will be interesting to follow the localization of a tagged version of Activin and test if it persists in early endosomes for longer time in ppl cell doublets compared to single cells.

The use of Ndr2 over-expression, Activin and light activated receptors (Opto-Actvr) to increase Nodal signaling also raises the question of how do these treatments compare to the physiological levels and modes of Nodal pathway activation within the embryo. Unfortunately, levels of endogenous Nodal ligands or Nodal receptor activation have not

been described in the zebrafish embryo, due to a lack of specific antibodies and/or appropriate transgenic lines. While it is likely that our approaches entail activation of Nodal signaling at higher rate than in the embryo, we tuned our experimental conditions to compare to endogenous situation as much as possible: i) Mz*oep* cells exposed to Activin were selected via FACS sorting so that only cells that expressed gsc::mEGFP at the same levels of WT ppl cells were used for further experiments; ii) Ndr2-EGFP was over-expressed at the minimum level necessary to obtain homogeneously induced embryos; within these over-expression levels, highly expressing cells formed cell-cell contacts of size comparable to the ones formed by endogenous ppl cells and low expressing cells comparable to the overall mesendoderm cell population (Fig. 3.3.1b); iii) activation of Opto-Actvr was performed only after shield stage (6 hpf). Given that very little is known on Oep and ligand independent signaling by Nodal receptors it was not possible to devise an assay to control for such effects in following Opto-Actvr activation.

We further show that cell-cell contact formation promotes *gsc* expression in ppl cells in culture and within the embryo. We assume that the effect of one cell-cell contact, that we measure in culture, is additive, resulting in greater increase of *gsc* expression in ppl cells i*n vivo* compared to ppl cells in culture. However, comparing rates of gsc expression between ppl cells in culture and *in vivo* is problematic due to differences in the experimental setup (confocal microscope for *in vitro* assays, two-photon for *in vivo*), developmental time window analyzed (50-170 min after shield stage in culture, 30-90 min after shield stage *in vivo*) and data normalization. When computing *gsc::mEGFP* expression rates of ppl cells *in vivo* as fold increase, similar to the analysis of ppl cells in culture (Fig. 3.2.1), we find values ranging from 1.11 to 3.00. Therefore, the increase in *gsc::mEGFP* detected in ppl cells in culture (single cells, 1.5; doublets; 1.7) falls within this range. However, if cell-cell contact formation may affect cell fate of ppl cells in culture remains unclear. Given our finding that the proportion of ppl cells turning into endoderm and expressing *sox17* depends on cell-cell contact duration, it would be interesting to know if *sox17* expression is more likely in single cells compared to doublets in culture. Unfortunately, this analysis was precluded by *sox17::EGFP* being expressed only at later stages of development and by ppl cells surviving in culture only for limited time. It would be interesting to test if ppl cells transplanted in ectopic positions and devoid of cell-cell contacts are more likely to express *sox17* than ppl cells forming clusters.

Interestingly, our stochastic model proposes that cell-cell contact formation coupled to the accumulation of Nodal pathway components allows ppl cells to “measure” the average

duration of cell-cell contacts - as opposed to only the number of cell-cell contacts - by a mechanism closely resembling kinetic proofreading (Fig. 4.1 a,b). Kinetic proofreading was first proposed to explain the comparatively small error rates in biosynthetic processes like protein synthesis or DNA replication[228], but was later shown to also constitute a mechanism with which signaling pathways can discriminate between few specific receptor binding substrates with long binding durations, and many unspecific binding substrates with short binding durations [229]. In the latter, discrimination is based on one or more nearly irreversible activation reactions after formation of the substrate-receptor complex and before induction of downstream signaling. This effective time delay results in differential pathway activation of long and short binding substrates even if the respective substrate-receptor complexes have equal concentration. The dynamics of ppl cell-cell contact formation and loss closely resemble the dynamics of substrate-receptor binding and unbinding. In this case, the delay of Nodal pathway activation after cell-cell contact formation due to the necessary prior localization of Nodal signaling pathway components at the cell-cell contact sites takes the role of the irreversible activation reaction crucial for kinetic proofreading[228] (Fig. 4.1 b). Our model proposes that due to this effective kinetic proofreading scheme less than a quarter of all cell-cell contacts with an average duration of one minute lead to pathway activation, whereas more than three quarters of contacts with an average duration of ten minutes lead to pathway activation (Fig. 4.1c). This prediction is consistent with our observation that cell-cell contact duration rather than the absolute number of cell-cell contact scales with *gsc*::mEGFP expression in ppl cells (Fig. 3.1.2). Collectively, these findings suggest that kinetic proofreading, originally described in the context of molecular processes such as protein synthesis, DNA replication and receptor-ligand interaction, represents a generic concept also applicable to morphogenetic processes, such as cell-cell contact formation.

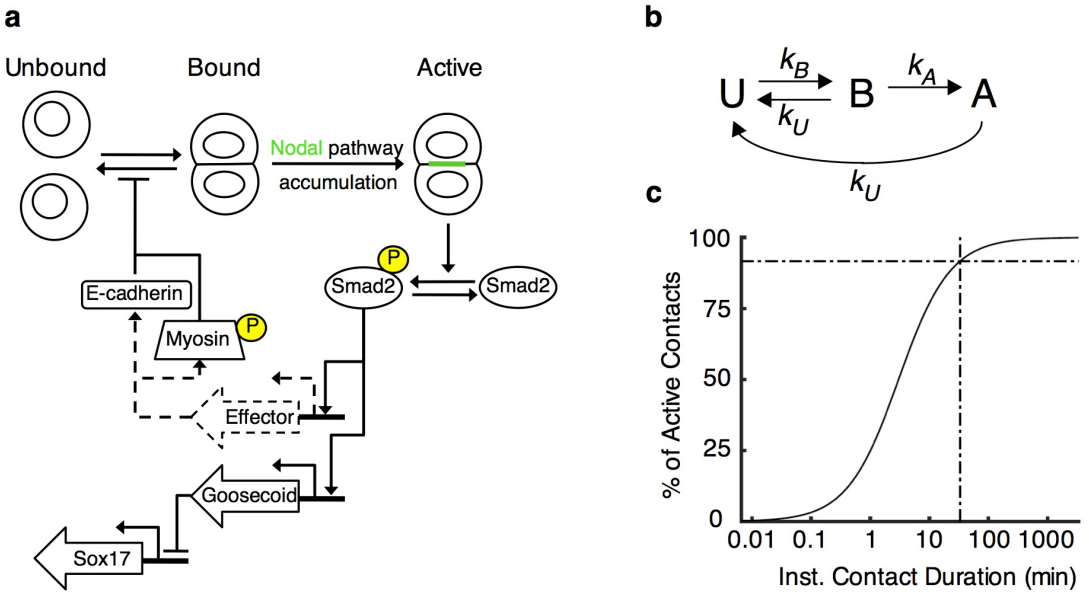

Fig. 4.1 - Positive feedback loop between cell-cell contact duration and nodal signaling: a multi-scale kinetic proofreading scheme

(**a**) Schematic representation of the positive feedback loop between cell-cell contact and nodal signaling. (**b**) Kinetic proofreading of ppl cells. The average number of cell-cell contacts $\langle B+A \rangle = \left(1+k_B/k_U\right)^{-1}$ only depends on the ratio between the contact formation rate constant k_B and the contact loss rate constant k_U, and is the same for cells forming many short or few long lasting contacts (i.e. when scaling k_B and k_U by the same constant). However, before a cell-cell contact increases Nodal signaling, components of the Nodal signaling pathway have to accumulate at the cell-cell contact site (rate constant k_A). Due to this time-delayed "activation" of contacts, cells can discriminate between short and long lasting contacts, even if the average number of contacts is the same. (**c**) Percentage of active cell-cell contact $\frac{A}{A+B} = \frac{k_A}{k_A+k_U}$ as a function of the instantaneous contact duration $T = k_U^{-1}$. Theory and simulation, Moritz Lang.

References

1. Waddington, C. H. *The strategy of the genes: a discussion of some aspects of theoretical biology*. (1957).
2. Conklin, E. G. *The Organization and Cell-lineage of the Ascidian Egg*. (1905).
3. Whittaker, J. R. Segregation during ascidian embryogenesis of egg cytoplasmic information for tissue-specific enzyme development. *Proc. Natl. Acad. Sci. U. S. A.* **70,** 2096–2100 (1973).
4. Nishida, H. & Sawada, K. macho-1 encodes a localized mRNA in ascidian eggs that specifies muscle fate during embryogenesis. *Nature* **409,** 724–729 (2001).
5. Wikramanayake, A. H., Huang, L. & Klein, W. H. beta-Catenin is essential for patterning the maternally specified animal-vegetal axis in the sea urchin embryo. *Proc. Natl. Acad. Sci. U. S. A.* **95,** 9343–9348 (1998).
6. Logan, C. Y., Miller, J. R., Ferkowicz, M. J. & McClay, D. R. Nuclear beta-catenin is required to specify vegetal cell fates in the sea urchin embryo. *Development* **126,** 345–357 (1999).
7. Weitzel, H. E. *et al.* Differential stability of beta-catenin along the animal-vegetal axis of the sea urchin embryo mediated by dishevelled. *Development* **131,** 2947–2956 (2004).
8. Kelly, C., Chin, A. J., Leatherman, J. L., Kozlowski, D. J. & Weinberg, E. S. Maternally controlled (beta)-catenin-mediated signaling is required for organizer formation in the zebrafish. *Development* **127,** 3899–3911 (2000).
9. Bellipanni, G. *et al.* Essential and opposing roles of zebrafish beta-catenins in the formation of dorsal axial structures and neurectoderm. *Development* **133,** 1299–1309 (2006).
10. Heasman, J. *et al.* Overexpression of cadherins and underexpression of beta-catenin inhibit dorsal mesoderm induction in early Xenopus embryos. *Cell* **79,** 791–803 (1994).
11. Fagotto, F., Guger, K. & Gumbiner, B. M. Induction of the primary dorsalizing center in Xenopus by the Wnt/GSK/beta-catenin signaling pathway, but not by Vg1, Activin or

Noggin. *Development* **124,** 453–460 (1997).

12. Nishida, H. Developmental potential for tissue differentiation of fully dissociated cells of the ascidian embryo. *Rouxs. Arch. Dev. Biol.* **201,** 81–87 (1992).
13. Nishida, H. Cell fate specification by localized cytoplasmic determinants and cell interactions in ascidian embryos. *Int. Rev. Cytol.* **176,** 245–306 (1997).
14. Goldstein, B. Establishment of gut fate in the E lineage of C. elegans: the roles of lineage-dependent mechanisms and cell interactions. *Development* **118,** 1267–1277 (1993).
15. Goldstein, B. Induction of gut in Caenorhabditis elegans embryos. *Nature* **357,** 255–257 (1992).
16. Tassy, O., Daian, F., Hudson, C., Bertrand, V. & Lemaire, P. A quantitative approach to the study of cell shapes and interactions during early chordate embryogenesis. *Curr. Biol.* **16,** 345–358 (2006).
17. Picco, V., Hudson, C. & Yasuo, H. Ephrin-Eph signalling drives the asymmetric division of notochord/neural precursors in Ciona embryos. *Development* **134,** 1491–1497 (2007).
18. Wu, M. Y. & Hill, C. S. TGF-β Superfamily Signaling in Embryonic Development and Homeostasis. *Dev. Cell* **16,** 329–343 (2009).
19. Rogers, K. W. & Schier, A. F. Morphogen gradients: from generation to interpretation. *Annu. Rev. Cell Dev. Biol.* **27,** 377–407 (2011).
20. Gurdon, J. B., Harger, P., Mitchell, A. & Lemaire, P. Activin signalling and response to a morphogen gradient. *Nature* **371,** 487–492 (1994).
21. Yu, S. R. *et al.* Fgf8 morphogen gradient forms by a source-sink mechanism with freely diffusing molecules. *Nature* **461,** 533–536 (2009).
22. White, R. J., Nie, Q., Lander, A. D. & Schilling, T. F. Complex regulation of cyp26a1 creates a robust retinoic acid gradient in the zebrafish embryo. *PLoS Biol.* **5,** e304 (2007).
23. Hagos, E. G. & Dougan, S. T. Time-dependent patterning of the mesoderm and

endoderm by Nodal signals in zebrafish. *BMC Dev. Biol.* **7,** 22 (2007).

24. Stern, C. D. *Gastrulation: From Cells to Embryo*. (CSHL Press, 2004).
25. Larsen, E. & McLaughlin, H. M. The morphogenetic alphabet: lessons for simple-minded genes. *Bioessays* **7,** 130–132 (1987).
26. Shook, D. R. & Keller, R. Morphogenic machines evolve more rapidly than the signals that pattern them: lessons from amphibians. *J. Exp. Zool. B Mol. Dev. Evol.* **310,** 111–135 (2008).
27. Sherrard, K., Robin, F., Lemaire, P. & Munro, E. Sequential activation of apical and basolateral contractility drives ascidian endoderm invagination. *Curr. Biol.* **20,** 1499–1510 (2010).
28. Leptin, M. & Grunewald, B. Cell shape changes during gastrulation in Drosophila. *Development* **110,** 73–84 (1990).
29. Sweeton, D., Parks, S., Costa, M. & Wieschaus, E. Gastrulation in Drosophila: the formation of the ventral furrow and posterior midgut invaginations. *Development* **112,** 775–789 (1991).
30. Martin, A. C. & Goldstein, B. Apical constriction: themes and variations on a cellular mechanism driving morphogenesis. *Development* **141,** 1987–1998 (2014).
31. Shook, D. R. & Keller, R. Epithelial type, ingression, blastopore architecture and the evolution of chordate mesoderm morphogenesis. *J. Exp. Zool. B Mol. Dev. Evol.* **310,** 85–110 (2008).
32. Montero, J.-A. *et al.* Shield formation at the onset of zebrafish gastrulation. *Development* **132,** 1187–1198 (2005).
33. Lyons, D. C., Kaltenbach, S. L. & McClay, D. R. Morphogenesis in sea urchin embryos: linking cellular events to gene regulatory network states. *Wiley Interdiscip. Rev. Dev. Biol.* **1,** 231–252 (2011).
34. Martins, G. G., Summers, R. G. & Morrill, J. B. Cells are added to the archenteron during and following secondary invagination in the sea urchin Lytechinus variegatus. *Dev. Biol.* **198,** 330–342 (1998).

35. Hart, N. H. & Donovan, M. Fine structure of the chorion and site of sperm entry in the egg ofBrachydanio. *J. Exp. Zool.* **227,** 277–296 (1983).
36. Kloc, M., Bilinski, S. & Etkin, L. D. The Balbiani body and germ cell determinants: 150 years later. *Curr. Top. Dev. Biol.* **59,** 1–36 (2004).
37. Marlow, F. L. & Mullins, M. C. Bucky ball functions in Balbiani body assembly and animal–vegetal polarity in the oocyte and follicle cell layer in zebrafish. *Dev. Biol.* **321,** 40–50 (2008).
38. Lu, F.-I., Thisse, C. & Thisse, B. Identification and mechanism of regulation of the zebrafish dorsal determinant. *Proceedings of the National Academy of Sciences* **108,** 15876–15880 (2011).
39. Tran, L. D. *et al.* Dynamic microtubules at the vegetal cortex predict the embryonic axis in zebrafish. *Development* **139,** 3644–3652 (2012).
40. Kimmel, C. B. & Law, R. D. Cell lineage of zebrafish blastomeres. *Dev. Biol.* **108,** 78–85 (1985).
41. Kane, D. A. & Kimmel, C. B. The zebrafish midblastula transition. *Development* **119,** 447–456 (1993).
42. Montero, J.-A., Kilian, B., Chan, J., Bayliss, P. E. & Heisenberg, C.-P. Phosphoinositide 3-kinase is required for process outgrowth and cell polarization of gastrulating mesendodermal cells. *Curr. Biol.* **13,** 1279–1289 (2003).
43. Dumortier, J. G., Martin, S., Meyer, D., Rosa, F. M. & David, N. B. Collective mesendoderm migration relies on an intrinsic directionality signal transmitted through cell contacts. *Proc. Natl. Acad. Sci. U. S. A.* **109,** 16945–16950 (2012).
44. Pézeron, G. *et al.* Live analysis of endodermal layer formation identifies random walk as a novel gastrulation movement. *Curr. Biol.* **18,** 276–281 (2008).
45. Kimmel, C. B., Ballard, W. W., Kimmel, S. R., Ullmann, B. & Schilling, T. F. Stages of embryonic development of the zebrafish. *Dev. Dyn.* **203,** 253–310 (1995).
46. Helde, K. A., Wilson, E. T., Cretekos, C. J. & Grunwald, D. J. Contribution of early cells to the fate map of the zebrafish gastrula. *Science* **265,** 517–520 (1994).

47. Kimmel, C. B., Warga, R. M. & Schilling, T. F. Origin and organization of the zebrafish fate map. *Development* **108,** 581–594 (1990).
48. Kimmel, C. B. & Warga, R. M. Tissue-specific cell lineages originate in the gastrula of the zebrafish. *Science* **231,** 365–368 (1986).
49. Ho, R. K. & Kimmel, C. B. Commitment of cell fate in the early zebrafish embryo. *Science* **261,** 109–111 (1993).
50. Carvalho, L. & Heisenberg, C.-P. The yolk syncytial layer in early zebrafish development. *Trends Cell Biol.* **20,** 586–592 (2010).
51. Wagner, D. S., Santiago, C., Park, K.-M., de la Torre Canny, S. G. & Wagner, D. S. Zebrafish poky/CHUK/IKK1 is required for epiboly and EVL differentiation. *Dev. Biol.* **331,** 451–452 (2009).
52. Sabel, J. L. *et al.* Maternal Interferon Regulatory Factor 6 is required for the differentiation of primary superficial epithelia in Danio and Xenopus embryos. *Dev. Biol.* **325,** 249–262 (2009).
53. Sagerström, C. G., Gammill, L. S., Veale, R. & Sive, H. Specification of the enveloping layer and lack of autoneuralization in zebrafish embryonic explants. *Dev. Dyn.* **232,** 85–97 (2004).
54. Krens, S. F. G., Möllmert, S. & Heisenberg, C.-P. Enveloping cell-layer differentiation at the surface of zebrafish germ-layer tissue explants. *Proc. Natl. Acad. Sci. U. S. A.* **108,** E9–10; author reply E11 (2011).
55. Schneider, S., Steinbeisser, H., Warga, R. M. & Hausen, P. Beta-catenin translocation into nuclei demarcates the dorsalizing centers in frog and fish embryos. *Mech. Dev.* **57,** 191–198 (1996).
56. Hashimoto, H. *et al.* Zebrafish Dkk1 functions in forebrain specification and axial mesendoderm formation. *Dev. Biol.* **217,** 138–152 (2000).
57. Shimizu, T. *et al.* Cooperative roles of Bozozok/Dharma and Nodal-related proteins in the formation of the dorsal organizer in zebrafish. *Mech. Dev.* **91,** 293–303 (2000).
58. Langdon, Y. G. & Mullins, M. C. Maternal and zygotic control of zebrafish dorsoventral

axial patterning. *Annu. Rev. Genet.* **45,** 357–377 (2011).

59. Piccolo, S., Sasai, Y., Lu, B. & De Robertis, E. M. Dorsoventral patterning in Xenopus: inhibition of ventral signals by direct binding of chordin to BMP-4. *Cell* **86,** 589–598 (1996).
60. Rebagliati, M. R., Toyama, R., Haffter, P. & Dawid, I. B. cyclops encodes a nodal-related factor involved in midline signaling. *Proc. Natl. Acad. Sci. U. S. A.* **95,** 9932–9937 (1998).
61. Dubrulle, J. *et al.* Response to Nodal morphogen gradient is determined by the kinetics of target gene induction. *Elife* **4,** (2015).
62. Feldman, B. *et al.* Zebrafish organizer development and germ-layer formation require nodal-related signals. *Nature* **395,** 181–185 (1998).
63. van Boxtel, A. L. *et al.* A Temporal Window for Signal Activation Dictates the Dimensions of a Nodal Signaling Domain. *Dev. Cell* **35,** 175–185 (2015).
64. Mathieu, J. Nodal and Fgf pathways interact through a positive regulatory loop and synergize to maintain mesodermal cell populations. *Development* **131,** 629–641 (2004).
65. Website. Available at: Thisse, B., Pflumio, S., FÃ¼rthauer, M., Loppin, B., Heyer, V., Degrave, A., Woehl, R., Lux, A., Steffan, T., Charbonnier, X.Q. and Thisse, C. (2001) Expression of the zebrafish genome during embryogenesis (NIH R01 RR15402). ZFIN Direct Data Submission (http://zfin.org). (Accessed: 21st January 2017)
66. Samarut, E., Fraher, D., Laudet, V. & Gibert, Y. ZebRA: An overview of retinoic acid signaling during zebrafish development. *Biochim. Biophys. Acta* **1849,** 73–83 (2015).
67. Schier, A. F. & Talbot, W. S. Molecular genetics of axis formation in zebrafish. *Annu. Rev. Genet.* **39,** 561–613 (2005).
68. Shimozono, S., Iimura, T., Kitaguchi, T., Higashijima, S.-I. & Miyawaki, A. Visualization of an endogenous retinoic acid gradient across embryonic development. *Nature* **496,** 363–366 (2013).
69. Green, J. B. A. & Sharpe, J. Positional information and reaction-diffusion: two big ideas in developmental biology combine. *Development* **142,** 1203–1211 (2015).

70. David, N. B. & Rosa, F. M. Cell autonomous commitment to an endodermal fate and behaviour by activation of Nodal signalling. *Development* **128,** 3937–3947 (2001).
71. Gritsman, K., Talbot, W. S. & Schier, A. F. Nodal signaling patterns the organizer. *Development* **127,** 921–932 (2000).
72. Chen, Y. & Schier, A. F. The zebrafish Nodal signal Squint functions as a morphogen. *Nature* **411,** 607–610 (2001).
73. Thisse, B., Wright, C. V. & Thisse, C. Activin- and Nodal-related factors control antero-posterior patterning of the zebrafish embryo. *Nature* **403,** 425–428 (2000).
74. Poulain, M. Zebrafish endoderm formation is regulated by combinatorial Nodal, FGF and BMP signalling. *Development* **133,** 2189–2200 (2006).
75. Griffin, K., Patient, R. & Holder, N. Analysis of FGF function in normal and no tail zebrafish embryos reveals separate mechanisms for formation of the trunk and the tail. *Development* **121,** 2983–2994 (1995).
76. Agathon, A., Thisse, C. & Thisse, B. The molecular nature of the zebrafish tail organizer. *Nature* **424,** 448–452 (2003).
77. Kishimoto, Y., Lee, K. H., Zon, L., Hammerschmidt, M. & Schulte-Merker, S. The molecular nature of zebrafish swirl: BMP2 function is essential during early dorsoventral patterning. *Development* **124,** 4457–4466 (1997).
78. Müller, P. *et al.* Differential diffusivity of Nodal and Lefty underlies a reaction-diffusion patterning system. *Science* **336,** 721–724 (2012).
79. Long, S., Ahmad, N. & Rebagliati, M. The zebrafish nodal-related gene southpaw is required for visceral and diencephalic left-right asymmetry. *Development* **130,** 2303–2316 (2003).
80. Tian, J., Andrée, B., Jones, C. M. & Sampath, K. The pro-domain of the zebrafish Nodal-related protein Cyclops regulates its signaling activities. *Development* **135,** 2649–2658 (2008).
81. Blanchet, M.-H. *et al.* Cripto recruits Furin and PACE4 and controls Nodal trafficking during proteolytic maturation. *EMBO J.* **27,** 2580–2591 (2008).

82. Schier, A. F. Nodal morphogens. *Cold Spring Harb. Perspect. Biol.* **1,** a003459 (2009).

83. Shen, M. M. Nodal signaling: developmental roles and regulation. *Development* **134,** 1023–1034 (2007).

84. Constam, D. B. Riding shotgun: a dual role for the epidermal growth factor-Cripto/FRL-1/Cryptic protein Cripto in Nodal trafficking. *Traffic* **10,** 783–791 (2009).

85. Itoh, F. *et al.* The FYVE domain in Smad anchor for receptor activation (SARA) is sufficient for localization of SARA in early endosomes and regulates TGF-beta/Smad signalling. *Genes Cells* **7,** 321–331 (2002).

86. Tsukazaki, T., Chiang, T. A., Davison, A. F., Attisano, L. & Wrana, J. L. SARA, a FYVE domain protein that recruits Smad2 to the TGFbeta receptor. *Cell* **95,** 779–791 (1998).

87. Batut, J., Howell, M. & Hill, C. S. Kinesin-mediated transport of Smad2 is required for signaling in response to TGF-beta ligands. *Dev. Cell* **12,** 261–274 (2007).

88. Inman, G. J. & Hill, C. S. Stoichiometry of active smad-transcription factor complexes on DNA. *J. Biol. Chem.* **277,** 51008–51016 (2002).

89. Schmierer, B., Tournier, A. L., Bates, P. A. & Hill, C. S. Mathematical modeling identifies Smad nucleocytoplasmic shuttling as a dynamic signal-interpreting system. *Proc. Natl. Acad. Sci. U. S. A.* **105,** 6608–6613 (2008).

90. Warmflash, A. *et al.* Dynamics of TGF- signaling reveal adaptive and pulsatile behaviors reflected in the nuclear localization of transcription factor Smad4. *Proceedings of the National Academy of Sciences* **109,** E1947–E1956 (2012).

91. Schulte-Merker, S. *et al.* Expression of zebrafish goosecoid and no tail gene products in wild-type and mutant no tail embryos. *Development* **120,** 843–852 (1994).

92. Kikuchi, Y. casanova encodes a novel Sox-related protein necessary and sufficient for early endoderm formation in zebrafish. *Genes Dev.* **15,** 1493–1505 (2001).

93. Alexander, J., Rothenberg, M., Henry, G. L. & Stainier, D. Y. R. casanova Plays an Early and Essential Role in Endoderm Formation in Zebrafish. *Dev. Biol.* **215,** 343–357 (1999).

94. Melby, A. E., Warga, R. M. & Kimmel, C. B. Specification of cell fates at the dorsal

margin of the zebrafish gastrula. *Development* **122,** 2225–2237 (1996).

95. Bisgrove, B. W., Essner, J. J. & Yost, H. J. Regulation of midline development by antagonism of lefty and nodal signaling. *Development* **126,** 3253–3262 (1999).
96. Chen, C. & Shen, M. M. Two Modes by which Lefty Proteins Inhibit Nodal Signaling. *Curr. Biol.* **14,** 618–624 (2004).
97. Thisse, C., Thisse, B., Halpern, M. E. & Postlethwait, J. H. Goosecoid expression in neurectoderm and mesendoderm is disrupted in zebrafish cyclops gastrulas. *Dev. Biol.* **164,** 420–429 (1994).
98. Sako, K. *et al.* Optogenetic Control of Nodal Signaling Reveals a Temporal Pattern of Nodal Signaling Regulating Cell Fate Specification during Gastrulation. *Cell Rep.* **16,** 866–877 (2016).
99. Jullien, J. & Gurdon, J. Morphogen gradient interpretation by a regulated trafficking step during ligand-receptor transduction. *Genes Dev.* **19,** 2682–2694 (2005).
100. Blanchet, M.-H. *et al.* Cripto localizes Nodal at the limiting membrane of early endosomes. *Sci. Signal.* **1,** ra13 (2008).
101. Garrod, D., North, A. J. & Chidgey, M. A. J. *The Adhesive Interaction of Cells*. (Elsevier, 1999).
102. Yap, A. S., Brieher, W. M. & Gumbiner, B. M. Molecular and functional analysis of cadherin-based adherens junctions. *Annu. Rev. Cell Dev. Biol.* **13,** 119–146 (1997).
103. Takeichi, M. Functional correlation between cell adhesive properties and some cell surface proteins. *J. Cell Biol.* **75,** 464–474 (1977).
104. Halbleib, J. M. & Nelson, W. J. Cadherins in development: cell adhesion, sorting, and tissue morphogenesis. *Genes Dev.* **20,** 3199–3214 (2006).
105. Hayashi, S. & Takeichi, M. Emerging roles of protocadherins: from self-avoidance to enhancement of motility. *J. Cell Sci.* **128,** 1455–1464 (2015).
106. Chen, X. & Gumbiner, B. M. Paraxial protocadherin mediates cell sorting and tissue morphogenesis by regulating C-cadherin adhesion activity. *J. Cell Biol.* **174,** 301–313 (2006).

107. Goonesinghe, A., Luan, X.-M., Hurlstone, A. & Garrod, D. Desmosomal cadherins in zebrafish epiboly and gastrulation. *BMC Dev. Biol.* **12,** 1 (2012).

108. Gumbiner, B. M. Regulation of cadherin-mediated adhesion in morphogenesis. *Nat. Rev. Mol. Cell Biol.* **6,** 622–634 (2005).

109. Babb, S. G. & Marrs, J. A. E-cadherin regulates cell movements and tissue formation in early zebrafish embryos. *Dev. Dyn.* **230,** 263–277 (2004).

110. Shimizu, T. *et al.* E-cadherin is required for gastrulation cell movements in zebrafish. *Mech. Dev.* **122,** 747–763 (2005).

111. Kane, D. A. *et al.* The zebrafish epiboly mutants. *Development* **123,** 47–55 (1996).

112. Warga, R. M. & Kane, D. A. A role for N-cadherin in mesodermal morphogenesis during gastrulation. *Dev. Biol.* **310,** 211–225 (2007).

113. Lele, Z. *et al.* parachute/n-cadherin is required for morphogenesis and maintained integrity of the zebrafish neural tube. *Development* **129,** 3281–3294 (2002).

114. Shapiro, L. *et al.* Structural basis of cell-cell adhesion by cadherins. *Nature* **374,** 327–337 (1995).

115. Nagar, B., Overduin, M., Ikura, M. & Rini, J. M. Structural basis of calcium-induced E-cadherin rigidification and dimerization. *Nature* **380,** 360–364 (1996).

116. Brieher, W. M., Yap, A. S. & Gumbiner, B. M. Lateral dimerization is required for the homophilic binding activity of C-cadherin. *J. Cell Biol.* **135,** 487–496 (1996).

117. Tomschy, A., Fauser, C., Landwehr, R. & Engel, J. Homophilic adhesion of E-cadherin occurs by a co-operative two-step interaction of N-terminal domains. *EMBO J.* **15,** 3507–3514 (1996).

118. Overduin, M. *et al.* Solution structure of the epithelial cadherin domain responsible for selective cell adhesion. *Science* **267,** 386–389 (1995).

119. Pokutta, S., Herrenknecht, K., Kemler, R. & Engel, J. Conformational changes of the recombinant extracellular domain of E-cadherin upon calcium binding. *Eur. J. Biochem.* **223,** 1019–1026 (1994).

120. Nose, A., Nagafuchi, A. & Takeichi, M. Expressed recombinant cadherins mediate cell

sorting in model systems. *Cell* **54,** 993–1001 (1988).

121. Nose, A., Tsuji, K. & Takeichi, M. Localization of specificity determining sites in cadherin cell adhesion molecules. *Cell* **61,** 147–155 (1990).

122. Nagafuchi, A. & Takeichi, M. Cell binding function of E-cadherin is regulated by the cytoplasmic domain. *EMBO J.* **7,** 3679–3684 (1988).

123. Ozawa, M., Baribault, H. & Kemler, R. The cytoplasmic domain of the cell adhesion molecule uvomorulin associates with three independent proteins structurally related in different species. *EMBO J.* **8,** 1711–1717 (1989).

124. Hinck, L., Näthke, I. S., Papkoff, J. & Nelson, W. J. Dynamics of cadherin/catenin complex formation: novel protein interactions and pathways of complex assembly. *J. Cell Biol.* **125,** 1327–1340 (1994).

125. Aberle, H. *et al.* Assembly of the cadherin-catenin complex in vitro with recombinant proteins. *J. Cell Sci.* **107 (Pt 12),** 3655–3663 (1994).

126. Drees, F., Pokutta, S., Yamada, S., Nelson, W. J. & Weis, W. I. Alpha-catenin is a molecular switch that binds E-cadherin-beta-catenin and regulates actin-filament assembly. *Cell* **123,** 903–915 (2005).

127. Yamada, S., Pokutta, S., Drees, F., Weis, W. I. & Nelson, W. J. Deconstructing the cadherin-catenin-actin complex. *Cell* **123,** 889–901 (2005).

128. Torres, M. *et al.* An alpha-E-catenin gene trap mutation defines its function in preimplantation development. *Proc. Natl. Acad. Sci. U. S. A.* **94,** 901–906 (1997).

129. Buckley, C. D. *et al.* Cell adhesion. The minimal cadherin-catenin complex binds to actin filaments under force. *Science* **346,** 1254211 (2014).

130. Shibamoto, S. *et al.* Association of p120, a tyrosine kinase substrate, with E-cadherin/catenin complexes. *J. Cell Biol.* **128,** 949–957 (1995).

131. Ishiyama, N. *et al.* Dynamic and Static Interactions between p120 Catenin and E-Cadherin Regulate the Stability of Cell-Cell Adhesion. *Cell* **141,** 117–128 (2010).

132. Thoreson, M. A. *et al.* Selective uncoupling of p120(ctn) from E-cadherin disrupts strong adhesion. *J. Cell Biol.* **148,** 189–202 (2000).

133. Anastasiadis, P. Z. *et al.* Inhibition of RhoA by p120 catenin. *Nat. Cell Biol.* **2,** 637–644 (2000).

134. Noren, N. K., Liu, B. P., Burridge, K. & Kreft, B. p120 catenin regulates the actin cytoskeleton via Rho family GTPases. *J. Cell Biol.* **150,** 567–580 (2000).

135. Magie, C. R., Pinto-Santini, D. & Parkhurst, S. M. Rho1 interacts with p120ctn and alpha-catenin, and regulates cadherin-based adherens junction components in Drosophila. *Development* **129,** 3771–3782 (2002).

136. Kourtidis, A., Ngok, S. P. & Anastasiadis, P. Z. p120 catenin: an essential regulator of cadherin stability, adhesion-induced signaling, and cancer progression. *Prog. Mol. Biol. Transl. Sci.* **116,** 409–432 (2013).

137. Yamada, S. & Nelson, W. J. Localized zones of Rho and Rac activities drive initiation and expansion of epithelial cell-cell adhesion. *J. Cell Biol.* **178,** 517–527 (2007).

138. Maitre, J.-L. *et al.* Adhesion Functions in Cell Sorting by Mechanically Coupling the Cortices of Adhering Cells. *Science* **338,** 253–256 (2012).

139. Engl, W., Arasi, B., Yap, L. L., Thiery, J. P. & Viasnoff, V. Actin dynamics modulate mechanosensitive immobilization of E-cadherin at adherens junctions. *Nat. Cell Biol.* **16,** 587–594 (2014).

140. Yap, A. S., Gomez, G. A. & Parton, R. G. Adherens Junctions Revisualized: Organizing Cadherins as Nanoassemblies. *Dev. Cell* **35,** 12–20 (2015).

141. Truong Quang, B.-A., Mani, M., Markova, O., Lecuit, T. & Lenne, P.-F. Principles of E-cadherin supramolecular organization in vivo. *Curr. Biol.* **23,** 2197–2207 (2013).

142. Wu, Y., Kanchanawong, P. & Zaidel-Bar, R. Actin-Delimited Adhesion-Independent Clustering of E-Cadherin Forms the Nanoscale Building Blocks of Adherens Junctions. *Dev. Cell* **32,** 139–154 (2015).

143. Lecuit, T. & Yap, A. S. E-cadherin junctions as active mechanical integrators in tissue dynamics. *Nat. Cell Biol.* **17,** 533–539 (2015).

144. Acharya, B. R. & Yap, A. S. Pli Selon Pli: Mechanochemical Feedback and the Morphogenetic Role of Contractility at Cadherin Cell-Cell Junctions. *Curr. Top. Dev.*

Biol. **117,** 631–646 (2016).

145. Stephenson, R. O., Yamanaka, Y. & Rossant, J. Disorganized epithelial polarity and excess trophectoderm cell fate in preimplantation embryos lacking E-cadherin. *Development* **137,** 3383–3391 (2010).

146. Tepass, U. *et al.* shotgun encodes Drosophila E-cadherin and is preferentially required during cell rearrangement in the neurectoderm and other morphogenetically active epithelia. *Genes Dev.* **10,** 672–685 (1996).

147. Levine, E., Lee, C. H., Kintner, C. & Gumbiner, B. M. Selective disruption of E-cadherin function in early Xenopus embryos by a dominant negative mutant. *Development* **120,** 901–909 (1994).

148. Lee, C. H. & Gumbiner, B. M. Disruption of gastrulation movements in Xenopus by a dominant-negative mutant for C-cadherin. *Dev. Biol.* **171,** 363–373 (1995).

149. Foty, R. A. & Steinberg, M. S. The differential adhesion hypothesis: a direct evaluation. *Dev. Biol.* **278,** 255–263 (2005).

150. Krens, S. F. G. & Heisenberg, C.-P. Cell sorting in development. *Curr. Top. Dev. Biol.* **95,** 189–213 (2011).

151. Winklbauer, R. Cell adhesion strength from cortical tension - an integration of concepts. *J. Cell Sci.* **128,** 3687–3693 (2015).

152. Ciruna, B. & Rossant, J. FGF signaling regulates mesoderm cell fate specification and morphogenetic movement at the primitive streak. *Dev. Cell* **1,** 37–49 (2001).

153. Kölsch, V., Seher, T., Fernandez-Ballester, G. J., Serrano, L. & Leptin, M. Control of Drosophila gastrulation by apical localization of adherens junctions and RhoGEF2. *Science* **315,** 384–386 (2007).

154. Wu, S.-Y. & McClay, D. R. The Snail repressor is required for PMC ingression in the sea urchin embryo. *Development* **134,** 1061–1070 (2007).

155. Nieto, M. A., Sargent, M. G., Wilkinson, D. G. & Cooke, J. Control of cell behavior during vertebrate development by Slug, a zinc finger gene. *Science* **264,** 835–839 (1994).

156. Chuai, M. & Weijer, C. J. Regulation of cell migration during chick gastrulation. *Curr.*

Opin. Genet. Dev. **19,** 343–349 (2009).

157. Schafer, G., Narasimha, M., Vogelsang, E. & Leptin, M. Cadherin switching during the formation and differentiation of the Drosophila mesoderm - implications for epithelial-to-mesenchymal transitions. *Development* **141,** e0907–e0907 (2014).

158. Weng, M. & Wieschaus, E. Myosin-dependent remodeling of adherens junctions protects junctions from Snail-dependent disassembly. *J. Cell Biol.* **212,** 219–229 (2016).

159. Arboleda-Estudillo, Y. *et al.* Movement directionality in collective migration of germ layer progenitors. *Curr. Biol.* **20,** 161–169 (2010).

160. Ulrich, F. *et al.* Wnt11 functions in gastrulation by controlling cell cohesion through Rab5c and E-cadherin. *Dev. Cell* **9,** 555–564 (2005).

161. Zhong, Y., Brieher, W. M. & Gumbiner, B. M. Analysis of C-cadherin regulation during tissue morphogenesis with an activating antibody. *J. Cell Biol.* **144,** 351–359 (1999).

162. Krieg, M. *et al.* Tensile forces govern germ-layer organization in zebrafish. *Nat. Cell Biol.* **10,** 429–436 (2008).

163. Maître, J.-L., Niwayama, R., Turlier, H., Nédélec, F. & Hiiragi, T. Pulsatile cell-autonomous contractility drives compaction in the mouse embryo. *Nat. Cell Biol.* **17,** 849–855 (2015).

164. Schötz, E.-M. *et al.* Quantitative differences in tissue surface tension influence zebrafish germ layer positioning. *HFSP J.* **2,** 42–56 (2008).

165. von der Hardt, S. *et al.* The Bmp gradient of the zebrafish gastrula guides migrating lateral cells by regulating cell-cell adhesion. *Curr. Biol.* **17,** 475–487 (2007).

166. Brieher, W. M. & Gumbiner, B. M. Regulation of C-cadherin function during activin induced morphogenesis of Xenopus animal caps. *J. Cell Biol.* **126,** 519–527 (1994).

167. Ogata, S. *et al.* TGF-beta signaling-mediated morphogenesis: modulation of cell adhesion via cadherin endocytosis. *Genes Dev.* **21,** 1817–1831 (2007).

168. Woo, S., Housley, M. P., Weiner, O. D. & Stainier, D. Y. R. Nodal signaling regulates endodermal cell motility and actin dynamics via Rac1 and Prex1. *J. Cell Biol.* **198,** 941–952 (2012).

169. Gao, L., McBeath, R. & Chen, C. S. Stem Cell Shape Regulates a Chondrogenic Versus Myogenic Fate Through Rac1 and N-Cadherin. *Stem Cells* (2010). doi:10.1002/stem.308

170. McBeath, R., Pirone, D. M., Nelson, C. M., Bhadriraju, K. & Chen, C. S. Cell shape, cytoskeletal tension, and RhoA regulate stem cell lineage commitment. *Dev. Cell* **6,** 483–495 (2004).

171. Engler, A. J., Sen, S., Lee Sweeney, H. & Discher, D. E. Matrix Elasticity Directs Stem Cell Lineage Specification. *Cell* **126,** 677–689 (2006).

172. Yennek, S., Burute, M., Théry, M. & Tajbakhsh, S. Cell Adhesion Geometry Regulates Non-Random DNA Segregation and Asymmetric Cell Fates in Mouse Skeletal Muscle Stem Cells. *Cell Rep.* **7,** 961–970 (2014).

173. Bellas, E. & Chen, C. S. Forms, forces, and stem cell fate. *Curr. Opin. Cell Biol.* **31,** 92–97 (2014).

174. Gilmour, D., Rembold, M. & Leptin, M. From morphogen to morphogenesis and back. *Nature* **541,** 311–320 (2017).

175. Larue, L. *et al.* A role for cadherins in tissue formation. *Development* **122,** 3185–3194 (1996).

176. Poh, Y.-C. *et al.* Generation of organized germ layers from a single mouse embryonic stem cell. *Nat. Commun.* **5,** 4000 (2014).

177. Warmflash, A., Sorre, B., Etoc, F., Siggia, E. D. & Brivanlou, A. H. A method to recapitulate early embryonic spatial patterning in human embryonic stem cells. *Nat. Methods* **11,** 847–854 (2014).

178. McCrea, P. D., Maher, M. T. & Gottardi, C. J. in *Current Topics in Developmental Biology* 129–196 (2015).

179. Logan, C. Y. & Nusse, R. The Wnt signaling pathway in development and disease. *Annu. Rev. Cell Dev. Biol.* **20,** 781–810 (2004).

180. Qian, X., Karpova, T., Sheppard, A. M., McNally, J. & Lowy, D. R. E-cadherin-mediated adhesion inhibits ligand-dependent activation of diverse receptor tyrosine kinases.

EMBO J. **23,** 1739–1748 (2004).

181. Klezovitch, O. & Vasioukhin, V. Cadherin signaling: keeping cells in touch. *F1000Res.* **4,** 550 (2015).

182. Lampugnani, M. G., Orsenigo, F., Gagliani, M. C., Tacchetti, C. & Dejana, E. Vascular endothelial cadherin controls VEGFR-2 internalization and signaling from intracellular compartments. *J. Cell Biol.* **174,** 593–604 (2006).

183. Curto, M., Cole, B. K., Lallemand, D., Liu, C.-H. & McClatchey, A. I. Contact-dependent inhibition of EGFR signaling by Nf2/Merlin. *J. Cell Biol.* **177,** 893–903 (2007).

184. Suyama, K., Shapiro, I., Guttman, M. & Hazan, R. B. A signaling pathway leading to metastasis is controlled by N-cadherin and the FGF receptor. *Cancer Cell* **2,** 301–314 (2002).

185. Cavallaro, U., Niedermeyer, J., Fuxa, M. & Christofori, G. N-CAM modulates tumour-cell adhesion to matrix by inducing FGF-receptor signalling. *Nat. Cell Biol.* **3,** 650–657 (2001).

186. Rudini, N. *et al.* VE-cadherin is a critical endothelial regulator of TGF-β signalling. *EMBO J.* **27,** 993–1004 (2008).

187. Grazia Lampugnani, M. *et al.* Contact inhibition of VEGF-induced proliferation requires vascular endothelial cadherin, beta-catenin, and the phosphatase DEP-1/CD148. *J. Cell Biol.* **161,** 793–804 (2003).

188. Haÿ, E. *et al.* N-cadherin interacts with axin and LRP5 to negatively regulate Wnt/beta-catenin signaling, osteoblast function, and bone formation. *Mol. Cell. Biol.* **29,** 953–964 (2009).

189. Desai, R. A., Gao, L., Raghavan, S., Liu, W. F. & Chen, C. S. Cell polarity triggered by cell-cell adhesion via E-cadherin. *J. Cell Sci.* **122,** 905–911 (2009).

190. Nallet-Staub, F. *et al.* Cell density sensing alters TGF-β signaling in a cell-type-specific manner, independent from Hippo pathway activation. *Dev. Cell* **32,** 640–651 (2015).

191. Michel, M., Raabe, I., Kupinski, A. P., Pérez-Palencia, R. & Bökel, C. Local BMP receptor activation at adherens junctions in the Drosophila germline stem cell niche.

Nat. Commun. **2,** 415 (2011).

192. Salazar-Ciudad, I., Jernvall, J. & Newman, S. A. Mechanisms of pattern formation in development and evolution. *Development* **130,** 2027–2037 (2003).

193. Shyer, A. E., Huycke, T. R., Lee, C., Mahadevan, L. & Tabin, C. J. Bending gradients: how the intestinal stem cell gets its home. *Cell* **161,** 569–580 (2015).

194. Westerfield, M. *The Zebrafish Book: A Guide for the Laboratory Use of Zebrafish (Danio Rerio)*. (2007).

195. Smutny, M. *et al.* Friction forces position the neural anlage. *Nat. Cell Biol.* (in press).

196. Cooper, M. S. *et al.* Visualizing morphogenesis in transgenic zebrafish embryos using BODIPY TR methyl ester dye as a vital counterstain for GFP. *Dev. Dyn.* **232,** 359–368 (2005).

197. Chung, W.-S. & Stainier, D. Y. R. Intra-endodermal interactions are required for pancreatic beta cell induction. *Dev. Cell* **14,** 582–593 (2008).

198. Gritsman, K. *et al.* The EGF-CFC protein one-eyed pinhead is essential for nodal signaling. *Cell* **97,** 121–132 (1999).

199. Kwan, K. M. *et al.* The Tol2kit: a multisite gateway-based construction kit for Tol2 transposon transgenesis constructs. *Dev. Dyn.* **236,** 3088–3099 (2007).

200. Villefranc, J. A., Amigo, J. & Lawson, N. D. Gateway compatible vectors for analysis of gene function in the zebrafish. *Dev. Dyn.* **236,** 3077–3087 (2007).

201. Inbal, A., Topczewski, J. & Solnica-Krezel, L. Targeted gene expression in the zebrafish prechordal plate. *Genesis* **44,** 584–588 (2006).

202. Grusch, M. *et al.* Spatio-temporally precise activation of engineered receptor tyrosine kinases by light. *EMBO J.* **33,** 1713–1726 (2014).

203. Yoder, M. D. & Gumbiner, B. M. Axial protocadherin (AXPC) regulates cell fate during notochordal morphogenesis. *Dev. Dyn.* **240,** 2495–2504 (2011).

204. Luu, O. *et al.* PAPC mediates self/non-self-distinction during Snail1-dependent tissue separation. *J. Cell Biol.* **208,** 839–856 (2015).

205. Medina, A., Araceli, M., Swain, R. K., Klaus-Michael, K. & Herbert, S. Xenopus paraxial

protocadherin has signaling functions and is involved in tissue separation. *EMBO J.* **23,** 3249–3258 (2004).

206. Blanco, M. J. *et al.* Snail1a and Snail1b cooperate in the anterior migration of the axial mesendoderm in the zebrafish embryo. *Development* **134,** 4073–4081 (2007).

207. Barone, V., Vanessa, B. & Carl-Philipp, H. Cell adhesion in embryo morphogenesis. *Curr. Opin. Cell Biol.* **24,** 148–153 (2012).

208. Maître, J.-L. *et al.* Asymmetric division of contractile domains couples cell positioning and fate specification. *Nature* **536,** 344–348 (2016).

209. Durdu, S. *et al.* Luminal signalling links cell communication to tissue architecture during organogenesis. *Nature* **515,** 120–124 (2014).

210. Witzel, S., Zimyanin, V., Carreira-Barbosa, F., Tada, M. & Heisenberg, C.-P. Wnt11 controls cell contact persistence by local accumulation of Frizzled 7 at the plasma membrane. *J. Cell Biol.* **175,** 791–802 (2006).

211. Ulrich, F. *et al.* Slb/Wnt11 controls hypoblast cell migration and morphogenesis at the onset of zebrafish gastrulation. *Development* **130,** 5375–5384 (2003).

212. Kim, S. H., Yamamoto, A., Bouwmeester, T., Agius, E. & Robertis, E. M. The role of paraxial protocadherin in selective adhesion and cell movements of the mesoderm during Xenopus gastrulation. *Development* **125,** 4681–4690 (1998).

213. DaCosta Byfield, S. SB-505124 Is a Selective Inhibitor of Transforming Growth Factor-Type I Receptors ALK4, ALK5, and ALK7. *Mol. Pharmacol.* **65,** 744–752 (2004).

214. Xu, W., Hou, Y., Hung, Y. S. & Zou, Y. A comparative analysis of Spearman's rho and Kendall's tau in normal and contaminated normal models. *Signal Processing* **93,** 261–276 (2013).

215. Warga, R. M. & Kane, D. A. One-eyed pinhead regulates cell motility independent of Squint/Cyclops signaling. *Dev. Biol.* **261,** 391–411 (2003).

216. Schier, A. F. Nodal Signaling in Vertebrate Development. *Annu. Rev. Cell Dev. Biol.* **19,** 589–621 (2003).

217. Trichas, G. *et al.* Nodal Dependent Differential Localisation of Dishevelled-2

Demarcates Regions of Differing Cell Behaviour in the Visceral Endoderm. *PLoS Biol.* **9,** e1001019 (2011).

218. Schmierer, B. & Hill, C. S. Kinetic Analysis of Smad Nucleocytoplasmic Shuttling Reveals a Mechanism for Transforming Growth Factor -Dependent Nuclear Accumulation of Smads. *Mol. Cell. Biol.* **25,** 9845–9858 (2005).
219. Losick, R. & Desplan, C. Stochasticity and cell fate. *Science* **320,** 65–68 (2008).
220. Meunier, C. & Verga, A. D. Noise and bifurcations. *J. Stat. Phys.* **50,** 345–375 (1988).
221. Gnügge, R., Dharmarajan, L., Lang, M. & Stelling, J. An Orthogonal Permease-Inducer-Repressor Feedback Loop Shows Bistability. *ACS Synth. Biol.* **5,** 1098–1107 (2016).
222. Warga, R. M. & Nüsslein-Volhard, C. Origin and development of the zebrafish endoderm. *Development* **126,** 827–838 (1999).
223. Davidson, E. H. *et al.* A genomic regulatory network for development. *Science* **295,** 1669–1678 (2002).
224. Ferrell, J. E., Jr. The Biochemical Basis of an All-or-None Cell Fate Switch in Xenopus Oocytes. *Science* **280,** 895–898 (1998).
225. Mitrophanov, A. Y. & Groisman, E. A. Positive feedback in cellular control systems. *Bioessays* **30,** 542–555 (2008).
226. Becskei, A., Attila, B. & Grusby, M. J. Contribution of IL-12R mediated feedback loop to Th1 cell differentiation. *FEBS Lett.* **581,** 5199–5206 (2007).
227. Brandman, O., Ferrell, J. E., Jr, Li, R. & Meyer, T. Interlinked fast and slow positive feedback loops drive reliable cell decisions. *Science* **310,** 496–498 (2005).
228. Hopfield, J. J. Kinetic proofreading: a new mechanism for reducing errors in biosynthetic processes requiring high specificity. *Proc. Natl. Acad. Sci. U. S. A.* **71,** 4135–4139 (1974).
229. McKeithan, T. W. Kinetic proofreading in T-cell receptor signal transduction. *Proc. Natl. Acad. Sci. U. S. A.* **92,** 5042–5046 (1995).

A. Appendix 1

Stochastic modeling of the positive feedback loop between cell-cell contact formation and nodal signaling in the ppl during zebrafish gastrulation. The work presented in this section was performed by Moritz Lang.